University of Liège
Faculty of Applied Sciences

ULg Promoter Pr. J.-P. Swings
ESA Supervisor R. Prieto Cerdeira

Master thesis

Ionosphere Crossing of GALILEO Signals

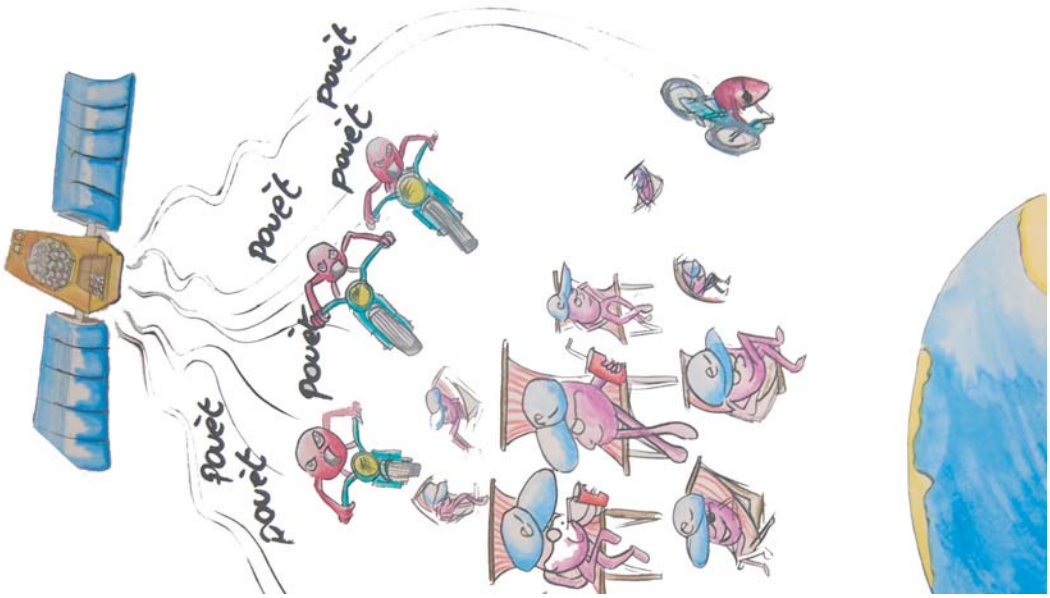

Benoît Bidaine
Last year for the master's degree in physics engineering
Field of space techniques
B.Bidaine@gmail.com

Academic year 2005 - 2006

University of Liège
Faculty of Applied Sciences

ULg Promoter Pr. J.-P. Swings
ESA Supervisor R. Prieto Cerdeira

Master thesis

Ionosphere Crossing of GALILEO Signals

Benoît Bidaine
Last year for the master's degree in physics engineering
Field of space techniques
B.Bidaine@gmail.com

Academic year 2005 - 2006

Ionosphere Crossing of GALILEO Signals

The **ionosphere** plays a crucial role in Global Navigation Satellite Systems (GNSS) accuracy. This electrically charged part of the atmosphere can **lead to errors in positioning** up to several tens of meters for single frequency receivers. Therefore its modelling constitutes an important field of study.

An **empirical model called NeQuick** has been chosen to evaluate the ionospheric contribution in GALILEO single frequency users correction. It generates electron densities for given space, time and solar activity conditions from a minimum set of anchor points characteristics. Its use with integration methods allows to calculate total electron contents (TEC) which are directly related to the ionospheric delay.

The current GALILEO baseline version of NeQuick is the one published by the Radiocommunication Sector of the International Telecommunication Union (ITU-R) in 2000. From that time, several improvements have been proposed and some problems have been discovered leading to the need of a better understanding and **comparison of** these different **versions** and an **analysis of** the **weaknesses**. For example research about new topside formulations is currently performed - a new simple proposal has been tested - and the consequences of the daily effective use of NeQuick, which is designed to work with monthly median situations, have to be better known.

A software tool with a Graphical User Interface (GUI) has then been developed for the analysis and a comparison between different versions and also between modelled and measured data has been performed. **Structuring and analysis** of the above-mentioned issues and results of the comparison are detailed in the present document. Solutions or possible paths to investigate solutions are also proposed.

Benoît Bidaine
Last year for the master's degree
in physics engineering
Field of space techniques

Board of supervisors

J.-P. Swings	R. Prieto Cerdeira	J.-C. Gérard	P. Beckers
Professor	Engineer	Professor	Professor
ULg (FS/AGO)	ESA (TEC-EEP)	ULg (FS/AGO)	ULg (FAS/A&M)
Promoter	Supervisor	Member	Member

Traversée de l'ionosphère par les signaux GALILEO

L'**ionosphère** joue un rôle crucial pour la précision des systèmes globaux de navigation par satellite (GNSS). Cette partie de l'atmosphère chargée électriquement peut **mener à des erreurs de positionnement** de plusieurs dizaines de mètres pour les récepteurs simple fréquence. Par conséquent sa modélisation constitue un domaine d'étude important.

Un **modèle empirique appelé NeQuick** a été choisi pour estimer la contribution de l'ionosphère à la correction destinée aux utilisateurs simple fréquence de GALILEO. Il génère des densités électroniques pour des conditions d'espace, de temps et d'activité solaire données à partir d'un ensemble minimum de caractéristiques de points d'ancrage. Son utilisation combinée à des méthodes d'intégration permet de calculer des contenus totaux en électrons (TEC) qui sont directement liés au délai ionosphérique.

La référence actuelle pour GALILEO est la version de NeQuick publiée par la Section Radiocommunication de l'Union Internationale des Télécommunications (ITU-R) en 2000. Depuis lors, plusieurs améliorations ont été proposées et certains problèmes ont été découverts d'où le besoin d'une meilleure compréhension et de la **comparaison de** ces diverses **versions** et une **analyse des faiblesses**. Par exemple des recherches au sujet de nouvelles formulations de la couche supérieure sont en cours - une nouvelle proposition simple a été testée - et les conséquences de l'utilisation effective journalière de NeQuick, construit pour fonctionner sur base de situations mensuelles moyennes, doivent être mieux connues.

Un logiciel muni d'une interface graphique (GUI) a donc été développé pour l'analyse et une comparaison entre différentes versions mais aussi entre des données issues de la modélisation et de mesures a été effectuée. **La structuration et l'analyse** des sujets cités ci-dessus et les résultats de la comparaison sont détaillés dans le présent document. Des solutions ou des pistes aboutissant potentiellement à des solutions sont également proposées.

Benoît Bidaine

Travail de fin d'études en vue de l'obtention du grade d'ingénieur civil physicien - filière techniques spatiales

Jury

J.-P. Swings	R. Prieto Cerdeira	J.-C. Gérard	P. Beckers
Professeur	Ingénieur	Professeur	Professeur
ULg (FS/AGO)	ASE (TEC-EEP)	ULg (FS/AGO)	ULg (FSA/A&M)
Promoteur	Tuteur	Membre	Membre


pouèt
pouèt
pouèt
pouèt
pouèt
pouèt

Acknowledgements

I could not begin the description of my work at ESA without thanking deeply Roberto Prieto Cerdeira, my supervisor, Antonio Martellucci and Bertram Arbesser-Rastburg from ESTEC TEC-EEP section, who never hesitated to spend time for me.

This wonderful experience was made possible by Peter Claes from the GALILEO Project and Jean-Pierre Swings, my promoter at ULg, towards who I am very grateful.

Everyday life at ESTEC has been really pleasant thanks to Roberto, Antonio and Bertram but also Ana, Cristina, Annalisa, Carolina, Donata, Hao, Cyril, Peter, Arturo, Antoine, Luca, Maarten, Marc, Ferran, Nicolas and Charles.

I wish also to acknowledge

Sandro Radicella, Pierdavide Coïsson and Bruno Nava from ARPL in Trieste as well as René Warnant from ROB in Brussels for their wise comments,

Olivier Dupont for the beautiful cover drawing,

Alison, Anne-Marie, Eric and all the people who supported me in my task and I could have forgotten.

My final thoughts go to Reinhart Leitinger whose knowledge I would have really been honoured to share.

Eppur si muove
[*And yet it does move!*]

Galileo Galilei
June 22nd, 1633

Contents

1 Introduction **1**

I A few guidelines **4**

2 GALILEO as a GNSS **5**

2.1 Navigation and GNSS 5

2.1.1 Fundamentals of satellite navigation 5

2.1.2 Several systems 6

2.1.3 GPS 7

2.2 GALILEO 9

2.2.1 General characteristics 9

2.2.2 Infrastructure 10

2.2.3 Comparison with GPS 11

2.3 Positioning error 12

3 Ionosphere as an atmospheric layer **14**

3.1 Ionization and atmosphere 14

3.2 Ionosphere 15

3.2.1 Vertical structure 15

3.2.2 Variations 16

3.2.3 Description 19

3.3 Ionospheric error 25

4 NeQuick as an ionospheric model **27**

4.1 Ionospheric models 27

4.1.1 Common points . . . 27
4.1.2 International Reference Ionosphere (IRI) . . . 27
4.1.3 Bent . . . 28
4.1.4 DGR family . . . 30
4.2 DGR "profiler" concept . . . 31
4.2.1 Principle . . . 31
4.2.2 Parameters determination from input data . . . 35
4.2.3 Evolution . . . 36
4.3 NeQuick . . . 37
4.3.1 Simple topside . . . 37
4.3.2 Implementation . . . 38
4.3.3 Electronic characteristics as output . . . 42
4.3.4 GALILEO ionospheric model for single-frequency receivers 44

II A broad analysis 46

5 NeQuick assessment 47
5.1 Analysis structure . . . 47
5.2 "Physical" behaviour . . . 49
5.2.1 "Physical" related questions . . . 49
5.2.2 Developments from 2001 . . . 49
5.2.3 Future developments . . . 52
5.3 "Effective" use . . . 54
5.3.1 Effective ionization Az . . . 54
5.3.2 "Effective" related questions . . . 55
5.4 Implementation . . . 56

6 Analysis tool 57
6.1 Main . . . 57
6.2 Modules . . . 59
6.2.1 Electron densities . . . 59
6.2.2 Profiles . . . 60
6.2.3 vTEC analysis . . . 62

6.2.4 sTEC analysis 64
6.2.5 Flux 66
6.3 Further developments 67

7 Tests **68**
7.1 Overall description 68
7.2 Profiles 71
7.3 vTEC 74
7.4 sTEC 76

III A path to the future **79**

8 Conclusion **80**
8.1 Benefits for GALILEO 80
8.2 Towards further related research 81

IV Appendixes **84**

A NeQuick details **85**
A.1 Variables and parameters 85
A.2 Version 1 (ITU-R) 86
A.3 Version 2 92

List of Figures **97**

List of Tables **98**

Bibliography **99**

Acronyms **106**

Chapter 1

Introduction

The first time I typed "Galileo Project" in Google, I was surprisingly directed to a website providing information on **Galileo Galilei**'s life and work[1].

This Italian scientist wrote and verified the basic law of falling bodies. He also built a telescope which he studied lunar craters with and discovered four moons revolving around Jupiter. He is maybe better known after his opposition to the Catholic Church about the Copernican heliocentric system which made him pronounce the famous words recalled in foreword of this study.

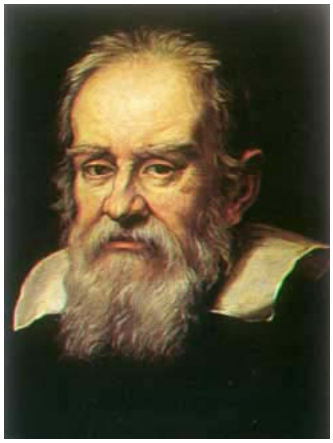

Figure 1.1: Galileo Galilei (1564 - 1642) - Original portrait by Justus Sustermans painted in 1636 [1]

[1] http://galileo.rice.edu

Of course I was looking for some information about the **GALILEO Project** in satellite navigation as I was going to spend three months working on it at ESTEC, in the Wave Interaction & Propagation section.

Apart from its obvious space related characteristic, I got involved into this field because of its following *features*:

- *gathering* - like every space project, it brings together lots of people with their own skills -,
- *topical* - first GALILEO satellite has been launched last December 28th -,
- *broad* - GALILEO is due to become a worldwide navigation system used for a lot of purposes -
- and *practical* - everyone can have a little idea of what my work will be useful for by thinking about personal car receivers for example.

Among the different concerns of the Wave Interaction & Propagation section, I focused on the *ionospheric effects on signals* dealing with the delay created by ionospheric electron content. This delay is crucial because of its relatively high value (up to $50m$) taking into account GALILEO's planned accuracy ($15m$ for single frequency users). It was the occasion for me to apply a major number of skills learnt during my studies: atmospheric physics and electromagnetism, numerical analysis and algorithmic, etc.

These explanations of my choices account somehow for the title worked out for my thesis and constitute a natural link to the first part **structure**, which includes guidelines allowing to understand my work and consider it in a global context. *GALILEO* signals are indeed intended to be used for navigation purpose like in other navigation satellite systems and they are submitted to different kinds of error sources (cf. chapter 2). In particular their *ionosphere* crossing plays a major role as above mentioned and is studied in the light of ionosphere properties described in chapter 3. In some situations, ionospheric *models* are needed e.g. for single frequency receivers (cf. chapter 4).

I studied one model into details, the one selected for GALILEO single frequency users which is called NeQuick. My work described in part II, consisted of a broad *analysis* of possible improvements (cf. chapter 5), the design of a *tool* allowing to show the relevance of proposed modifications (cf. chapter 6) and the demonstration of its use through different kinds of *tests* (cf. chapter 7).

Finally I completed the text with a set of **tools**. A joined *CD* contains the different programs and files cited throughout the document as well as a couple of documents included in the *bibliography* which constitutes the second tool. It gathers the references for each chapter. A list of acronyms is also provided at the end.

Part I

A few guidelines

Chapter 2

GALILEO as a GNSS

2.1 Navigation and GNSS

2.1.1 Fundamentals of satellite navigation

To drive a person between two locations, which is the goal of **navigation**, different tools exist. The most simple is a map on which the traveller can follow the road he wants to take. He had first to choose his way and, above all, he must know his position at any time. If he remains sufficiently careful, he knows where he is because he knows where he came from but, if he looses himself, he needs indications to find his way back. He would then be very interested in a device giving him directly his position, which is made possible through satellite navigation.

The most common concept used in this field is called **time of arrival** (TOA) ranging [11]: the propagation time t of a signal travelling from an emitter (in this case, a satellite) to a receiver is measured and multiplied by the speed of the signal (here, the speed of light $c \approx 3\ 10^8 m\ s^{-1}$) to obtain the emitter-to-receiver distance R called range.

$$R = t\ c \tag{2.1}$$

The receiver consequently stands on a sphere centred about the satellite. Using three satellites (**trilateration**) allows to locate the receiver on three spheres centred about the three satellites (cf. figure 2.1). The intersection gives the exact wanted position.

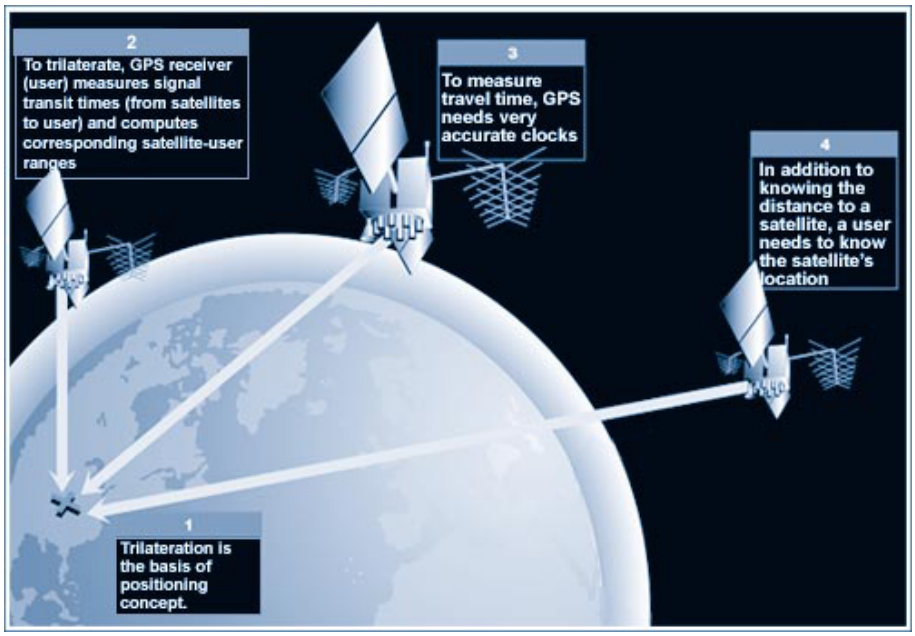

Figure 2.1: Satellite navigation principle [6]

This presupposes

- that the satellites positions, called ephemerides, are accurately known
- and that clocks on board the satellites and the receiver are synchronized.

To achieve this last goal, the satellites carry atomic clocks which are very well synchronized together and the TOA to a fourth satellite is measured by the receiver in order to determine its clock offset towards the satellites time base.

2.1.2 Several systems

Since more than forty years, satellite navigation developed through different systems [10].

The most important ones, providing a worldwide coverage, are the US NAVSTAR Global Positioning System (GPS) and the Russian Global Navigation Satellite System (GLONASS). They are referred to as Global Navigation Satellite Systems (**GNSS**) and will be joined by the European GALILEO Project.

To enhance their accuracy and offer more functionalities, augmentations were designed which can be either space-based, such as a geostationary satellite overlay service, or ground-based. Four of these systems are currently running or under development to supply a region of the world with local services and

to be interoperable: the US Wide Area Augmentation System (WAAS), the European Geostationary Navigation Overlay System (EGNOS) – the first step towards GALILEO –, the Japanese Multifunctional transport Satellite space-based Augmentation System (MSAS) and the Indian GPS and GEO Augmented Navigation system (GAGAN) which are called Satellite-Based Augmentation System (**SBAS**).

Finally some **other** local satellite systems which can use different techniques than TOA ranging can be mentioned: the Chinese BeiDou (Chinese name for Ursa Major constellation) system which uses two-way range measurements or the Japanese Quasi-Zenith Satellite System.

2.1.3 GPS

GPS constitutes undeniably the most known and used satellite navigation system. Its development by the GPS Joint Program Office (JPO ; [8]) began in the late sixties on the **basis** of several **military services** among which Transit.

It is a dual-use system as it presents two **services**.

1. The Precise Positioning Service (PPS) is designed for military and authorized users. With its two carrier frequencies (L1: 1575.42 MHz and L2: 1227.6 MHz), it provides a positioning accuracy[1] of $22m$.

2. The Standard Positioning Service (SPS) is designated for civil community. It uses only the L1 frequency and gives a positioning accuracy of $25m$ now that selective availability is turned off (cf. FAQ in [6]).

The latter is one of two **intentional errors** added for security concerns into the publicly available navigation signals.

1. *Selective Availability* (SA) consists of a satellite clock frequency manipulation resulting in the generation of the carrier waves and codes with varying wavelengths and errors in the description of the satellite orbit in the ephemeris data sent in the broadcast message. With SA imposed, the typical positioning error extends to about $100m$ but hopefully it was terminated on May 1, 2000.

2. The second to be mentioned is *Anti Spoofing* (AS) which alters GPS signals by changing the characteristics of the code.

[1] Throughout the chapter, the positioning accuracies are given 2 drms, 95%, horizontal. Twice the distance root mean square, 2 drms, is the radius of a circle containing at least 95% of all possible points obtained with the corresponding system at any one place. Beside this indicative number, other performance measures exist for navigation: timing accuracy, vertical accuracy, availability, continuity of service, integrity, etc.

The infrastructure dedicated to GPS is divided in three **segments**.

1. The *Space* segment (cf. figures 2.2 and 2.3) includes the 24 operational out of the 29 currently in orbit satellites of a MEO constellation [13]. They are located on six orbital planes at $20200km$ with 55° inclination and have a period of 12 hours.

2. The *Control* segment consists of six Monitor Stations (MSs: Hawaii, Kwajalein, Ascension Island, Diego Garcia, Colorado Springs, Cape Canaveral), three Ground Antennas (GAs: Ascension Island, Diego Garcia, Kwajalein) and a Master Control Station (MCS: Colorado Springs) [6]. The MSs check the orbit and clock of all satellites in view, accumulating data. This information is processed at the MCS to update each satellite's navigation message. Updated information is transmitted to each satellite via the GAs.

3. The *User* segment comprises the receivers that have been designed to decode the signals from the satellites for the purposes of determining position, velocity and time.

Figure 2.2: GPS satellite (Block IIA) (Credit: NASA)

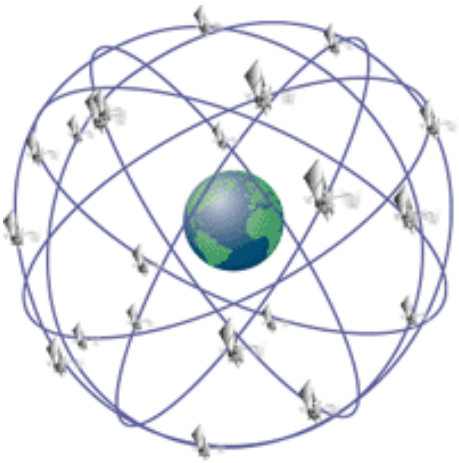

Figure 2.3: GPS constellation [6]

2.2 GALILEO

2.2.1 General characteristics

Unlike GPS, the European GALILEO system was originally designed for **civil** purposes [15]. It is due to enhance performance and availability by comparison with GPS but also to ensure *interoperability* with the US system. Furthermore it will include *integrity* information so the user have confident levels of the reliability of the position determination.

Five **services** will be available in the framework of GALILEO.

1. The *Open Service* (OS) will provide positioning, velocity and timing information accessible free of direct charges. Suitable for mass-market applications, its positioning accuracy will depend on its operation mode, $15m$ or $24m$ (depending on the frequency ; cf. section 3.3) in single frequency and $4m$ in dual frequency.

2. The *Commercial Service* (CS) will offer added value services on payment of a fee such as traffic information or map updates. With the same specification than OS, it will be managed by the GALILEO Operating Company (GOC).

3. The *Safety of Life* service (SoL) will be used for safety critical applications where lives could be endangered by unnoticed degradation of system performance such as maritime, aviation and rail. Its dual frequency use with the same above-mentioned accuracy will be combined with integrity monitoring and notification.

4. Reserved to government-authorized users requiring a higher level of protection, the *Public Regulated Service* (PRS) will also supply both single and dual frequency operations[2] with an integrity capability.

5. Finally GALILEO will support *Search and Rescue* activities (SAR) of the international COSPAS/SARSAT cooperative effort.

These services open a wide range of **applications**. For a total cost of 3.4 billion € , GALILEO is intended to create 100000 jobs and a market for equipment and services worth some 200 billion € per year till 2013. It will include transport, energy, finance, agriculture and fishing, personal navigation, emergency and crisis management, recreation, etc.

To reach these promising ambitions, the European Commission (EC) [5] and ESA [4] set up a particular company structure, the *GALILEO Joint Undertaking* (GJU) [9], which enabled to raise public and private funding in order to lead the **development** divided into three phases.

[2]The accuracy of the latter will be limited to $6.5m$.

1. The *Development and In-Orbit Validation* started in 2002 and currently reaches its peak. It includes the consolidation of mission requirements, the launch of the first experimental satellite GIOVE-A on December 28th, 2005, the development of three more satellites and ground-based components and, thanks to these four pioneering satellites, the validation of the system in orbit.

2. The *Deployment* will ensure the construction and launch of the remaining 26 satellites and the installation of the complete ground segment.

3. Finally the *Initial Service Provision* is waited for 2008 and will mark the beginning of Commercial Operations.

The latest step in this process consisted of the release on May 23rd, 2006 of the signal (SIS) characteristics.

2.2.2 Infrastructure

The navigation signals will be broadcast through three carrier **frequencies** (E5: 1191.795 MHz ; E6: 1278.95 MHz ; L1: 1575.42 MHz) by the satellites of the Space segment.

The infrastructure is indeed composed of three **segments** like GPS:

1. the *Space* segment (cf. figures 2.4 and 2.5) consisting of a MEO constellation of 27 (+3 spare) satellites on three orbital planes at 23222km with 56° inclination and period of 14 hours [3] ;

2. the *Ground* segment comprising two main systems known as the Ground Control Segment (GCS) and the Ground Mission Segment (GMS) i.e. 40 GALILEO Sensor Stations (GSSs) and Telemetry, Tracking and Command stations (TT&Cs) with role similar to MSs, 9 UpLink Stations (ULSs) with role similar to GAs, an interconnecting communication network, two GALILEO Control Centres (GCCs) with role similar to MCS (the GCS includes the TT&C stations and one GCC and the GMS, the rest) [7] ;

3. and the *User* segment including the receivers.

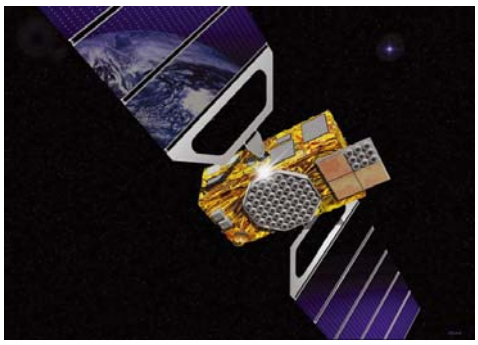

Figure 2.4: GALILEO satellite (Credit: ESA)

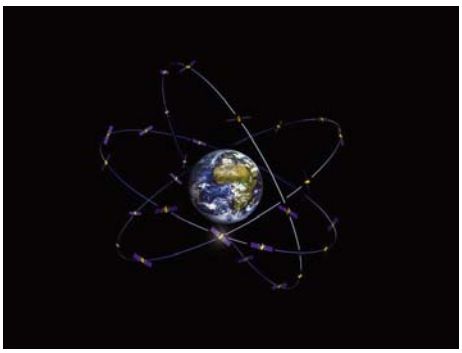

Figure 2.5: GALILEO constellation (Credit: ESA)

2.2.3 Comparison with GPS

Table 2.1 gives an indicative comparison between GPS and Galileo main features.

	GPS	GALILEO
Basic obedience	Military	Civilian
Number of services	2	5
Number of carrier frequencies	2	3
Horizontal accuracy for civilian users (SPS/OS) $[m]$	25	15
Number of available civil frequencies	1	3
Integrity	no	yes
Search and Rescue services	no	yes
Number of satellites (operational/in orbit)	24/29	27/30
Average altitude $[km]$	20200	23222
Number of orbital planes	6	3
Inclinations $[^\circ]$	55	56
Period [hours]	12	14
Ground stations (MS/GSS+TT&C)	6	45
Antennas (GA/ULS)	3	9
Control stations (MCS/GCC)	1	2

Table 2.1: Comparison between GPS and GALILEO

2.3 Positioning error

Among the effects affecting the performance of a navigation satellite system, some are directly related to the positioning error. They come from systems and atmospheric **issues** (cf. figure 2.6) which can be grouped as follows[12].

1. *Ephemeris* errors occur when the navigation message does not transmit the correct satellite location (cf. subsection 2.1.1).
2. The precision of the *clock* on board each satellite (cf. subsection 2.1.1) has to be taken into account.
3. The *ionosphere* constitutes a major source of error as signals are delayed by free electrons when they cross this atmospheric layer (cf. section 3.3).
4. The *troposphere* provokes also a delay depending on local temperature, pressure and humidity.
5. *Multipath* stands for parasite reflections in the environment of the receiver.
6. Finally the *receiver* itself causes error because of thermal noise, software accuracy and inter-channel biases.

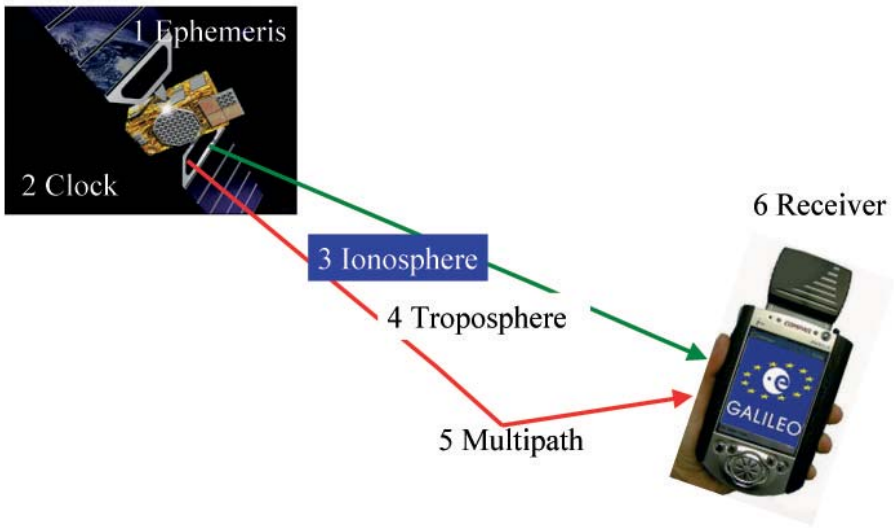

Figure 2.6: Different components of the positioning error

Getting back to the fundamentals of satellite navigation (cf. subsection 2.1.1) allows to understand better how positioning error is **computed** from the above mentioned effects. It is indeed divided into two steps.

1. First of all the impact of each effect on satellite-to-receiver range measurements is considered. The sum of these contributions constitutes a *ranging error* called the User Equivalent Range Error (UERE).

2. This number is multiplied by a *geometric factor*, the Dilution of Precision (DOP)[3] always greater than one, depending on the configuration of the satellites used by the receiver to calculate its position.

$$\epsilon = DOP * UERE \tag{2.2}$$

The different components of the UERE can be seen as **residual ranging errors** resulting from too simple modelling of each effect. Their orders of magnitude are given in table 2.2) which show clearly the need for a careful attention to ionosphere, the core of this study.

1. Ephemeris	$1-2m$
2. Clock	$1-2m$
3. Ionosphere	$cm-50m$
4. Troposphere	dm
5. Multipath	$1-2m$
6. Receiver	$0.3-2m$

Table 2.2: Different components of the residual positioning error [14]

[3]In fact different formulas exist involving different DOPs corresponding to different positioning errors (horizontal, vertical, etc.).

Chapter 3

Ionosphere as an atmospheric layer

3.1 Ionization and atmosphere

Between the satellites and the receiver, the navigation signals travel through the atmosphere, the layer of gases and dust surrounding the Earth: they are submitted to **atmospheric refraction** [28].

The properties of the atmosphere vary according to the height above Earth so that it can be **divided** into several layers (cf. figure 3.1). The most common division follows the evolution of temperature: in the troposphere up to about $15km$, it decreases ; it increases in the stratosphere which extends to $50km$; the mesosphere sees it going down again till $80km$; finally it rises in the thermosphere.

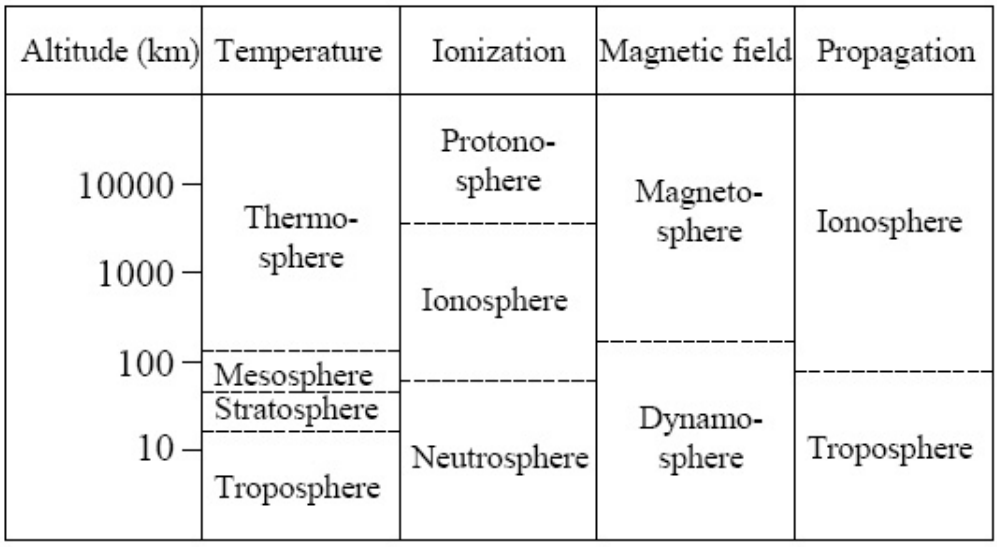

Figure 3.1: Possible subdivisions of the Earth's atmosphere [28]

For **propagation purpose**, the signal interaction with the atmosphere is considered, leading to two layers.

1. In the non-ionized part called *troposphere*, from the surface to $70km$, the propagation of radio waves depends on temperature, pressure and humidity.
2. In the ionized part called *ionosphere*, above $70km$, the free electrons affect the propagation.

3.2 Ionosphere

3.2.1 Vertical structure

To take into account the ionospheric effects on signal propagation, the characterization of the ionospheric electron density is important even if it reaches only a thousandth of neutral atmosphere at maximum. It originates in the action of the sun UV radiation on the atmospheric constituents so that its level results from a **compromise** between the ionization level increasing with height and the atmospheric constituents density decreasing with altitude giving birth to a schematic height profile represented in figure 3.2. The part below the peak is referred to as the bottomside (cf. figure 3.3) and the part above as the topside.

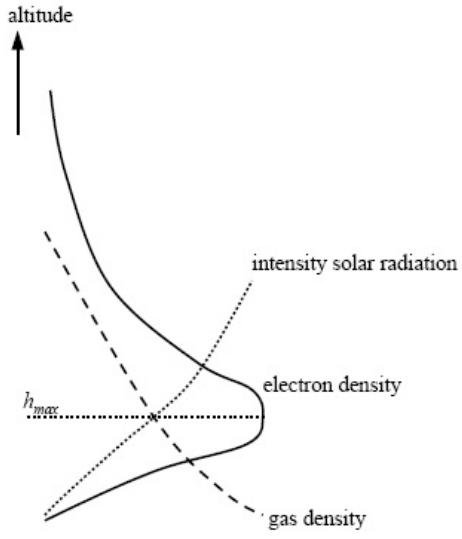

Figure 3.2: Global profile of electron density, gas density and intensity of solar radiation with altitude [28]

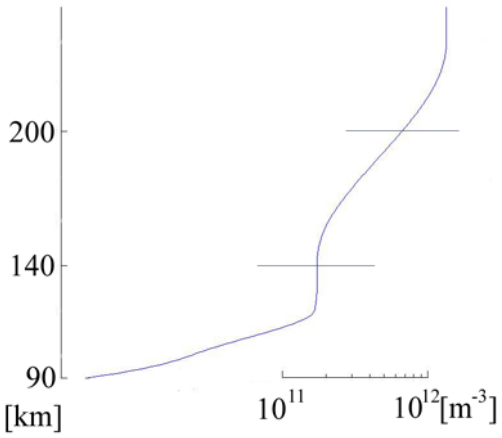

Figure 3.3: Typical bottomside vertical electron density profile

Having a deeper look to the shape of a typical profile, different horizontal **layers** are usually isolated (from ground to space) [22]:

1. the D layer which disappears at night by recombination between positive ions and electrons ;
2. the E layer, the first to have been studied by Appleton who gave it the name of the electric field, where the major ions are O_2^+ and NO^+ ;
3. the F_1 layer, composed mainly of O^+ ions, which goes up into the F_2 layer at night ;
4. the F_2 layer, the most dense one containing also mainly O^+ ions, which peaks at about $350km$;
5. and the *protonosphere* above $1000km$, constituted of H^+ ions according to its name.

Table 3.1 gives the orders of magnitude of height and electron densities of the three main ionospheric layers herein considered.

Layer	E	F_1	F_2
Height $[km]$	$90-140$	$140-200$	$200-\infty$
Daytime electron density $[el.\ m^{-3}]$	10^{11}	$5\ 10^{11}$	10^{12}
Nighttime electron density $[el.\ m^{-3}]$	$5\ 10^{9}$	–	10^{11}

Table 3.1: Horizontal layers in the ionosphere [28]

3.2.2 Variations

The shape of electron density profiles varies according to different influences [19] which could be understood considering the following simple **scheme**.

- Cause = sun
- Consequence = electron density
- Constraint = geomagnetic field

The **solar activity** influence conditions more or less the time evolution of the electron density profile. This intrinsic solar radiation but also the way it acts on the atmosphere follow cycles of different length, beginning with the shortest:

1. the *time-of-day* cycle, related to the solar radiation presence or absence resulting in higher or lower electron densities (cf. table 3.1) ;
2. the *season* cycle, related to the sun height above the horizon and the length of interaction path through the atmosphere giving birth to unexpected features such as the winter anomaly (larger peak electron density in winter than in summer) during the day at middle latitudes ;
3. and the 11-year *solar* cycle of the radiated energy for wavelength below 200 *nm* showing most of the time a linear relationship with electron densities.

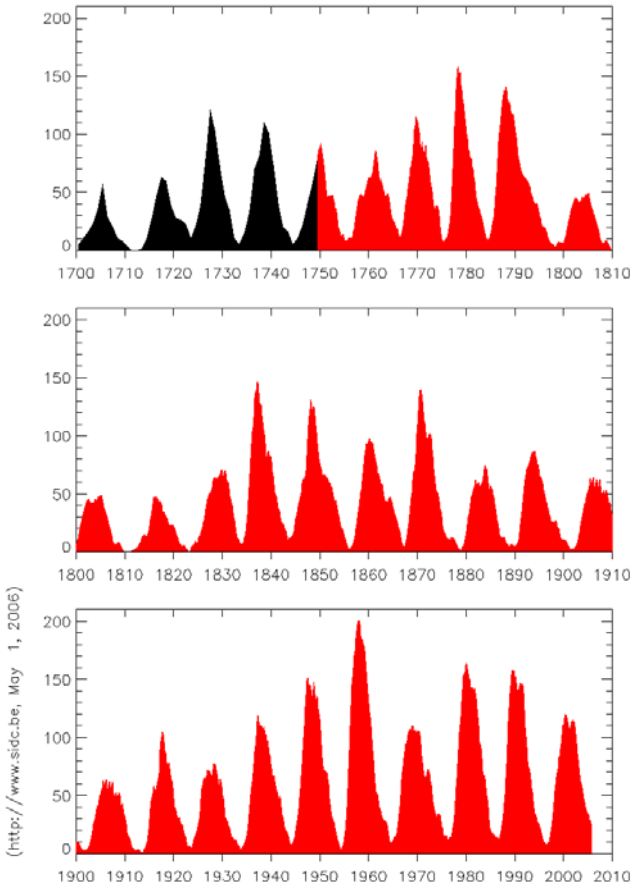

Figure 3.4: General behaviour of the sunspot number (Credit: SIDC, RWC Belgium, World Data Center for the Sunspot Index, Royal Observatory of Belgium)

The latter is usually described through two indices strongly related to each other [21],[16].

1. The *relative sunspot number* R, called the number of Wolf from the Swiss astronomer who introduced it in 1848, is based on the counting of cluster of sunspots (number g) and individual sunspots (number s).

$$R = k\ (10g + s) \tag{3.1}$$

   The factor k (usually lower than 1) depends on the observer and is intended to execute the conversion to the original scale. Figure 3.4 shows its evolution and highlights its main advantage of having been computed for more than 150 years. All this data is available from the Sunspot Index Data Center (SIDC) in Brussels [30].

2. The *solar radio noise flux* at $10.7cm$ wavelength $F10.7$ (corresponding to a frequency of 2800 MHz) is measured in $10^{-22}\ W\ m^{-2}\ Hz^{-1}$ and originates in the sun chromosphere. It has been recorded in Ottawa from 1947 and is available from the US National Geophysical Data Center (NGDC) [27].

Beside time conditions, space conditions are linked to the second influence from **geomagnetism**. The ionosphere follows the shape of the geomagnetic field and shows distinctive features such as the equatorial anomaly (cf. figure 3.5). Geomagnetic storms have also to be taken into account because they produce tremendous growth of the electron densities. They can be detected by means of the K-index, a quasi-logarithmic local index of the 3-hourly range in magnetic activity [16]. Planetary Kp values are available from the GeoForschungsZentrum in Potsdam [20]. They range between 0 and 9 and denotes a storm when they exceed 5.

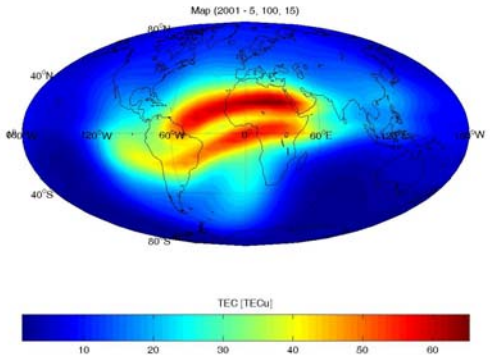

Figure 3.5: vTEC map example from NeQuick version 1 (ITU-R) (May, average solar flux – $\Phi = 100$ –, 15h universal time)

Figure 3.6 proposes a summary of the general ionospheric variations:

1. *position* into the geomagnetic field,
2. *season* related to the level of ionization from the sun,
3. *solar activity* defining the power of ionization
4. and *time-of-day* linked to the presence of the source of ionization.

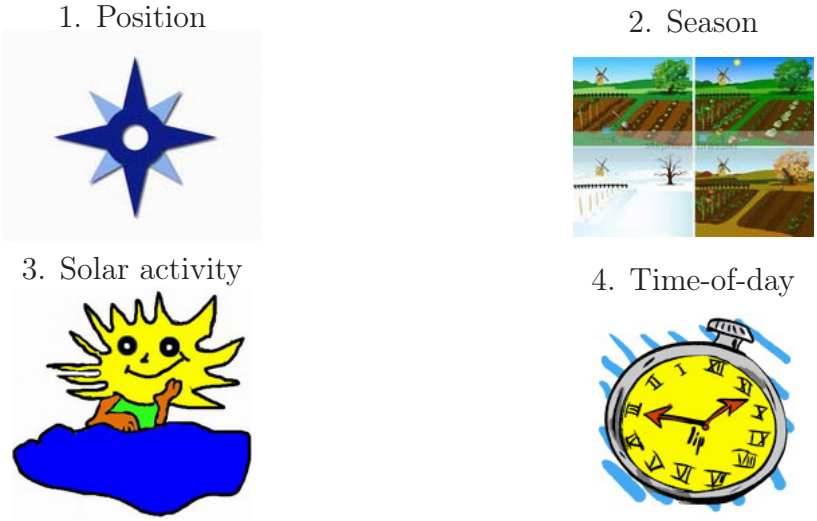

Figure 3.6: General ionospheric variations

3.2.3 Description

In order to describe the shape of the electron density profiles, tools called **ionosonde parameters**, including critical frequencies and transmission factors, are used taking into account the above-mentioned variations. Some considerations about wave propagation through the ionosphere allow to understand their *meaning* [29].

As ionosphere is a dispersive medium, the behaviour of a ray refracting in an ionospheric layer L[1] depends on its frequency f and its initial elevation angle $\frac{\pi}{2} - a_T$ (cf. figure 3.7). It can

- be reflected and come back to the Earth at a certain distance from its emission place known as "sender" (low frequencies ; low elevation angles) ;
- or cross the ionosphere (high frequencies ; high elevation angles).

[1]This general discussion can be applied to the layers of our interest. L stands then for the layer index which possible values are E, F_1 and F_2.

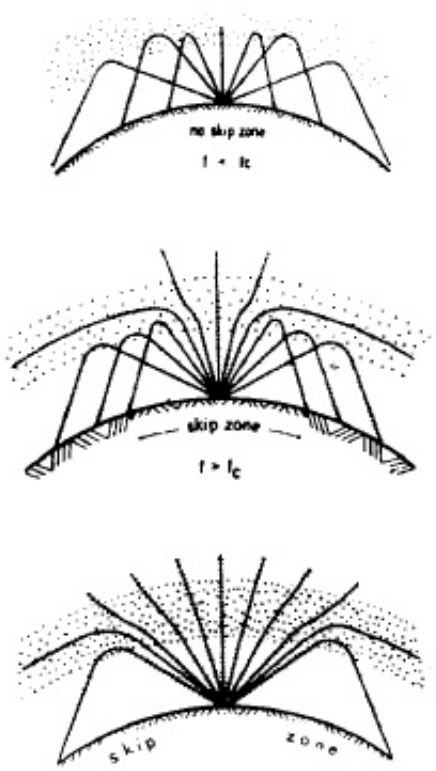

Figure 3.7: Ray geometry (sender on Earth) for different frequencies [29]

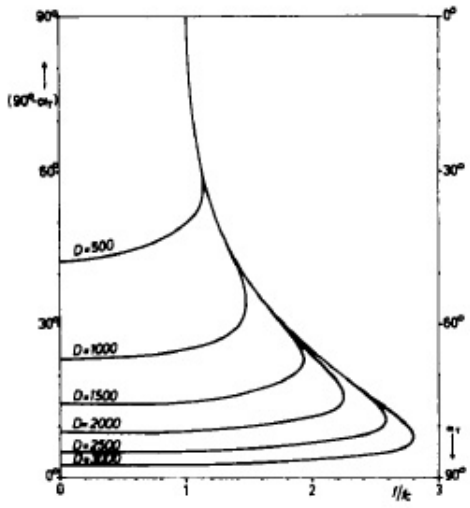

Figure 3.8: Elevation angle $\frac{\pi}{2} - a_T$ as a function of f/f_0 - Distance as parameter [29]

Below a certain frequency (first situation in figure 3.7), called the *critical frequency* f_0L $[MHz]$, the ray cannot cross the ionosphere for any elevation angle. The layer is somehow dense enough to reflect the ray in all situations – for vertical incidence in particular – so that the critical frequency is linked to the maximum electron density NmL $[10^{11}\ el.\ m^{-3}]$[2] of the layer [18].

$$NmL = 0.124\ f_0L^2 \tag{3.2}$$

Above that frequency (other situations in figure 3.7), a zone around the sender, called "skip zone", exists which cannot be reached by reflection. In other words, at a fixed frequency greater than the critical frequency corresponds a minimum distance of reception. If the latter is now fixed, the corresponding maximum frequency is defined as the maximal usable frequency MUF (cf. figure 3.8).

[2]These units are preferred regarding the characteristic orders of magnitude of electron densities in table 3.1.

Considering the F_2 layer, the standard $MUF(3000)F_2$ is obtained for a distance of $3000km$. The *transmission factor* $M(3000)F_2$ comes then from the division of $MUF(3000)F_2$ by f_0F_2 and is linked to the height $h_{max}^{F_2}$ where the electron density reaches its maximum value, called the layer peak (cf. equation A.8).

The **general variations of the ionosphere** are described through so-called "maps" i.e. their values are calculated on the basis of measured data – from vertical incidence soundings at a certain number of ground stations all over the world – by means of empirical equations (cf. appendix A.2 for the ionospheric model used in this study). The most common maps allow to compute monthly medians, describing well the evolution during a day but showing no difference from day to day during the same month.

f_0E and f_0F_1 appear to be closely correlated so that, in the ionospheric model used in this study, f_0F_1 is calculated from f_0E (cf. equations A.19 and A.20). They depend in general

- on *solar activity* through the monthly solar radio flux at $10.7cm$ wavelength Φ $[10^{-22}\ W\ m^{-2}\ Hz^{-1}]$;
- and on *position, season and time-of-day* through the cosine of the zenith angle of the sun χ $[^\circ]$.[3]

The nighttime behaviour of the F_1 layer is also taken into account by equalling f_0F_1 to 0 during the night.

The treatment of f_0F_2 and $M(3000)F_2$, which are related to the main ionospheric layer F_2, is more complex regarding their more complicated variations towards time and latitude [29]. They are generated by means of numerical maps

- based on monthly sets of coefficients defining the map – the most common sets were released by the CCIR in 1967 and define the so-called "CCIR maps" ;
- and consisting in a Fourier time series (cf. equation A.21) where the two big influences described in subsection 3.2.2 can be highlighted.

The *seasonal* variation is obvious regarding the definition of the CCIR maps – one for each month.

[3] In the particular case mentioned, a last dependence on *position and season* can be noticed through the latitude ϕ and the month used to define the weighting coefficient a_E.

The *solar influence* appears in the very first combination of the basic coefficients according to the most of the time linear relationship with solar activity (cf. subsection 3.2.2). To represent the latter, the appropriate parameter was found to be the monthly smoothed sunspot number R_{12} (cf. figure 3.9) defined as follows [23].

$$R_{12} = \frac{1}{12}\left[\frac{R_{n-6}}{2} + \sum_{k=n-5}^{n+5} R_k + \frac{R_{n+6}}{2}\right] \tag{3.3}$$

R_k is the mean of the daily sunspot numbers for a single month k.

R_{12} is the smoothed index for the month represented by $k = n$.

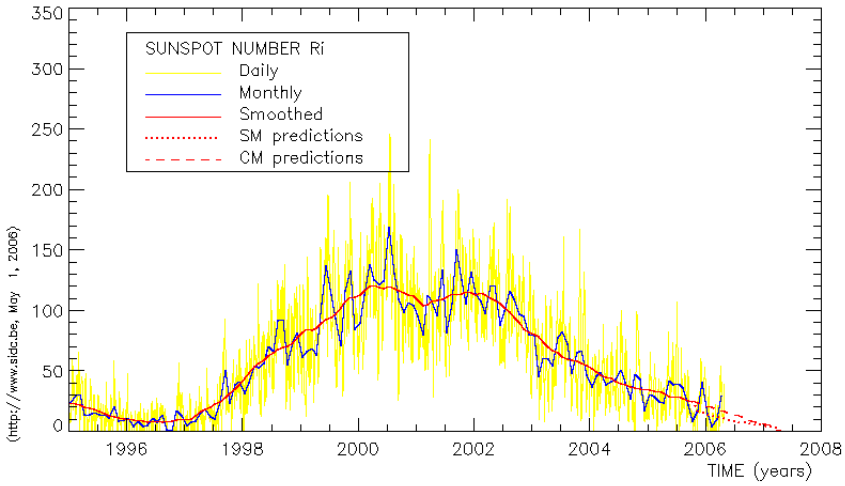

Figure 3.9: Comparison between sunspot numbers (Credit: SIDC, RWC Belgium, World Data Center for the Sunspot Index, Royal Observatory of Belgium)

R_{12} can be converted to monthly smoothed solar flux Φ_{12} (cf. figure 3.10) which estimates Φ with a good agreement to compute f_0E or f_0F_1.

$$\Phi_{12} = 63.7 + 0.728\ R_{12} + 8.9\ 10^{-4}\ R_{12}^2 \tag{3.4}$$

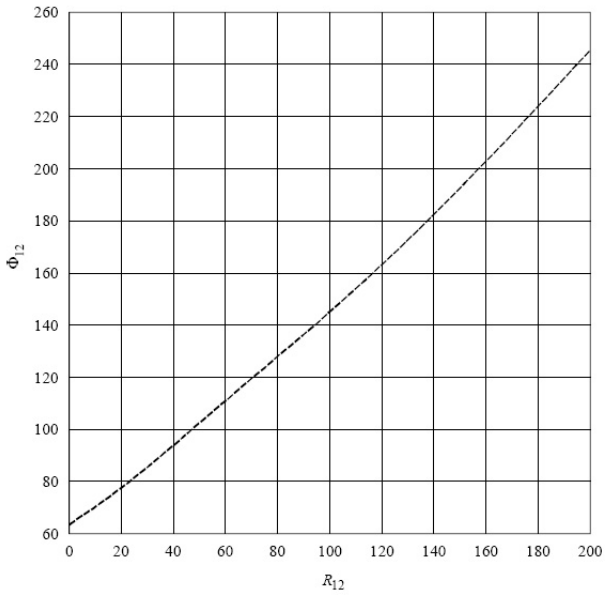

Figure 3.10: Relationship between R_{12} and Φ_{12} [23]

The basic coefficients, which can be grouped by two, one for low solar activity associated at $R_{12} = 0$ and the other for high solar activity associated at $R_{12} = 100$, are combined linearly following the current value of R_{12} (cf. equation A.22). For the highest solar activity conditions, the dependence on solar activity is not linear any more so that it is recommended to clamp R_{12} (resp. Φ_{12}) at 150 (resp. 193) [25]. Typical values of solar indices are given in table 3.2.

Solar activity	R_{12}	Φ_{12}
Low	0	63.7
Average	50	100
High	100	150
Highest	150	193

Table 3.2: Typical values of solar indices

f_0F_2 and $M(3000)F_2$ are also related to the *time* variation as the coefficients resulting from the above described combination are multiplied just after by the appropriate trigonometric function of the universal time UT.

The geographic coordinate functions G_k constitutes the last tool to be considered (cf. equation A.23). It shows the influence of

- *position* through latitude ϕ [°] and longitude θ [°]
- and the *geomagnetic field* through a new parameter, the modified dip latitude (MODIP) μ [°] defined in equation 3.5.

$$\tan \mu = \frac{I}{\sqrt{\cos \phi}} \tag{3.5}$$

I [°] denotes the geomagnetic dip.

ϕ [°] denotes the geographic latitude.

It was first used by RAWER in [29] to build a continuous, physically consistent description of MUF. It was indeed necessary to consider a physical system of interpolation between the spots of data given by the inhomogeneous station's network in order to represent correctly features such as the equatorial anomaly (cf. figure 3.5) even over oceans. Figure 3.11 shows the similarity with the shape of the magnetic field.

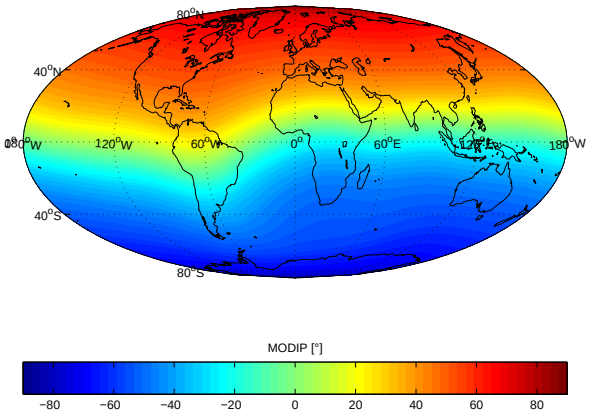

Figure 3.11: Shape of μ

In parallel with figure 3.6, table 3.3 summarizes the main variables used to describe the general variations of the ionospheric electron density profile.

1. Position ϕ [°], θ [°], μ [°]	2. Season month
3. Solar activity Φ_{12} [10^{-22} W m^{-2} Hz^{-1}], R_{12}	4. Time-of-day UT [hours]

Table 3.3: Main variables for general ionospheric variations

3.3 Ionospheric error

After the physical discussion introducing the tools used to describe ionosphere, a short mathematical development will link propagation issues to positioning error (cf. section 2.3). When a wave is submitted to atmospheric refraction (cf. section 3.1), it interacts with the particles of the atmosphere so that its velocity[4] v $[m\ s^{-1}]$ becomes lower than the speed of light c $[m\ s^{-1}]$. Their ratio is defined as the **refractive index** n which depends on the electron density N $[10^{11}\ el.\ m^{-3}]$ and the frequency f $[MHz]$ as ionosphere is dispersive [17] [5].

The commonly used first order approximation is given by the following equation.

$$\begin{aligned} n = \frac{c}{v} &= 1 + \frac{1}{2}\frac{f_p^2}{f^2} \\ f_p &= \sqrt{10\ A\ N} \\ A = \frac{e^2}{4\pi^2 m_e \epsilon_0} &\approx 80.6 m^3 s^{-2} \end{aligned} \tag{3.6}$$

f_p $[MHz]$ denotes the electron plasma frequency.

$e = 1.60218\ 10^{-19} C$ denotes the electron charge.

$m_e = 9.10939\ 10^{-31} kg$ denotes the electron mass.

$\epsilon_0 = 8.85419\ 10^{-12} F\ m^{-1}$ denotes the permittivity of free space.

The **measured range** s $[m]$ between two points – herein a satellite and a receiver – can be simplified as the result of the integration of a time element along the ray path, giving the propagation time longer than in vacuum, and the multiplication by the speed of light c.

$$\begin{aligned} s &= c \int_{sat.}^{rec.} dt = c \int_{sat.}^{rec.} \frac{ds}{v} \\ &= \int_{sat.}^{rec.} n\ ds = \int_{sat.}^{rec.} 1 + \frac{10\ A\ N}{2\ f^2}\ ds \\ &= \int_{sat.}^{rec.} ds + \frac{5\ A}{f^2} \int_{sat.}^{rec.} N\ ds \end{aligned} \tag{3.7}$$

[4] This development is intentionally limited to group – as opposed to phase – characteristics as the ionospheric residual error introduced in section 2.3 is linked to the group delay.

[5] [26] gives a complete description of ionospheric effects on GPS. The following discussion is limited to the purpose of this study.

The first integral can be approximated to the geometric range and the second integral, related by difference to the ionospheric delay, is defined as the **total electron content** (TEC), sTEC for a slant ray, vTEC for a vertical ray. The relation between TEC and the ionospheric range error $\Delta s[m]$ depends then on the frequency in the following way (TEC in $TECu = 10^{16}\ el.m^{-2}$ and f in MHz) [2].

$$\Delta s = 40.3\ 10^4\ \frac{TEC}{f^2} \tag{3.8}$$

For L1 (1575.42 MHz), 1 $TECu$ corresponds approximately to an error of 0.16 m.

Equation 3.8 underlines the need of an **accurate knowledge** of TEC which can be obtained thanks to different techniques.

1. Taking advantage of the dispersive property of ionosphere, *dual frequency* receivers use two frequencies to measure two ionospheric delays corresponding to the same TEC which is determined by subtracting the time forms of equation 3.8 for these two frequencies from each other.

$$\Delta s_2 - \Delta s_1 = 40.3\ 10^4\ TEC \left(\frac{1}{f_2^2} - \frac{1}{f_1^2}\right)$$
$$\Rightarrow TEC = 10^{-4} \frac{c\ (\Delta t_2 - \Delta t_1)}{40.3} \frac{f_1^2 f_2^2}{f_1^2 - f_2^2} \tag{3.9}$$

2. For *single frequency* users, TEC has to be modelled using the tools described in subsection 3.2.3.

Chapter 4

NeQuick as an ionospheric model

4.1 Ionospheric models

4.1.1 Common points

The ionospheric models described in this section own several common characteristics.

1. They are **empirical** models based on measured data.
2. They use **CCIR numerical maps** described in subsection 3.2.3.
3. They consist in combinations of **analytical profiles** for different height intervals.

4.1.2 International Reference Ionosphere (IRI)

The International Reference Ionosphere (IRI) constitutes the first model to be described for it is the **most accurate and** the **most known** one [46]. This international project was originally created in the late sixties by a Working Group formed by COSPAR and URSI to build an empirical standard model of the ionosphere, based on all available data sources. Yearly updates are performed during special IRI Workshops.

For given location, time and date, IRI **generates** profiles of electron density, electron temperature, ion temperature and ion composition in the altitude range from about $50km$ to about $2000km$ as well as the electron content. It provides monthly averages in the non-auroral ionosphere for magnetically quiet conditions and is divided into 6 layers.

It takes advantage of several **data sources** among which the worldwide network of ionosondes, the powerful incoherent scatter radars (Jicamarca, Arecibo, Millstone Hill, Malvern, St. Santin), the ISIS and Alouette topside sounders and in situ instruments on several satellites and rockets.

Figure 4.1 shows the level of details obtained with IRI for a worldwide vTEC map but, for our purpose – satellites at altitudes higher than $20000km$ –, the $2000km$ **limit** is not suitable.

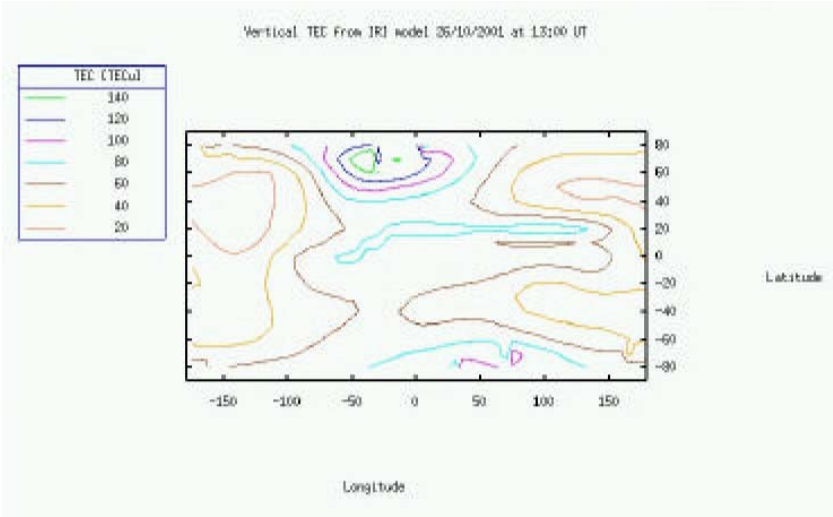

Figure 4.1: IRI vTEC map example [51]

4.1.3 Bent

The original Bent model was created in 1972 to describe the ionospheric **electron density** as a function of latitude, longitude, time, season, and solar radio flux [46]. It is divided in 5 layers using parabolas and exponential profiles.

The model is based on less **data sources** than IRI: about 50,000 Alouette topside ionograms (1962-1966), 6,000 Ariel 3 in situ measurements (1967-1968), and 400,000 bottomside ionograms (1962-1969).

As it is **simpler** than IRI (cf. figure 4.2) – for example, it does not include the lower layers (D, E, F_1) –, it shows worst results but it has also the advantage of higher computational speed so that it has been chosen as basis for GPS Klobuchar single-frequency algorithm in 1987 ([40]).

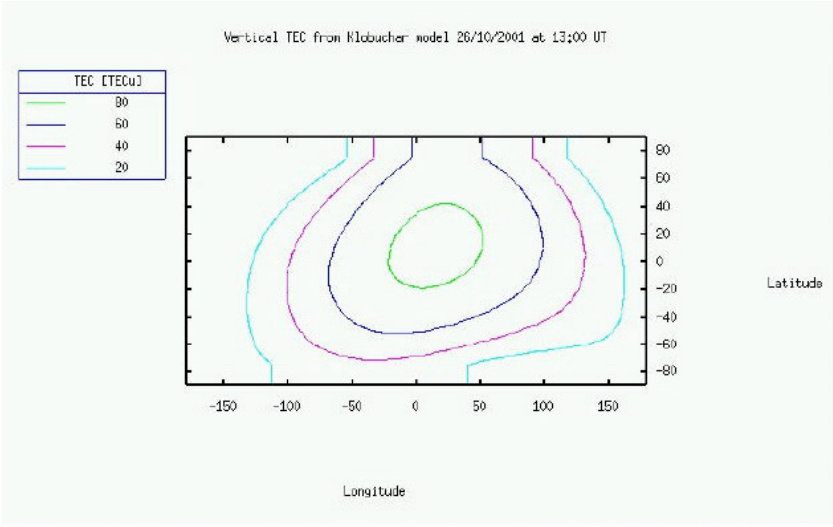

Figure 4.2: KLOBUCHAR vTEC map example [51]

This **algorithm** installed in the receiver uses height broadcast coefficients from the navigation message to compute vTEC which is then multiplied by an obliquity factor at the mean ionospheric height ($350km$) to obtain sTEC (cf. figure 4.3). It assumes a thin layer spherically stratified ionosphere and provides a 50% RMS correction of the ionospheric time-delay.

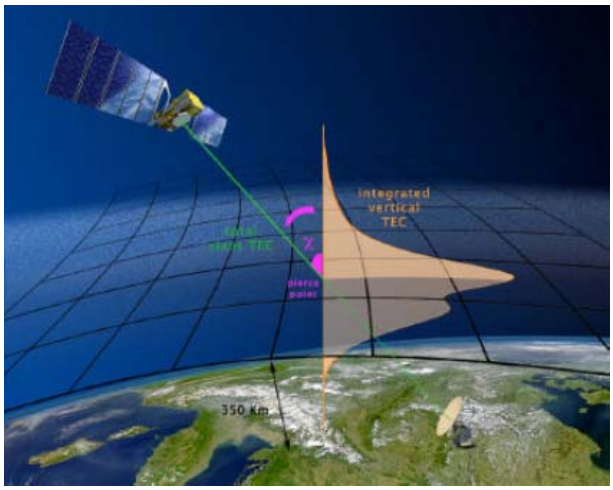

Figure 4.3: KLOBUCHAR algorithm scheme [51]

4.1.4 DGR family

In 1990, Di Giovanni and Radicella, two Italian scientists, proposed a new method based on **Epstein layers** to calculate the electron density in the ionosphere (cf. section 4.2).

This so-called DGR "profiler" concept, using the peaks of the E, F_1 and F_2 layers as anchor points, gave birth in the following decade to **three models** [37] which differ in their representation of the topside i.e. the region above the F_2-layer peak. Depending on the latter complexity and computational time required, they are used for different applications.

1. The simplest model using no additional parameter was called *NeQuick* and suits ionospheric applications. It has been adopted by the ITU-R recommendation for TEC modelling (cf. figure 4.4).

2. By taking into account the change of gradients in the topside profile associates to the $O^+ - H^+$ transition, *COSTprof* is preferred for ionospheric and plasmaspheric satellite to ground applications such as the electron density distribution model of the COST 251 action.

3. Finally *NeUoG-plas* presents the most precise plasmasphere description using a magnetic field aligned formulation for an H^+ diffusive equilibrium above 2000 km. Therefore it takes place in assessment studies involving satellite to satellite propagation of radio waves.

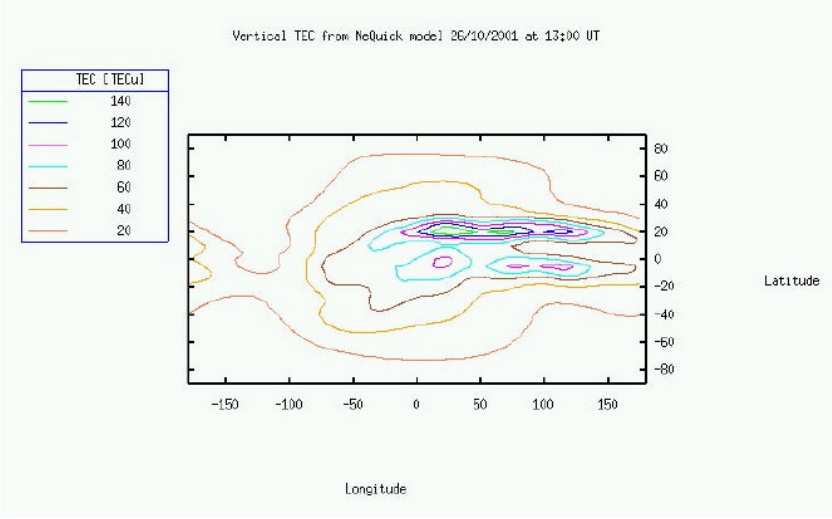

Figure 4.4: NeQuick vTEC map example [51]

Thanks to its computational speed where its name comes from, NeQuick was chosen for the calculation of **ionospheric UERE contribution** for EGNOS and GALILEO so that it constitutes the very basis of our concerns (cf.

section 4.3). Unlike Klobuchar algorithm, NeQuick is used along the ray path to generate electron densities which are then integrated to obtain sTEC (cf. figure 4.5). It represents then a 3D ionosphere and is intended to provide a 75% or better RMS correction of the ionospheric time-delay.

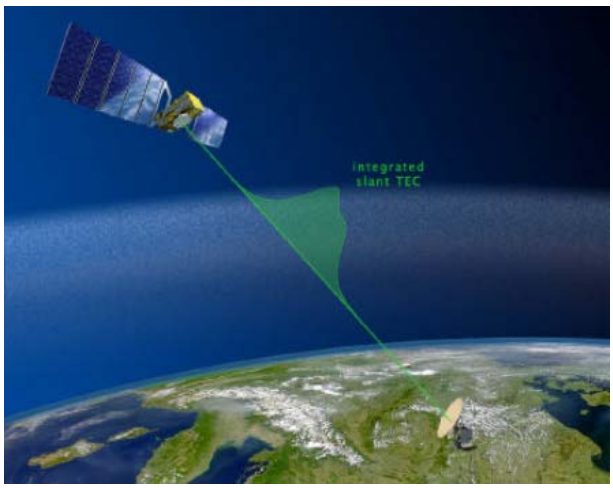

Figure 4.5: NeQuick algorithm scheme [51]

4.2 DGR "profiler" concept

4.2.1 Principle

The DGR models show a **common bottomside** description: up to the F_2-layer peak, they consist of a sum of Epstein layers [35]. One of the topside treatments (NeQuick) is further discussed in subsection 4.3.1.

The shape of an Epstein layer representing the electron density $N(h)$ [10^{11} $el.\ m^{-3}$][1] is given by the following function [53].

$$N(h) = 4\ N_{max}\ \frac{e^{\frac{h-h_{max}}{B}}}{(1+e^{\frac{h-h_{max}}{B}})^2} \tag{4.1}$$

N_{max} [10^{11} $el.\ m^{-3}$] denotes the peak amplitude.

h_{max} [km] denotes the height of the peak.

B [km] denotes the thickness parameter [2].

[1] These units are preferred regarding the characteristic orders of magnitude of electron densities in table 3.1.

[2] We can find an interesting interpretation of B by calculating the surface under the curve

The following graphs give a good idea of the variation of the curve as a function of each parameter.

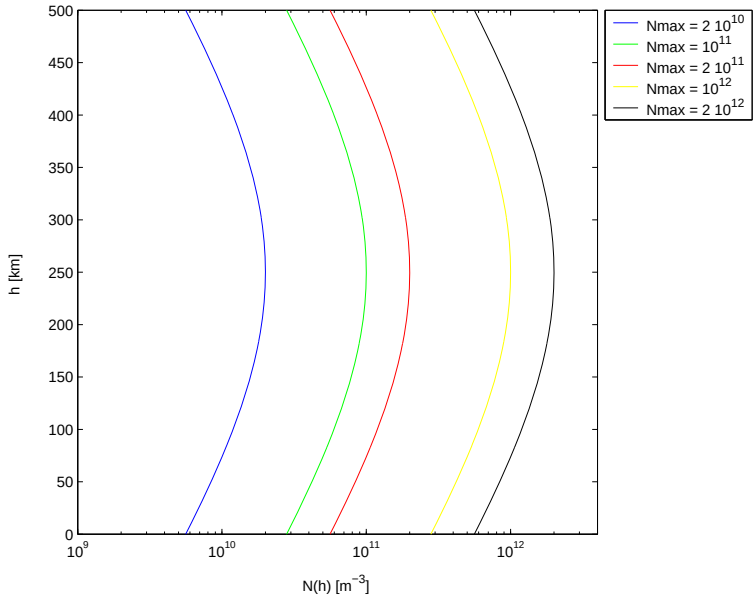

Figure 4.6: Peak amplitude N_{max} sensibility

as follows by posing $x = e^{\frac{h-h_{max}}{B}}$.

$$\begin{aligned} C &= \int_{-\infty}^{+\infty} 4\ N_{max}\ \frac{e^{\frac{h-h_{max}}{B}}}{(1+e^{\frac{h-h_{max}}{B}})^2} dh \\ &= 4\ N_{max} \int_0^{+\infty} \frac{B}{(1+x)^2} dx \\ &= 4\ N_{max}\ B \left[\frac{-1}{1+x}\right]_0^{+\infty} \\ &= 4\ N_{max}\ B \end{aligned} \tag{4.2}$$

$4B$ and N_{max} are then the edge of a rectangle with same surface.

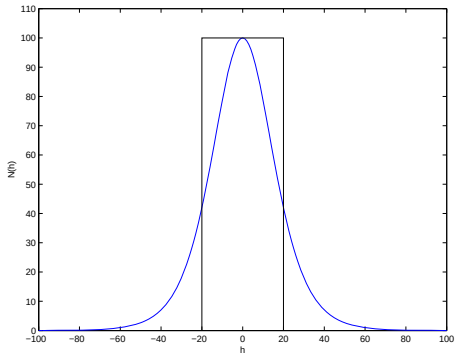

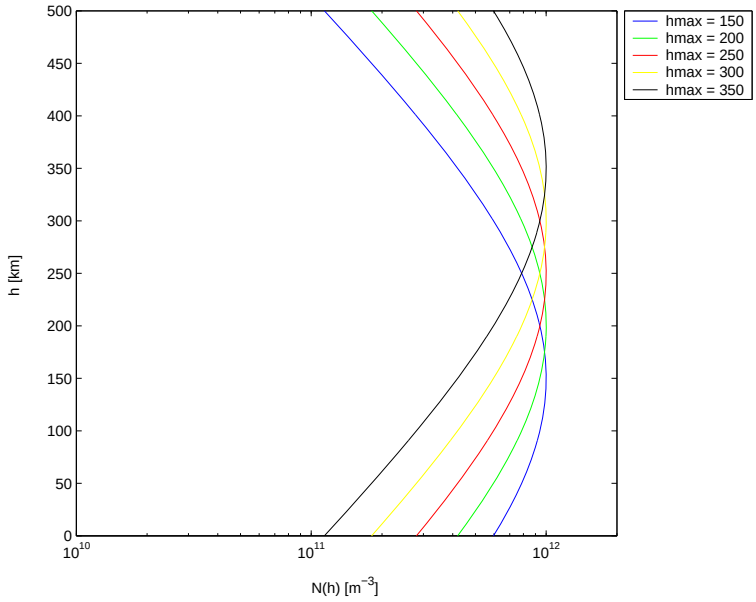

Figure 4.7: Peak height h_{max} sensibility

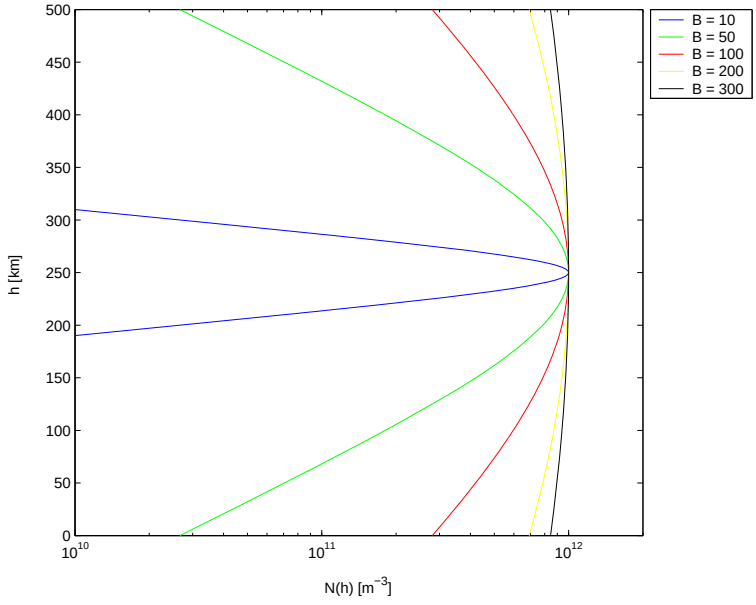

Figure 4.8: Thickness parameter B sensibility

To model the electron density of ionosphere, the best agreement was found by **dividing each layer** - E, F_1 and F_2 with corresponding peak characteristics N_{max}^L and h_{max}^L [3] - into its lower and its upper part by using two different

[3] Throughout this section, L stands for the layer index which possible values are E, F_1 and F_2.

thickness parameters, respectively B^L_{bot} and B^L_{top} [48]. The parameters determination is detailed in subsection 4.2.2.

Depending on the current height, bottom or top layers are chosen and the electron density results from the sum of the three components as follows.

$$\begin{aligned} N(h) &= \sum_L N^L(h) \\ &= \sum_L 4\ N^L_{max}\ \frac{e^{\frac{h-h^L_{max}}{B^L}}}{(1+e^{\frac{h-h^L_{max}}{B^L}})^2} \end{aligned} \tag{4.3}$$

Figure 4.9 shows the **shape** of the five components and their sum for characteristic values of the Epstein parameters in table 4.1.

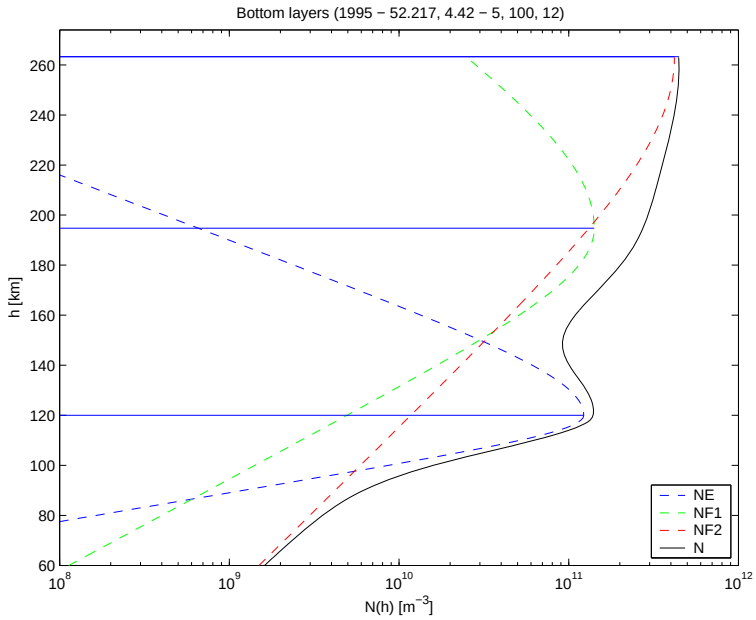

Figure 4.9: Bottomside profile example (ESTEC location – $52.217^{\circ}N,\ 4.42^{\circ}E$ –, May, average solar flux – $\Phi_{12} = 100$ –, midday universal time)

	E	F_1	F_2
N^L_{max} $[10^{11}\ el.\ m^3]$	1.23	1.42	4.2
h^L_{max} $[km]$	120	195	263
B^L_{bot} $[km]$	5	15.8	29
B^L_{top} $[km]$	11.3	22.6	

Table 4.1: Epstein parameters corresponding to figure 4.9

4.2.2 Parameters determination from input data

The Epstein parameters introduced in the previous subsection can be seen as intermediate parameters between the final profile and the input data based on measurements i.e. the ionosonde parameters, the critical frequencies f_0L and the transmission factor $M(3000)F_2$, described in subsection 3.2.3.

The **peak amplitudes** N^L_{max} are derived from the global electron densities at the peak height of layer L NmL [10^{11} $el.$ m^3] [48]

- neglecting the E layer when considering the F_1 and F_2 layers
- and assuming the amplitude of the F_1 layer at the F_2 peak.

$$\begin{aligned} N^E_{max} &= N(h^E_{max}) - N^{F_1}(h^E_{max}) - N^{F_2}(h^E_{max}) \\ &= NmE - N^{F_1}(h^E_{max}) - N^{F_2}(h^E_{max}) \end{aligned} \tag{4.4}$$

$$\begin{aligned} N^{F_1}_{max} &= N(h^{F_1}_{max}) - N^E(h^{F_1}_{max}) - N^{F_2}(h^{F_1}_{max}) \\ &= NmF_1 - N^{F_2}(h^{F_1}_{max}) \end{aligned} \tag{4.5}$$

$$\begin{aligned} N^{F_2}_{max} &= N(h^{F_2}_{max}) - N^E(h^{F_2}_{max}) - N^{F_1}(h^{F_2}_{max}) \\ &= NmF_2 - N^{F_1}(h^{F_2}_{max}) \\ &= NmF_2 - 0.1\ NmF_1 \end{aligned} \tag{4.6}$$

The global electron densities at the peak height of layer L NmL are calculated from the critical frequencies f_0L by means of equation 3.2 (e.g. table 4.2).

The **peak heights** are defined through more complicated empirical equations apart from h^E_{max} which is fixed at $120km$ (cf. equation A.8 to A.10). $h^{F_1}_{max}$ depends on NmF_1 and the magnetic dip I where $h^{F_2}_{max}$ is described by means of the ratio f_0F_2/f_0E and the transmission factor $M(3000)F_2$.

Finally the main **thickness parameters** are $B^{F_2}_{bot}$ and $B^{F_1}_{top}$ as the others are based on the latter or fixed at a certain value (cf. equations A.11 to A.18). $B^{F_2}_{bot}$ is calculated from NmF_2 and $(dN/dh)_{max}$, the gradient of $N(h)$ at the characteristic point at the base of the F_2 layer i.e. the first derivative of equation 4.1 for F_2 layer at the inflection point. $B^{F_1}_{top}$ is obtained from equation 4.1 and the same assumption as in equation 4.6.

Table 4.1 gives an example of the values of the Epstein parameters and lets guess the relation between $B^{F_1}_{top}$ and $B^{F_1}_{bot}$ (multiply by 0.7) and B^E_{top} (one half when F_1 is present) and the constant value of B^E_{bot} ($5km$).

Table 4.2 contains the **ionosonde parameters** corresponding to the example in figure 4.9. The critical frequencies logically grows with the height of the corresponding layers. These values are computed by means of equations

A.19 to A.23 for the specified situation using the CCIR maps as explained in subsection 3.2.3.

	E	F_1	F_2	$M(3000)F_2$
f_0L $[MHz]$	3.35	4.69	6	2.94
NmL $[10^{11}$ $el.$ $m^3]$	1.39	2.73	4.46	

Table 4.2: Ionosonde parameters and peak height electron densities corresponding to figure 4.9

4.2.3 Evolution

As mentioned in subsection 4.1.4, the DGR approach using **three Epstein layers** – one for each ionospheric layer – was first proposed in 1990 [35]. It was then improved in 1995 (cf. subsection 4.2.1) by dividing each layer into its top and bottomside leading to a bottomside formulation constituted of **five** so-called **semi-Epstein layers**.

Further improvements were obtained around 1999 from two main modifications [42].

1. The **lowest part** (below $100km$) was replaced by the bottomside of a **Chapman layer** (cf. equation 4.7 for the principle and A.1 for final version).

$$N(h) = N_0\, e^{1-\, b\frac{h-h_0}{H_0}\, -\, e^{-\frac{h-h_0}{H_0}}} \qquad (4.7)$$
$$b = 1 - \left[\frac{1}{N(h)}\frac{dN}{dh}(h)\right]_{h=h_0}$$

   $h_0 = 100km$

   N_0 $[10^{11}$ $el.$ $m^{-3}]$ denotes the electron density at $h = h_0$.

   $H_0 = 10km$

2. A **fading out effect** was added to the E and F_1 layers **in the vicinity of the F_2 layer peak** to ensure that the electron density at the F_2 layer peak corresponds exactly to f_0F_2 providing the direct calculation of $N_{max}^{F_2}$ from f_0F_2 by means of formula 3.2. Equation 4.6 was then replaced by the following equation.

$$N_{max}^{F_2} = 0.124\ (f_0F_2)^2$$

   To implement this effect, the arguments of the exponential functions corresponding to E and F_1 in equation 4.3 were multiplied by a coefficient $\zeta(h) = e^{\frac{10}{1+2|h-h_{max}^{F_2}|}}$. The resulting equations are presented in section A.2.

Figure 4.10 shows the resulting profile for the same conditions as figure 4.9.

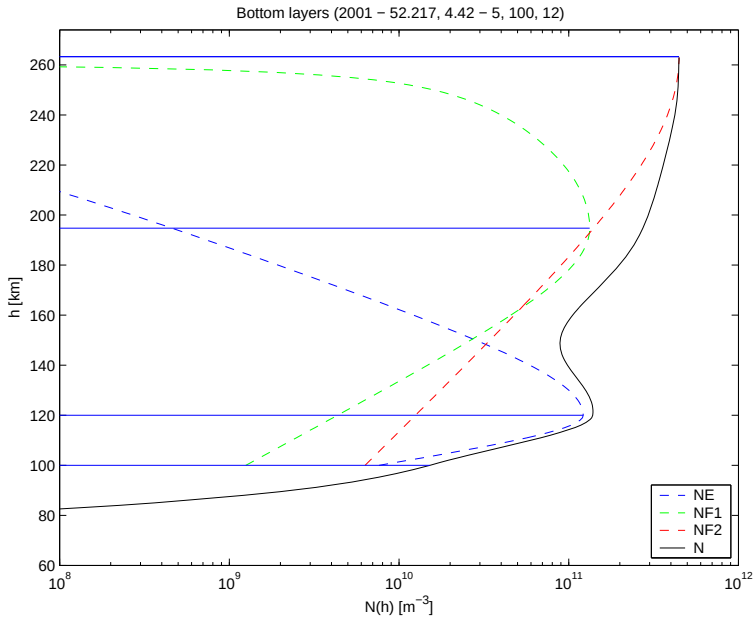

Figure 4.10: Bottomside profile example from NeQuick version 1 (ITU-R) (ESTEC location – $52.217^{\circ}N$, $4.42^{\circ}E$ –, May, average solar flux – $\Phi_{12} = 100$ –, midday universal time)

[49] explains this overall evolution and extends it to the **topside** which allows to differentiate between the models of the DGR family (cf. subsection 4.1.4). It was consequently not presented in this general overview of the DGR "profilers" and constitutes the first step in the description of NeQuick, the quick-run model chosen for GALILEO purpose.

4.3 NeQuick

4.3.1 Simple topside

The most simple way to take the topside into account is to consider it as a **sixth semi-Epstein layer**. However it received a different thickness parameter which evolved from the beginning, even before constituting the difference between the three models of the DGR family.

The first idea was to *adapt* modelled TEC values to measurements [48] using an additional parameter k for the top F_2 layer, considering only this layer and getting back to the meaning of the thickness parameter B (cf. footnote in subsection 4.2.1).

$$\begin{aligned} TEC &= TEC_{bot} + TEC_{top} = 2\ N_{max}^{F_2}\ B_{bot}^{F_2} + 2\ N_{max}^{F_2}\ B_{top}^{F_2} \\ &= 2\ N_{max}^{F_2}\ B_{bot}^{F_2}\ (1+k) \end{aligned} \tag{4.8}$$

The thickness parameter was then given by the equation $B_{top}^{F_2} = k\ B_{bot}^{F_2}$ where k could range from 2 to 8 (cf. equations A.13 for k).

An even better agreement was found [49] using a coefficient ν and replacing $B_{top}^{F_2}$ by a new *height dependent* thickness parameter H (cf. equation A.3) reaching the current form of the profile which is shown in figure 4.11 with $B_{top}^{F_2} = 46.2km$.

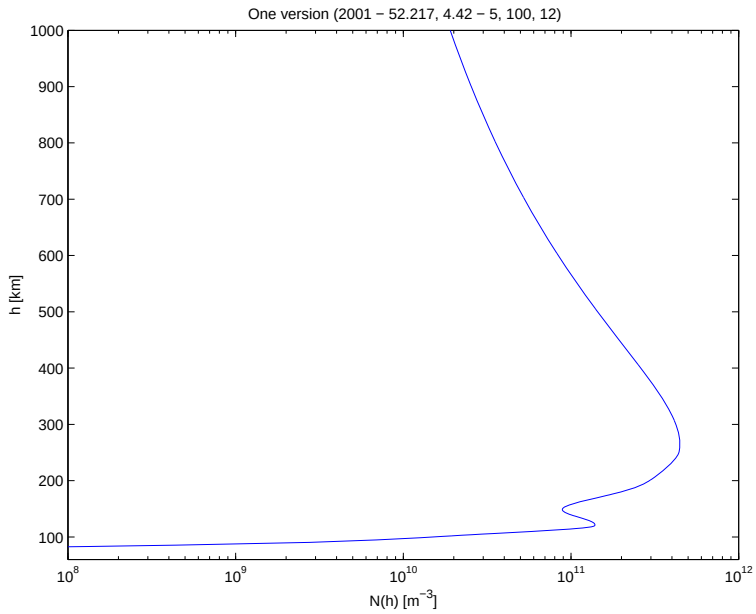

Figure 4.11: Profile example from NeQuick version 1 (ITU-R) (ESTEC location – $52.217^{\circ}N$, $4.42^{\circ}E$ –, May, average solar flux – $\Phi_{12} = 100$ –, midday universal time)

4.3.2 Implementation

Now that the overall principle of NeQuick has been widely discussed, the implementation of the equations in appendix A.2 has to be introduced. NeQuick was originally built in **FORTRAN 77**, was submitted to and accepted by the ITU-R in 2000 and was revised in 2002. It is downloadable from the Inter-

net [39] and is referred to either as version 1, ITU-R or 2001 as it was first described in an article from 2001 [49].

The file NeQuick_ITUR.for [4] contains NeQuick model which **variables and parameters** (cf. appendix A.1) correspond to the general ionospheric variations (cf. table 3.3) beginning with its input arguments:

1. *position* with height `h` (h), latitude `alat` (ϕ) and longitude `along` (θ),
2. *season* with month `mth`,
3. *solar activity* with monthly smoothed value of $F10.7$ `flx` (Φ_{12})
4. and *time-of-day* with universal time `UT` (UT).

The basic parameters are then computed from these inputs and from CCIR maps (files CCIRxx.asc) as described in subsection 3.2.3. They still correspond to the origin and constraint of the ionosphere i.e.

1. *solar activity* with `flx` limited to 193 for the highest solar activity conditions (cf. relationship with solar activity described in subsection 3.2.3) and converted to `R12` (R_{12}) by means of equation 3.4
2. and *geomagnetism* with MODIP `xMODIP` (μ) from magnetic dip `Dip` (I).

   The latter is calculated from the magnetic or dip latitude `dipl` (λ) by a dipole approximation [36] (cf. equation 4.9).

$$\tan I = 2\ tan\lambda \tag{4.9}$$

   Dip latitude comes itself from a 3rd order Lagrange interpolation [43],[56] on a grid[5] of data stored in the file diplats.asc.

Getting now to **implementation structure** (cf. figure 4.12), the first distinctive feature is the existence of two *entry points* allowing to bypass related operations if time conditions (season, solar activity and time-of-day) do not change between two calls to NeQuick.

- eldens, with only position input (`h`, `alat` and `along`), is designed to consider slant rays.
- For even simpler vertical profiles, vert requires only height input (`h`).

[4] cf. zip file or "NeQuick1.1\NeQuickG77" directory in "Tools" directory on joined CD
[5] 5° in latitude and 10° in longitude

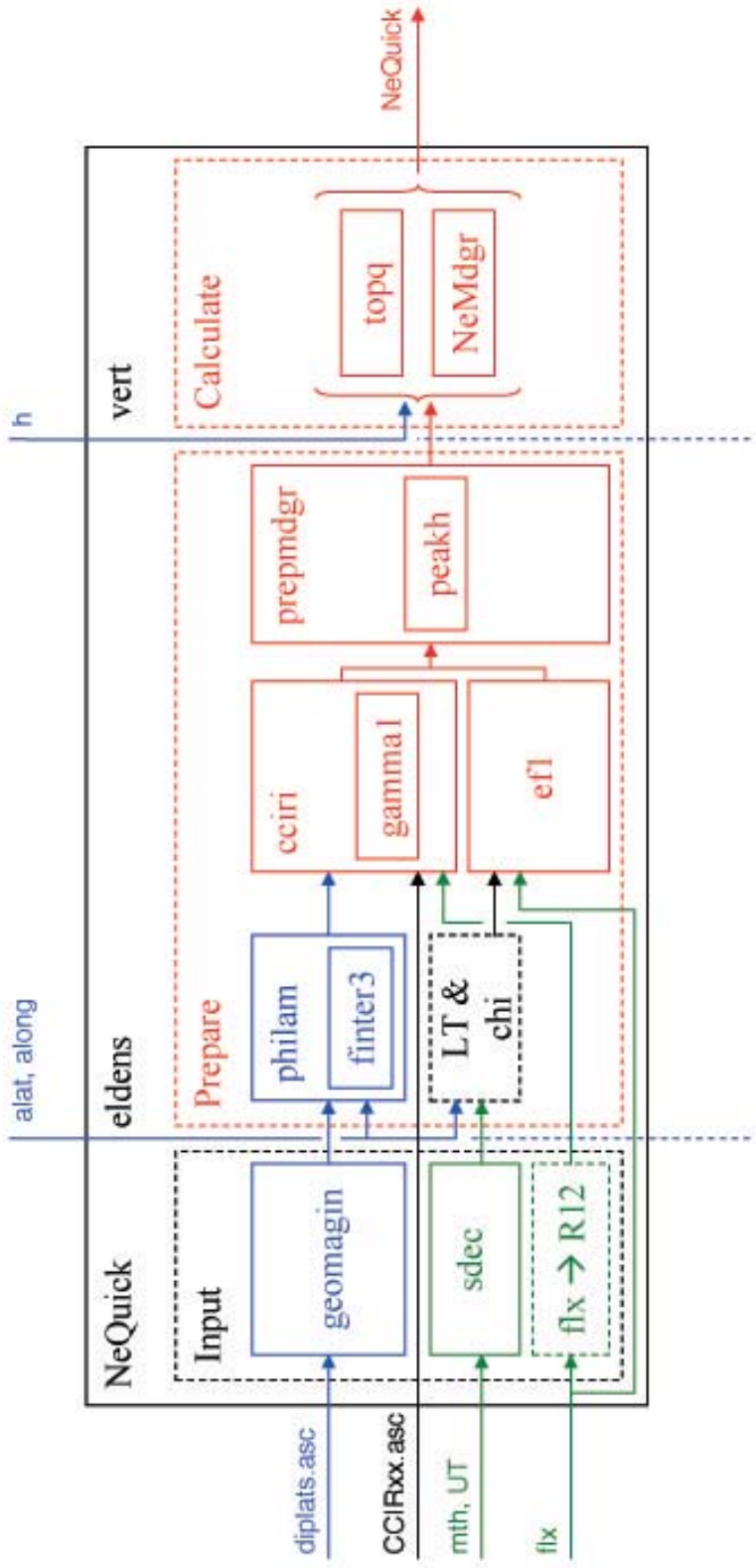

Figure 4.12: NeQuick structure

Three main steps making use of different functions and subroutines can be isolated (left upper part in blue related to space conditions, left lower part in green to time conditions, in black to both and rest in red to parameters and output calculations).

The *input* step includes the reading of space related data and initialization of time conditions.

- geomagin reads dip latitude grid from diplats.asc.
- sdec calculates sun declination necessary to compute the zenith angle of the sun `chi` (χ).
- `flx` is compared to 193, limited to that maximum value if necessary and finally converted to `R12`.

The *preparation* step allows to calculate basic and intermediate parameters.

- philam provides appropriate dip latitude by means of finter3 (Lagrange interpolation function). Then `Dip` and `xMODIP` are computed.
- Local time `LT` (LT) is calculated and is used with sun declination zenith angle of the sun `chi`.
- cciri loads appropriate CCIR map (for current month), adapts the coefficients to current `R12` and calls gamma1 (cf. equations A.24) to generate `foF2` (f_0F_2) and `M3000` ($M(3000)F_2$). ef1 calculates `foE` (f_0E) and `foF1` (f_0F_1) (implementation of equations A.19 and A.20).
- prepmdgr generates the Epstein parameters from the ionosonde parameters (cf. equations A.4 to A.6, A.9 to A.11, A.13 and A.15 to A.18). It calls peakh to calculate `hmF2` ($h_{max}F_2$) (cf. equation A.8).

Finally the *calculation* step generates electron density by means of the analytical profiles.

- If above the F_2 layer peak ($h > h^{F_2}_{max}$), topq is called to return the electron density in the topside into NeQuick and to the calling program (cf. equation A.3).
- For the bottomside, NeMdgr uses the Epstein parameters from prepmdgr to compute the electron density (cf. A.1 when $h < 100$ and A.2 else) before returning the handle to the main program.

Throughout NeQuick, djoin is used for *piecewise functions* implementation (cf. equation A.27) and fexp for *exponential functions* (cf. equation A.28).

4.3.3 Electronic characteristics as output

In order to **use NeQuick**, which is only a function, additional drivers are necessary such as eldens_ITUR.for and slQu.for, published in the same package, which ask input data to the user[6].

- eldens gives *single values of electron densities and height profiles.*
- slQu extends the possible calculations to *slant profiles and TEC* using a 2nd order Gauss-Legendre quadrature associated to a Richardson extrapolation [44],[57].

A scheme of slQu structure is proposed in figure 4.13 on the basis of its constitutive functions and subroutines.

Two subroutines ensure **input** operations.

- rays asks for *space* conditions (upper left part in blue) i.e. ray endpoints coordinates and calls then naut to calculate ray perigee properties and zenith angle and gcirc to get the properties of the great circle between ray endpoints, mainly azimuth.
- dat_t_sa takes care of the other conditions (*date, time and solar activity* ; lower left part in green) and is followed by NeQuick initialization to these conditions. Entry points eldens and vert can then be used only with space input values (dotted arrows).

The program is then divided into **two parts** according to its two different uses (right part in red).

1. The *slant profiles* calculation is held by geogra subroutine and eld function. The first gives height and geographic coordinates of successive points along the ray from its coordinates (zenith angle, azimuth and distance from perigee). The second computes electron density at the same points from the same parameters.
2. To generate *TEC* values, numerical integration functions gintv for vertical situations and gint else are called. They are based on second order Gauss-Legendre quadrature.

Finally all the **results** are stored into the file slQu.dat.

[6]New drivers (dens.for for electron densities, param.for and prof.for for profiles, vTEC.for for vTEC analysis, sTEC.for for sTEC analysis) have been built in the framework of the analysis tool described in chapter 6. They can be found on the joined CD into the "Code" directory of the GUI software.

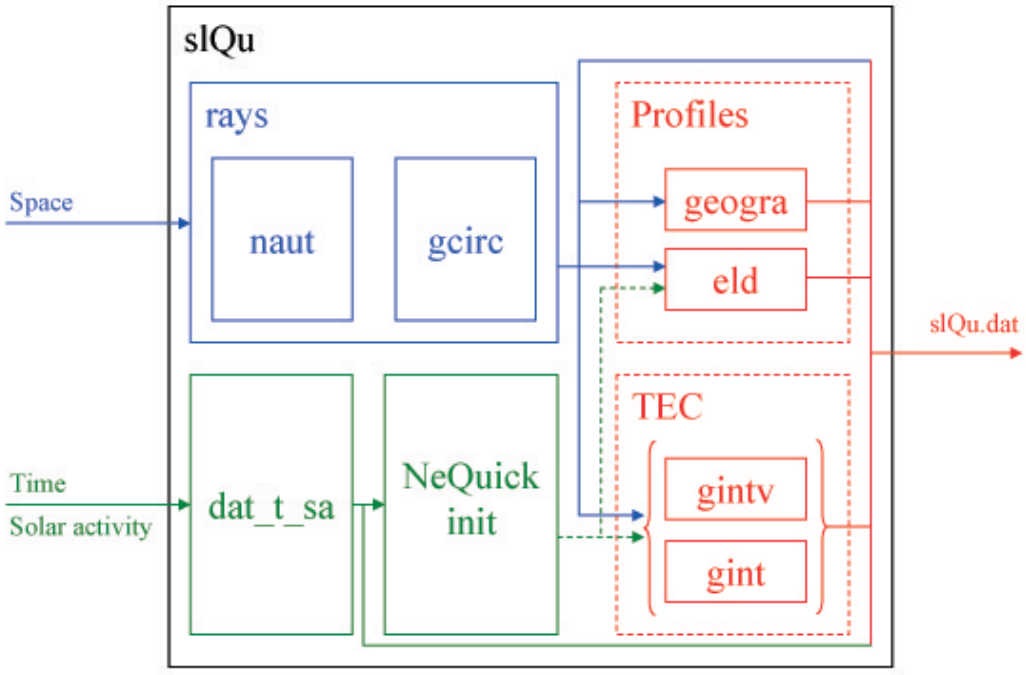

Figure 4.13: slQu structure

Using the second functionality and getting TEC allows then to go back to the ionospheric error (cf. section 3.3). An online version of NeQuick to compute TEC is also available [38].

4.3.4 GALILEO ionospheric model for single-frequency receivers

The tool to model TEC has been described but, as it provides monthly averages, it has to be completed by a proper algorithm in order to give **daily values**.

The solution was found [33] by using an *effective ionization level* Az for the whole world, applicable for a period of typically 24 hours, representing solar activity instead of solar flux $F10.7$ (Φ_{12}).

Its implementation follows the notice latitudinal – in fact the MODIP – dependence of NeQuick error by means of *three coefficients*.

$$Az = a_0 + a_1\ \mu + a_2\ \mu^2 \tag{4.10}$$

The actual ranges of values for the different parameters follows.

$$\begin{aligned} 10 < Az < 300 \\ 10 < a_0 < 300 \\ -1.19 < a_1 < 0.83 \\ -0.0251 < a_2 < 0.0349 \end{aligned} \tag{4.11}$$

As NeQuick overestimates TEC in equatorial regions and underestimates it in polar areas, Az will look like a smile (cf. figure 4.14).

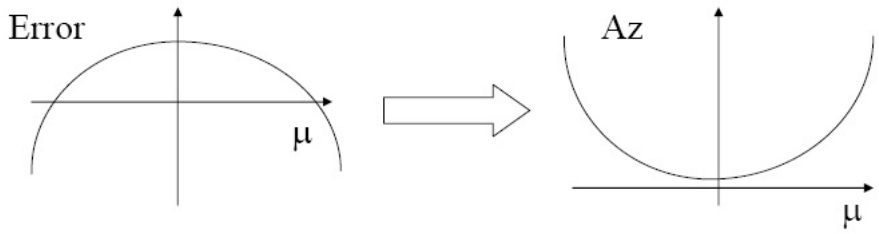

Figure 4.14: Principle of the effective ionization level Az

The three coefficients will be calculated and broadcasted to the user through the following *procedure*[7] (cf. figure 4.15).

1. For every GSS and every 20 minutes, sTEC will be measured ($sTEC_{meas}$) for each satellite in sight above an elevation mask angle of 30°. Every 24 hours, the set of measurements will be compared to modelled values with Az as unknown ($sTEC_{mod}(Az)$) in order to obtain the optimum Az for that day and GSS minimizing the mean-square error.

$$\Delta sTEC^2 = \sum |sTEC_{meas} - sTEC_{mod}(Az)|^2 \tag{4.12}$$

2. a_0, a_1 and a_2 will be computed at one GCC through a least-squares second degree polynomial fit of all GSS defined by their MODIP.

3. The receiver will run NeQuick using Az from previous day[8] to calculate TEC and ionospheric delay by means of equation 3.8.

This procedure is due to correct at least 75% RMS of the ionospheric delay which is twice better than for GPS algorithm.

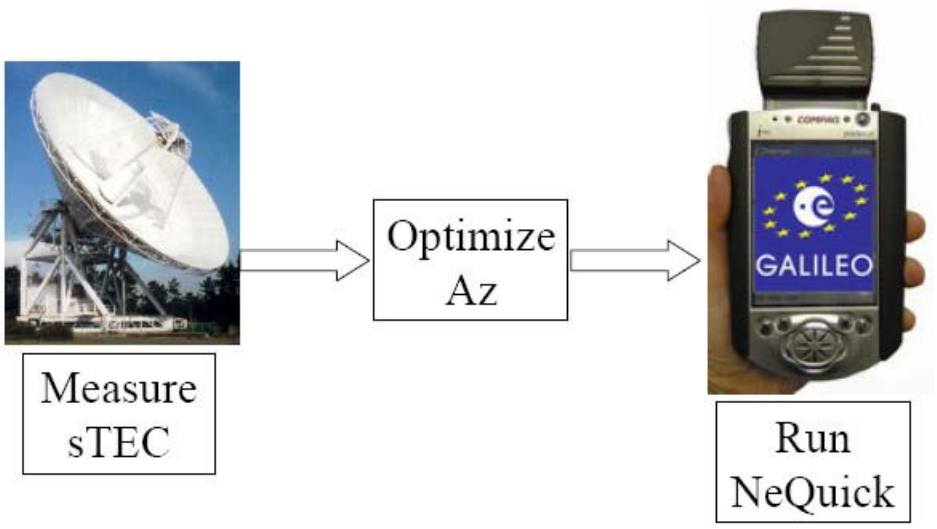

Figure 4.15: GALILEO single-frequency algorithm

[7]For understanding purpose, simplifications have voluntary been included.

[8]Three input arguments replace `flx` into NeQuick and a new function is added to compute Az for current MODIP (cf. "Tools\NeQuick1.1.1_Az" directory on joined CD).

Part II

A broad analysis

Chapter 5

NeQuick assessment

5.1 Analysis structure

This study focuses on NeQuick detailed functioning and is intended to achieve the following **goals**: provide a structured and complete description of *potential improvements* of NeQuick and *begin* the *analysis* of these improvements.

The first is developed in this chapter which states or proposes solutions or path to solutions. According to the second, chapter 6 introduces the analysis tool built to highlight the improvements resulting from the different proposed modifications and chapter 7 describes methods to realize tests and gives first results.

The broad analysis is based on the question **"How to use NeQuick for GALILEO single frequency receivers?"** which was divided into four issues (cf. figure 5.1)[1].

1. The *understanding* leading to the description in part I allowed to draw up a list of questions related to different topics.[2]

2. The main topic (cf. section 5.2) concerns the so-called *"physical"* behaviour of NeQuick, when it works with monthly medians (latitudinal dependence of error mentioned in subsection 4.3.4, etc.).

3. In parallel the *"effective"* use described in subsection 4.3.4 implies a series of problems to be solved (cf. section 5.3).

4. Finally purely *implementation* questions related to programming languages and numerical methods have to be considered (cf. section 5.4).

[1] cf. Excel file on CD in "Analysis" directory
[2] This list is included in the "Analysis\Questions" directory on joined CD.

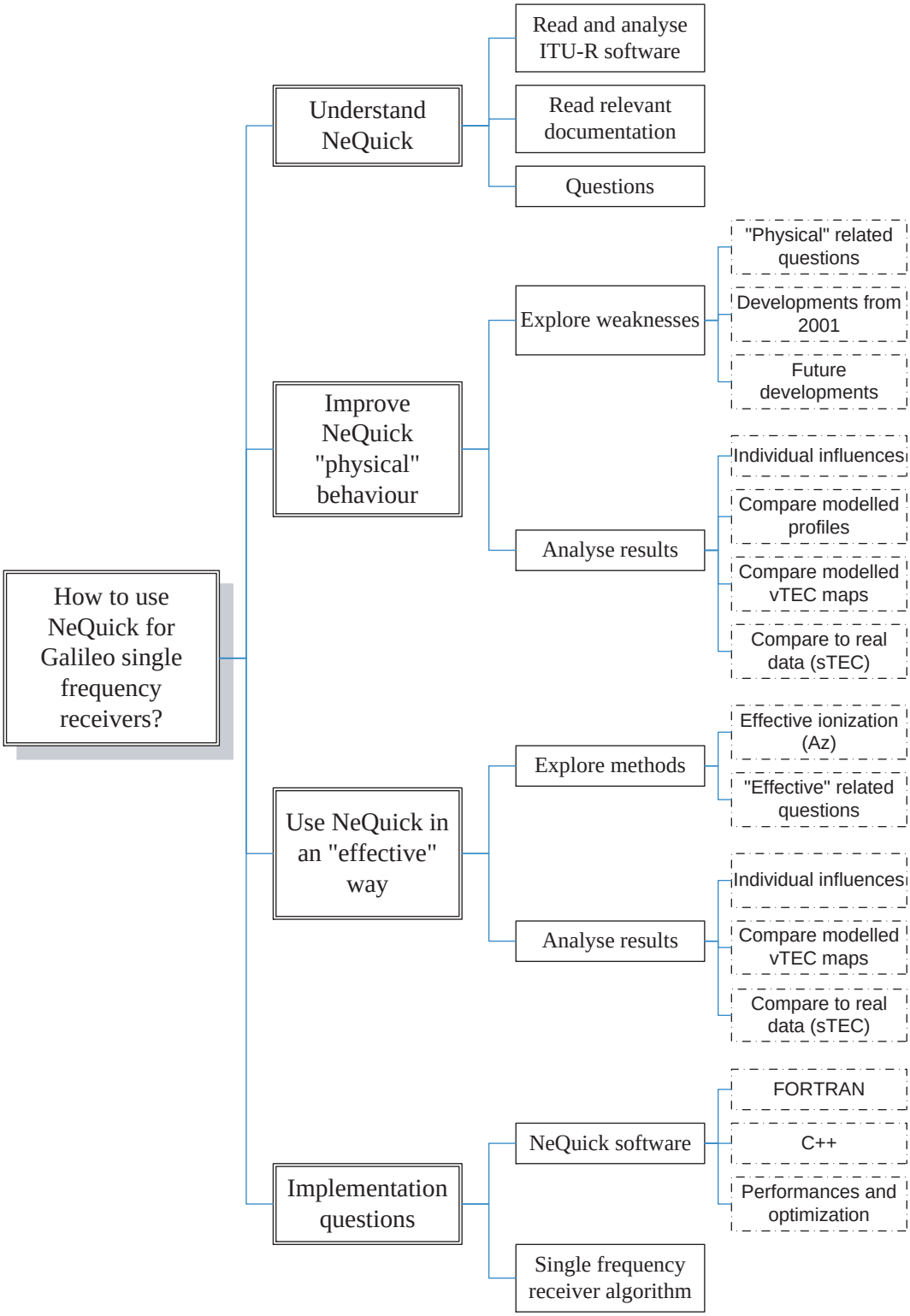

Figure 5.1: Analysis structure

5.2 "Physical" behaviour

5.2.1 "Physical" related questions

The **latitudinal dependence** of error is linked to the use of `alat` parameter with empirical coefficients which can be noticed in different **tools** throughout the model.

1. A *variable*, the MODIP, is computed from latitude so that, in parallel with associated equations, functions and subroutines, its related file should be studied for updates or different definition (basic variable different from dip latitude, different kind of grid).

2. The *basic parameters*, consisting of the ionosonde parameters, are also based on files – and corresponding equations, functions and subroutines – that could be updated and built differently. For example, they could use directly the solar flux instead of the sunspot number.

3. The *intermediate parameters*, including the Epstein and k parameters, are indirectly concerned as their equations, functions and subroutines use the basic parameters.

4. Finally the *topside* formulation is undergoing current research because the most important problems are thought to come from its too high simplicity and because, up to now, less data, from topside sounders for instance, was available to compare the model with measurements [59].

5.2.2 Developments from 2001

Modifications corresponding to the tools mentioned in previous subsection have already been proposed but not taken into account for GALILEO purpose.

These developments were named after their year of release and can be seen as the following of the evolution described in subsection 4.2.3: version 1990 corresponds to the DGR approach (three Epstein layers for bottomside), version 1995 includes the first improvements (five semi-Epstein layers for bottomside) and version 2001 (ITU-R or version 1) constitutes the current **baseline**.

In 2002 – it was however only published in 2005 [62] –, the definition for f_0F_1 was revisited (cf. equation A.35) so that **simplifications** were introduced for $h_{max}^{F_1}$ (cf. equation A.30) and the thickness parameters (cf. equations A.32 to A.34). Peak amplitudes were also modified (cf. equation A.29 and related explanation). This new formulation, called NeQuick 2002, corresponding to tools 2 and 3 of previous subsection, avoids strange structures and strong gradients in the E and F_1 layers (e.g. evolution for $B_{top}^{F_1}$, from figures 5.2 to 5.3).

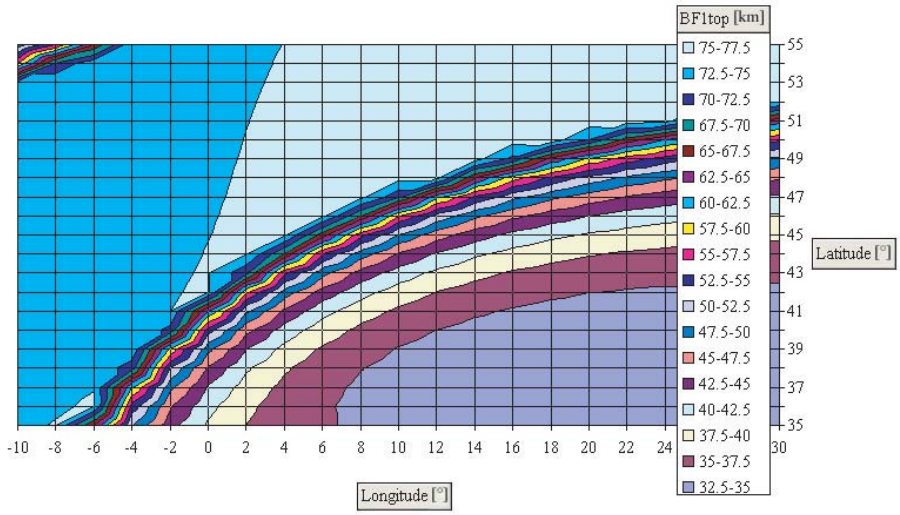

Figure 5.2: $B_{top}^{F_1}$ map from NeQuick 2001 (November, $\Phi_{12=122}$, 11h universal time)

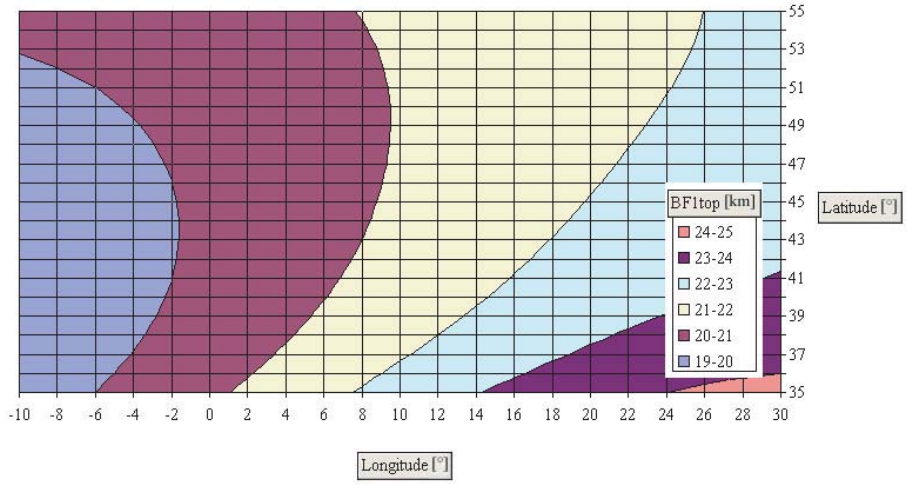

Figure 5.3: $B_{top}^{F_1}$ map from NeQuick 2002 (November, $\Phi_{12=122}$, 11h universal time)

Two improvements were presented in 2005. The first [58] is referred to as 2005a and involves tool 3 as the two formulas for topside **k parameter** were replaced by a unique one (cf. equation A.31).

The second constitutes a very deep revising and is not yet published. As a consequence, it was worked out from the code[3]. It is called 2005b or version 2 and is related to the proposal of **new input data files** for tools 1 and 2,

1. a *MODIP* file (modip_9.asc) instead of the dip latitude file (diplats.asc)
2. and *simplified ITU-R maps* (CCsimXX.asc replacing ccirXX.asc).

The latest correspond to a spherical harmonics approximation which does not use latitude anymore and replaces universal time by local time (cf. equation A.37) so that smaller scale structures which have no data base and do not reflect a realistic monthly median ionosphere could be removed. The roles of $h_{max}^{F_2}$ and $M(3000)F_2$ have also been inverted as $h_{max}^{F_2}$ is now computed by means of a numerical map. A summary of all the modifications can be found in appendix A.3.

By comparison with figure 4.12, equations, functions and subroutines were consequently modified.

1. For *MODIP*,
   - geomagin turned to amodin (reading of modip_9.asc instead of diplats.asc) ;
   - philam was replaced by amodip (direct interpolation of MODIP instead of dip latitude first) ;
   - and `Dip` calculation and dipole approximation were removed.
2. The *simplified maps* caused
   - cciri to turn to peakf ;
   - gamma1 to be replaced by Foureco (cf. equation A.38), sphharm (spherical harmonics with associated Legendre polynomials) and sphreco (cf. equation A.37) ;
   - and prepmdgr to evolve to prepep including $M(3000)F_2$ calculation (cf. equation A.36).

Each of these versions have been implemented[4] in the analysis tool (cf. chapter 6) and the consequences of these modifications are presented in chapter 7.

[3] cf. "Tools\NeQuick2" directory on joined CD

[4] The source codes can be found into the "Code" directory of the GUI software or into "Analysis\Model evolution" on joined CD.

5.2.3 Future developments

As mentioned in subsection 5.2.1, it seems that most of the errors come from the topside so that attempts for new formulations are suitable. This study proposes a simple evolution replacing the semi-Epstein profile from the ITU-R version (2001), first by a Chapman layer (NeQuick 2006a) and then by an **hybrid involving a Chapman layer** just above the F_2 peak **changing** fast **into a modified Epstein layer** (NeQuick 2006b).

This idea is based on the reading of [60] highlighting the need for new techniques to represent the transition between 0^+ and H^+ dominated ionosphere and of [59] advising a Chapman layer up to about $400km$ above F_2 layer peak. A compromise was then found by

- representing that transition (cf. figure 5.4) without new parameter by means of a Chapman and the original modified Epstein formulations – the unknown thickness parameters were arbitrarily chosen as $B_{top}^{F_2}$ (cf. equation A.13) for the Chapman layer and H (cf. equation A.12) for Epstein formulation ;
- and using an exponential transition to model the unknown transition height which is undergoing current research.

The derived equation follows[5] and an example of resulting profile in given in figure 5.5.

$$
\begin{aligned}
N(h) &= \frac{Ep(h)\ e^{50\ (Ch(h)-Ep(h))} + Ch(h)}{e^{50\ (Ch(h)-Ep(h))} + 1} \\
Ch(h) &= N_{max}^{F_2}\ e^{0.5\left(1-\frac{h-h_{max}^{F_2}}{B_{top}^{F_2}}\ -\ e^{-\frac{h-h_{max}^{F_2}}{B_{top}^{F_2}}}\right)} \\
Ep(h) &= 4\ N_{max}^{F_2}\ \frac{e^{\frac{h-h_{max}^{F_2}}{H}}}{\left(1+e^{\frac{h-h_{max}^{F_2}}{H}}\right)^2}
\end{aligned}
\tag{5.1}
$$

The hybrid formulation is also used with the latest version (2005b ; version 2) and is then referred to as NeQuick 2006.

The proposals are of course also implemented in the analysis tool (cf. chapter 6) and consequences are also presented in chapter 7 even if it should not give accurate results straight away i.e. without parameters adaptation.

[5] The corresponding code can be found on joined CD in the "Analysis\Topside" directory.

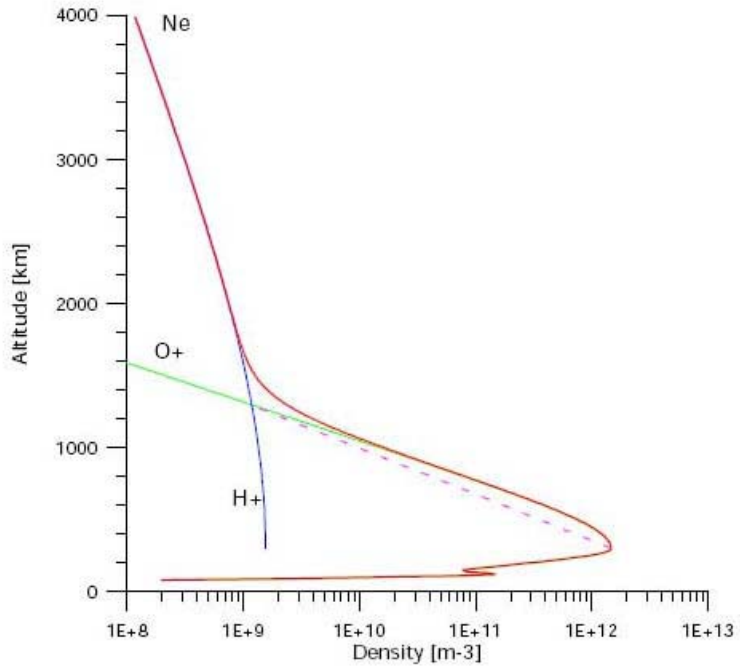

Figure 5.4: Transition between 0^+ and H^+ dominated ionosphere [60]

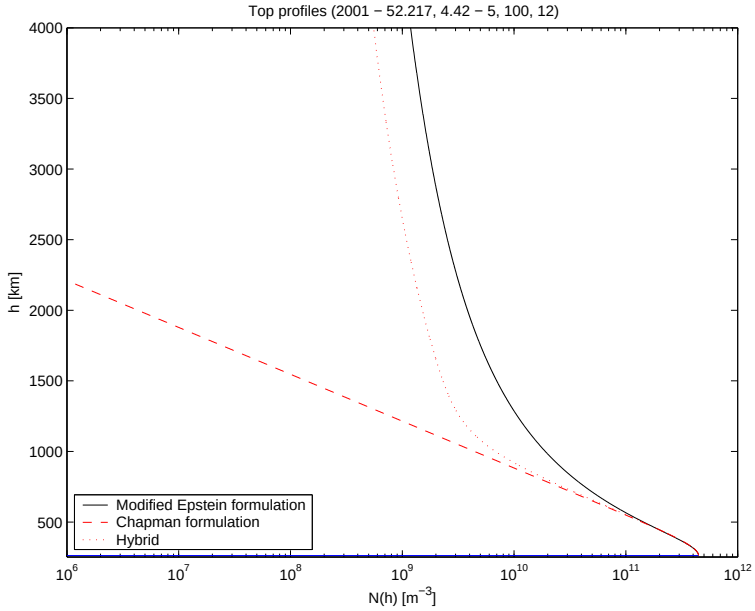

Figure 5.5: Proposed topside formulations and NeQuick version 1 (ITU-R) (ESTEC location – $52.217^{\circ}N$, $4.42^{\circ}E$ –, May, average solar flux – $\Phi_{12} = 100$ –, midday universal time)

5.3 "Effective" use

5.3.1 Effective ionization Az

Going now towards the daily use of NeQuick in the single frequency algorithm described in subsection 4.3.4, the Az calculation procedure deserves some comments.

- First of all the resulting **time and space conditions** could be imposed differently i.e. Az could be calculated for different regions instead of globally and more often than once every day for example.
- Direct consequences have also to be noticed as **new limits** have to be imposed (cf. figure 5.7).
    1. About *higher* limits, the daily use extends the variables domain so that the limit on flux at 193 has to be removed (cf. subsection 4.3.2).
    2. As Az is designed to push up TEC in polar regions and pull it down in equatorial regions, possible unrealistic values such as negative f_0F_2 (cf. figure 5.6)[6] or NaN conditions resulting from negative square-roots using $M(3000)F_2$ (cf. equation A.8) could appear. *Lower* limits have then to be added into cciri subroutine (for version 2, in peakf for f_0F_2 and no more for $M(3000)F_2$ as the square-roots disappeared).

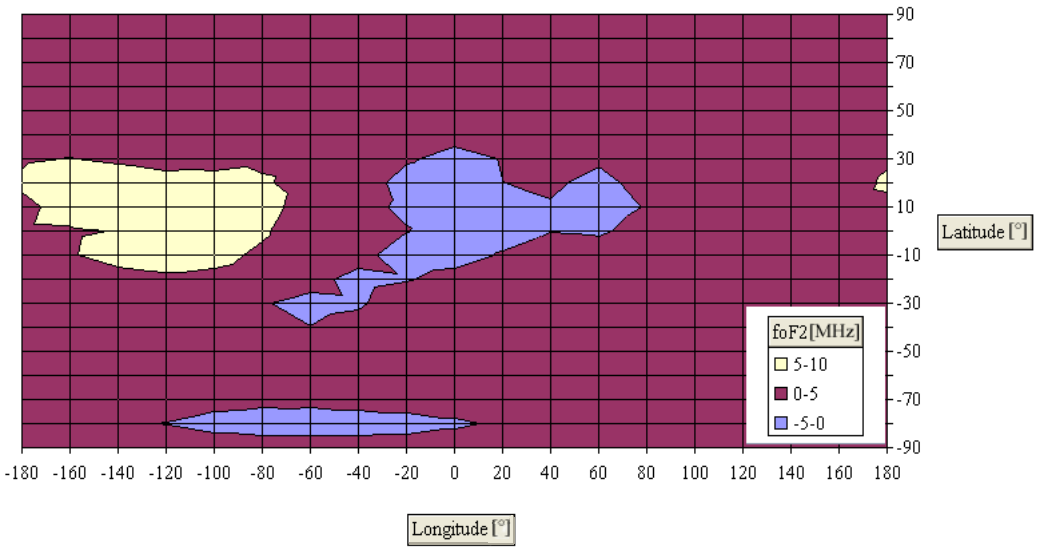

Figure 5.6: f_0F_2 map for $Az = 10$ (ESTEC location – $52.217^{\circ}N$, $4.42^{\circ}E$ –, May, midnight universal time)

[6] cf. "Analysis\Data analysis\Ionosonde\Ionosonde param (ccir)" directory on joined CD

The following qualitative description will improve the understanding of these modifications.

One of the purpose of Az implementation is to force too high modelled TEC in comparison with measured TEC to decrease. According to the monotonously increasing relationship with solar activity, the solar flux is replaced by a lower value of Az giving lower values of f_0F_2. But at a time – when f_0F_2 reaches 0 –, decreasing the solar activity parameter (Az) does not decrease electron density and TEC anymore because of the second order relationship of the global electron density at the F_2 layer peak NmF_2 on f_0F_2 (cf. equation 3.2). The means to decrease TEC further should then be found elsewhere and anyway negative values of f_0F_2 should be avoided.

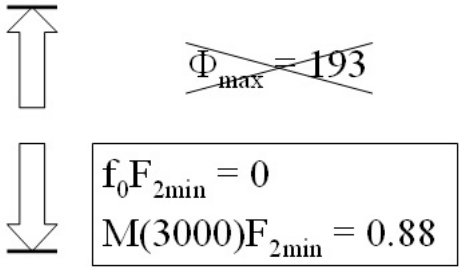

Figure 5.7: New "effective" limits

5.3.2 "Effective" related questions

Instead of considering NeQuick as a black box, an **intermediate approach** could be applied to use NeQuick daily. Beside feeding it with the effective ionization level Az, the use of daily values could lead to intrinsic modifications of the model (the "black box" is then put back to the CCIR files which will remain adapted for monthly values).

1. The *characteristic levels of solar activity* used for the very first combination of coefficients (cf. subsection 3.2.3), currently $R_{12} = 0$ for low and $R_{12} = 100$ for high, could be revaluated regarding the domain extension described in previous subsection. For example $R^* = 200$ could be chosen to represent high solar activity level (R^* denotes the daily effective sunspot number).

2. A *new relationship between flux and sunspot number* should consequently be built, linking Az to R^*, or Az could be directly used instead of the sunspot number.

5.4 Implementation

This broad analysis would not be complete without taking into account the questions related to the language used to implement the model and associated drivers and to the numerical tools chosen such as interpolation or integration methods.

A **C++** NeQuick source code version has indeed also been developed[7]. It is the conversion to C++ source code from an evolved version of FORTRAN NeQuick version 1 (ITU-R):

- the modifications leading to *version 2002* described in subsection 5.2.2 are included ;
- a *MODIP file* has already been taken into account (modip2001.asc) ;
- it is supposed to be used with *Az* (*"effective" use* with different input parameters – cf. subsection 4.3.4) ;
- and the *integration routine* has been *redesigned*.

This last point, concerning the **integration method**, constitutes precisely the most interesting example of implementation questions.

As mentioned in subsection 4.3.3, the ITU-R software uses a Gauss-Legendre quadrature. However other integration methods were compared [61] and it appeared that an adaptive Kronrod quadrature $G_7 - K_{15}$ gives better results.

This method involves two *characteristics*: [63]

1. the reuse of abscissas from previous iterations as part of the new set of points due to Kronrod, whereas usual Gaussian quadrature would require recomputation of all abscissas at each iteration
2. and the possibility – knows as adaptative– to adapt to the function to integrate, feeling the shape and increasing the number of abscissas when the function grows fast, not knowing a priori its characteristics.

It gives *better results* in terms of

1. number of function calls (divided by 15),
2. average of relative error (decreased by 20%),
3. and total computational time (on a slant profile, 40 times less).

Beside purely code optimization, this method could consequently be generalized and the C++ version could become the basic version.

[7] cf. "Tools\NeQuick1.1\NeQuickC++" directory on joined CD

Chapter 6

Analysis tool

6.1 Main

In order to **use NeQuick** in an efficient way and to visualize and store the results easily, a combination of FORTRAN programs and Matlab scripts appeared suitable. By means of Matlab GUI Builder, a GUI (cf. figure 6.1) was created to call different modules, each one running corresponding FORTRAN drivers and reading the results to show them as numbers or graphics[1].

By launching NeQuick[2] from Matlab, the user can

1. calculate *electron densities* by means of NeQuick_dens (cf. subsection 6.2.1) ;
2. plot electron density *profiles* by means of NeQuick_profiles (cf. subsection 6.2.2) ;
3. perform *vTEC analysis* by means of NeQuick_vTEC (cf. subsection 6.2.3) ;
4. and perform *sTEC analysis* on GPS data by means of NeQuick_sTEC (cf. subsection 6.2.4).

An auxiliary tool is also available to convert smoothed monthly sunspot numbers into corresponding *fluxes* or to look for past measured values of these parameters (cf. subsection 6.2.5).

If the user knows only *local time*, he can find a map of time zones (Timezones.gif) in the "Tools" directory and use it to find universal time.

[1]The software can be found on the joined CD into the "GUI" directory and used after having followed the procedure described in the file "Read me".

[2]Type "Nequick" after having changed the current directory to the one containing the software.

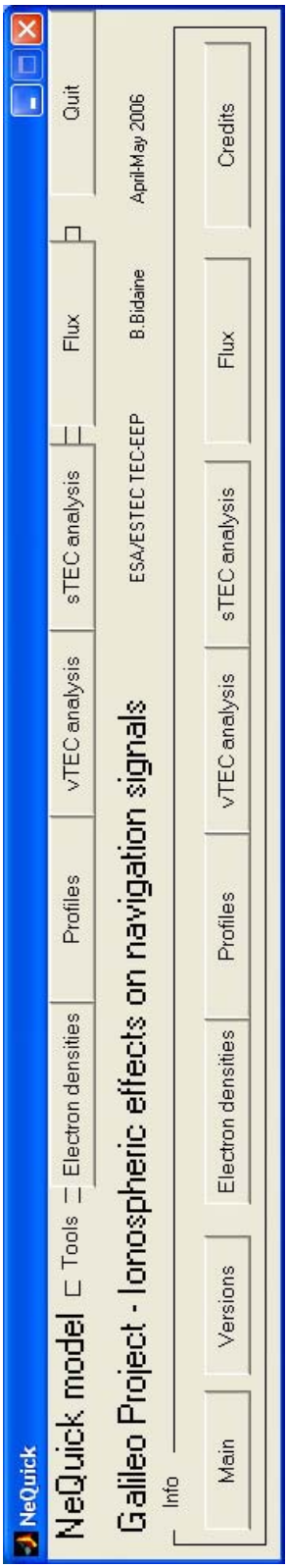

Figure 6.1: Main GUI

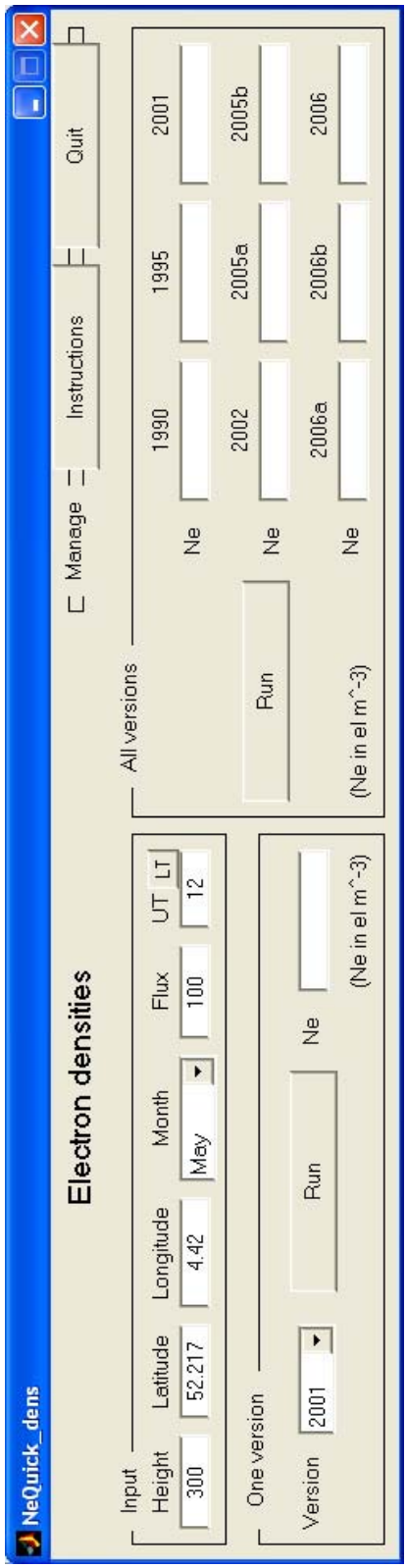

Figure 6.2: Electron densities module

6.2 Modules

6.2.1 Electron densities

The package (NeQuick_dens.fig, NeQuick_dens.m, and "Tools\dens" directory) allows to **calculate electron densities** from NeQuick model in two different ways.

By launching NeQuick_dens from Matlab (cf. figure 6.2), the user can calculate electron densities for

- *one version* of NeQuick (from "One version" frame)
- or *all versions* of NeQuick (from "All versions" frame).

He must execute the four following **steps**:

1. specify *input conditions* including height, latitude, longitude, month, flux and UT (in "Input" frame) ;
2. for "One version", select the *relevant version* in the "One version" frame ;
3. and push the *"Run"* button to calculate the corresponding electron densities (Ne in $el.m^{-3}$) appearing in the corresponding field.

6.2.2 Profiles

The package (NeQuick_profiles.fig, NeQuick_profiles.m, "Tools\param", "Tools\prof" and "Tools\Matlab_aux" directories) allows to **plot electron density profiles** from NeQuick model in a set of different ways.

By launching NeQuick_profiles from Matlab (cf. figure 6.3), the user can plot, in the same figure, electron density profiles for

- *one version* of NeQuick (from "One version" frame) ;
- *two versions* of NeQuick (from "Two versions" frame) ;
- *all versions* of NeQuick or only the ones *before or after 2001* (ITU-R) version (from "More versions" frame) ;
- the decomposition of the *bottomside* into its different layers (from "Bottom layers" frame) ;
- a comparison between Modified Epstein, Chapman and hybrid formulation for the *topside* (from "Topside profiles" frame) ;
- or a *comparison* between maximum five profiles for the same version (from "Comparison" frame).

He must execute the following **steps**:

1. specify *height characteristics* including minimum, maximum and step (in "Height" frame) ;
2. specify *input conditions* including latitude, longitude, month, flux and UT (in "Input" frame or "Comparison frame" in the last case) ;
3. select the *relevant version(s)* in the corresponding frame ;
4. and push the *"Plot"* button to calculate the corresponding electron density profile(s) and create the wanted figure.

The **figures** are saved in jpg files in the "Output_figures\Profiles" directory.

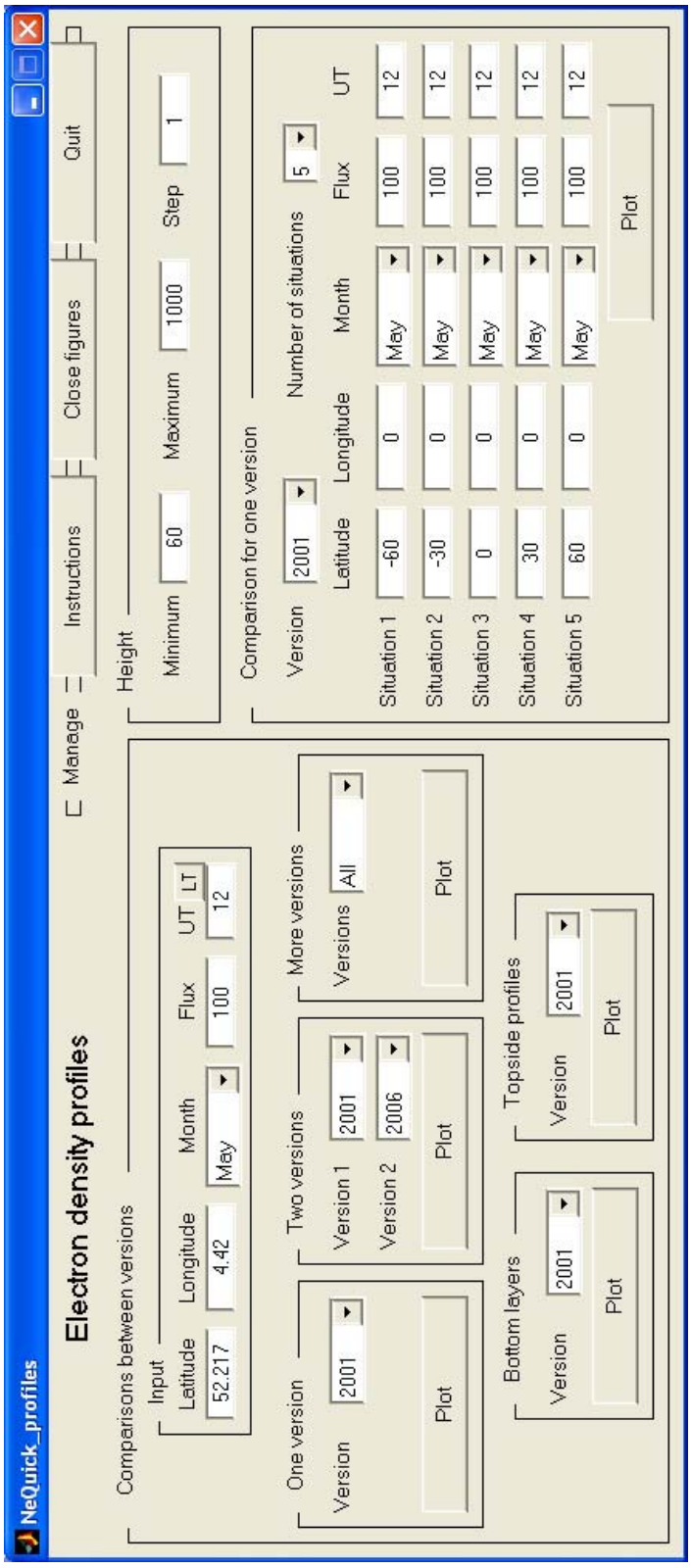

Figure 6.3: Profiles module

6.2.3 vTEC analysis

The package (NeQuick_vTEC.fig, NeQuick_vTEC.m, "Tools\vTEC" and "Tools\ m_map"[3] directories) allows to **analyse** vertical total electron contents (**vTEC**) from NeQuick model in a set of different ways.

By launching NeQuick_vTEC from Matlab (cf. figure 6.4), the user can

- plot *maps of vTEC* for one version of NeQuick (from "One version" frame) ;
- plot *maps of absolute and relative vTEC differences* between two versions of NeQuick (from "Differences" frame) ;
- calculate *global bias, maximum and RMS* of absolute and relative vTEC differences between two versions (from "Global" frame) ;
- or plot *curves of bias, maximum and RMS* of absolute and relative vTEC differences between two versions (from "Dependences" frames).

He must execute the following **steps**:

1. specify *space characteristics* including height (minimum, maximum), latitude and longitude (minimum, maximum and step) (in "Space" frame) ;
2. specify *input conditions* including month, flux and UT (in corresponding "Input" frames) ;
3. select the *relevant version(s)* in the corresponding frame ;
4. and push the *corresponding button* to calculate the corresponding vTEC values and/or create the wanted figures (to use the "Dependences" tools, the "Global" tool has to have been run before in order to calculate vTEC values).

The **calculated characteristics** are saved in txt files in the "Output_data\vTEC" directory. The **figures** are saved in jpg files in the "Output_figures\vTEC" directory.

[3]This directory contains M_Map mapping package for Matlab from University of British Columbia (http://www.eos.ubc.ca/~rich).

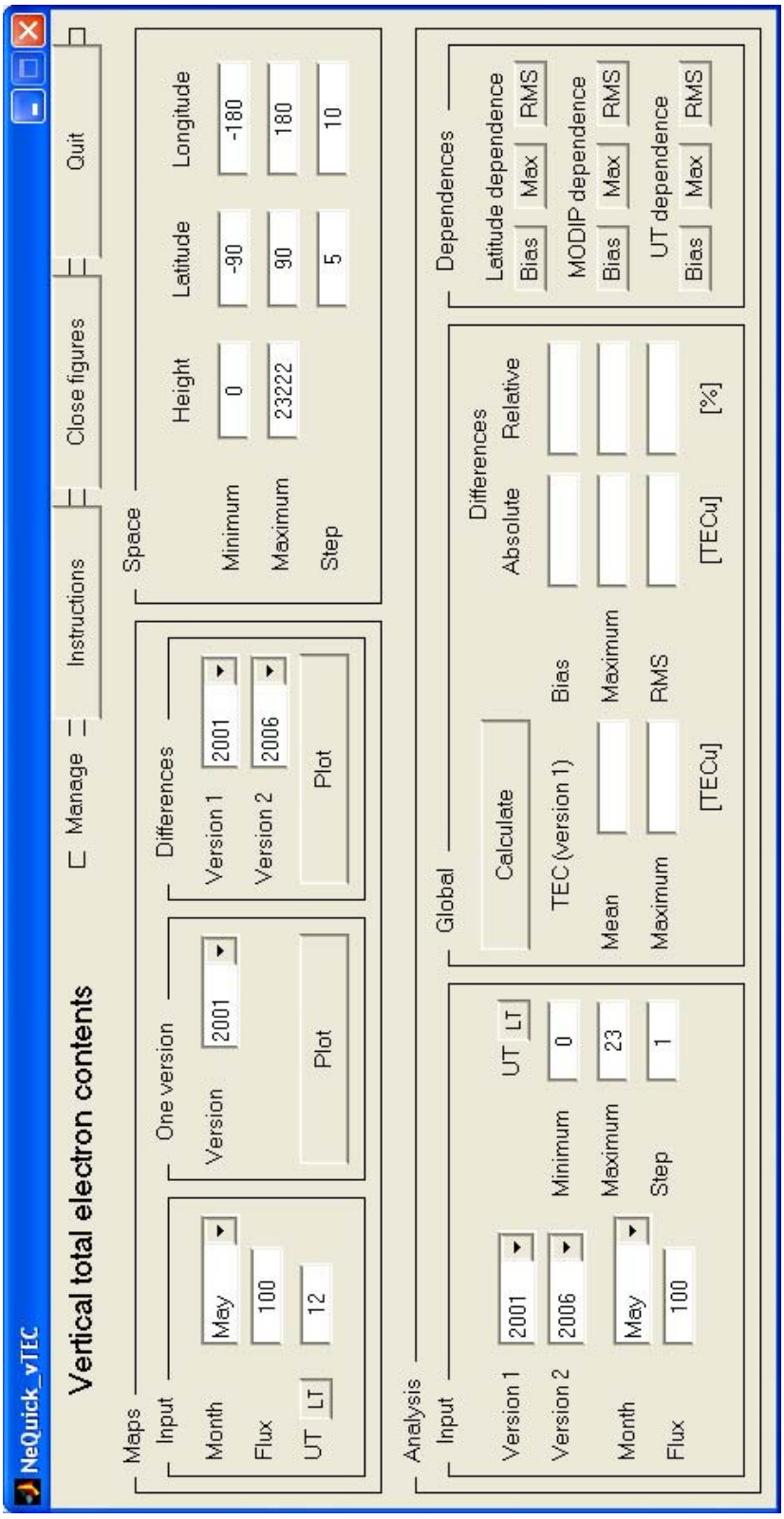

Figure 6.4: vTEC analysis module

6.2.4 sTEC analysis

The package (NeQuick_sTEC.fig, NeQuick_sTEC.m, "Tools\sTEC" and "To ols\m_map" directory) allows to **compare sTEC from NeQuick model to GPS data**[4] in a set of different ways.

By launching NeQuick_sTEC from Matlab (cf. figure 6.5), the user can

- create *working files* (toc.txt and char.txt) containing table of contents and space (station label, latitude and longitude) and time (first ut, last ut, missing ut) characteristics of GPS data ;
- calculate *global bias, maximum and RMS* of absolute and relative sTEC differences between modelled values from NeQuick and GPS data (from "Global" frame) ;
- or plot *curves of bias, maximum and RMS* of absolute and relative sTEC differences between modelled values from NeQuick and GPS data (from "Dependences" frame).

He must execute the following **steps**:

1. push *"Build TOC" and "Gather characteristics"* buttons when using GPS data for the first time ;
2. specify *input conditions* (in "Input" frame) ;
3. and push the *corresponding button* to calculate the corresponding sTEC values and/or create the wanted figures (to use the "Dependences" tools, the "Global" tool has to have been run before in order to calculate sTEC values).

The **calculated characteristics** are saved in txt files in the "Output_data \sTEC\yyyy\yyyy_mm" directory where yyyy stands for the chosen year and mm for the chosen month. The **figures** are saved in jpg files in the "Out put_figures\sTEC\yyyy\yyyy_mm" directory where yyyy stands for the cho-sen year and mm for the chosen month.

[4]The data available are described in section 7.1.

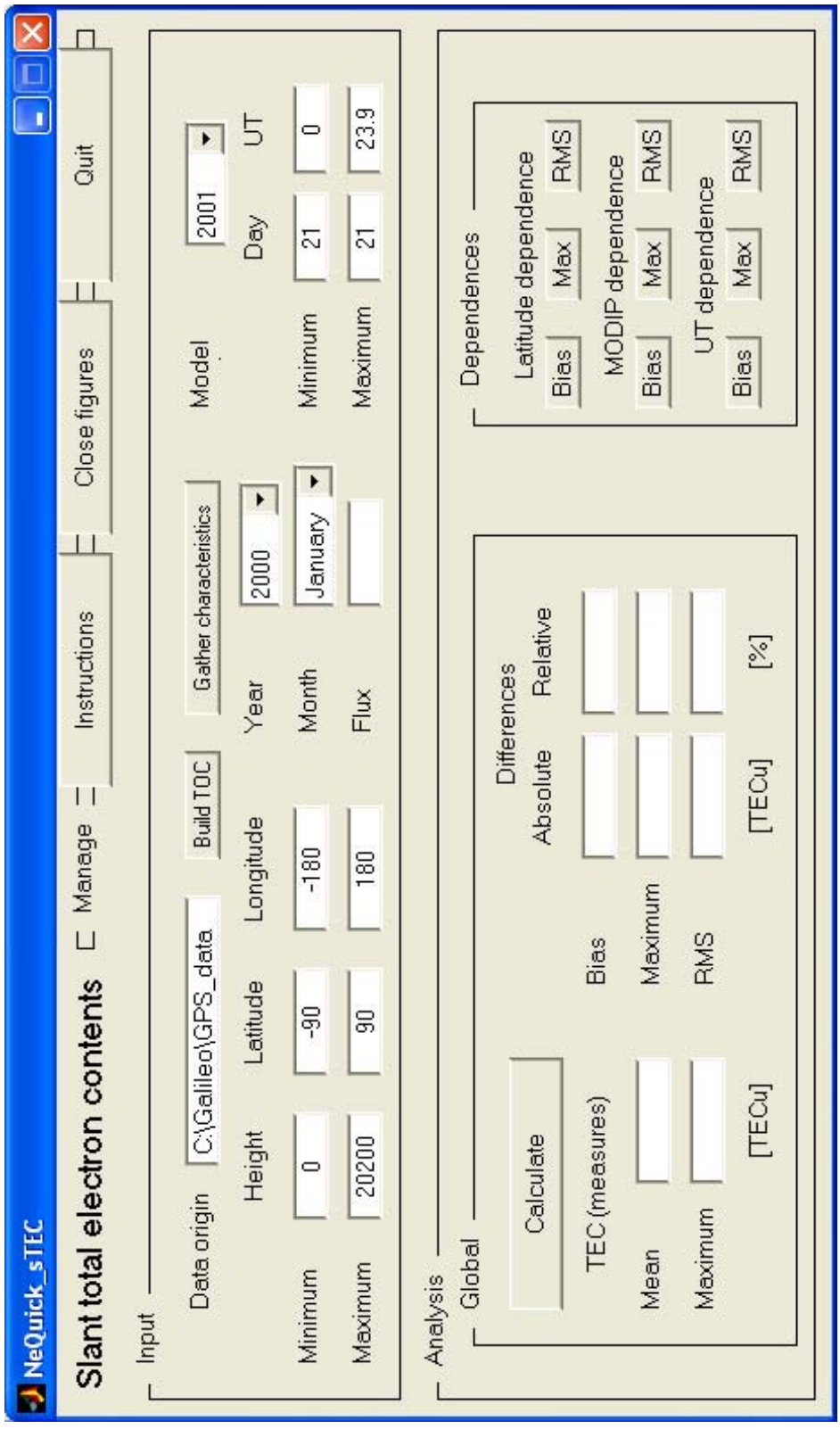

Figure 6.5: sTEC analysis module

6.2.5 Flux

The package (NeQuick_flux.fig, NeQuick_flux.m, "Input\R12" and "Tools\Flux" directories) allows to **find unknown fluxes from known smoothed monthly sunspot numbers** (R12 ; given by the user or from SIDC Brussels).

By launching NeQuick_flux from Matlab (cf. figure 6.6), the user can

- *update* the latest recorded values from SIDC (conversion of monthssn.dat into R12.dat by means of convR12.exe) ;
- give a *value of R12 or* look for it into *past measured values* ;
- and *convert* it into corresponding fluxes by means of the formula 3.4.

To know if an **update** is necessary, the user can press the "Last update?" button and read the month and year defining the version of monthssn.dat in use.

According to this date, *values of R12* are available till seven months before (e.g.: if the "Last update" is "May 2006", the last available value is from October 2005) because of the way R12 is calculated (use of six following monthly average sunspot numbers). Consequently, the user should not try to get values of R12 after six months before the "Last update".

If the value found by the program begins with a negative sign, it is *provisional* (valid for the few last available values).

To update SIDC file, the user needs to *download* monthssn.dat from SIDC website[5] in Input\R12 and to press the "Update" button.

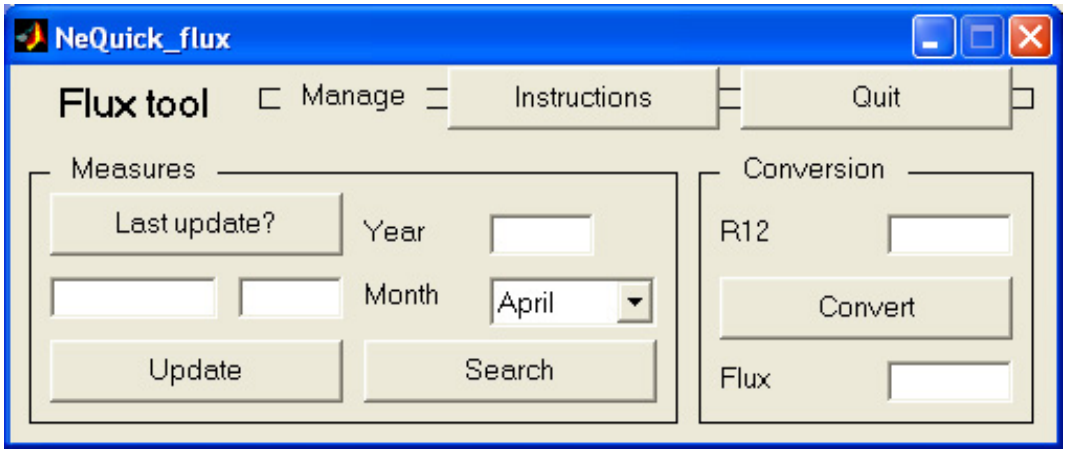

Figure 6.6: Flux module

[5] http://sidc.oma.be/sunspot-data or directly http://sidc.oma.be/DATA/monthssn.dat

6.3 Further developments

Several **new functionalities** could be added to this tool.

First of all *tests of input validity* (no negative heights, UT between 0 and 24, etc.) *and error messages* should be performed. With this version, the user must take care of the input values he gives to the program.

In order to plot *slant profiles*, an extension of NeQuick_profiles could be built to ask for latitude and longitude of the second point.

vTEC and sTEC could be calculated only for *one situation* (show one value like in NeQuick_dens) and their dependences should receive a means to *control* if the *"Global" calculation* was performed and, if not, to launch it. The *MODIP dependence* should also be implemented.

Better projections for vTEC maps could also be chosen depending on specified area.

Finally *sTEC* comparison could be performed for *several years and months.*

Chapter 7

Tests

7.1 Overall description

Thanks to the analysis tool described in chapter 6, a wide range of tests can be performed in order to characterize improvement proposals for NeQuick. A suitable sequence involves three **kinds of tests**.

1. A *profiles* analysis allows to visualize the precise consequences of the modifications.

2. Global consequences can be considered by means of a *vTEC* analysis including vTEC maps and differences study by comparison to the ITU-R baseline (computation of daily bias, maximum and RMS of absolute and relative differences - globally, by latitude, by UT).

3. Finally the *sTEC* analysis is crucial because it consists of a comparison with real data providing error values (daily bias, max and RMS of absolute and relative differences - globally, by latitude, by UT). The current version of the analysis tool is adapted to use sTEC measurements from IGS stations for every GPS satellite in sight every 10 minutes. They were extracted from RINEX files of year 2000 and 2004.

Table 7.1 gives the different formulas used in vTEC and sTEC analysis.

$\langle\rangle$ denotes an average calculation.

TEC_{ref} denotes the reference TEC value i.e. NeQuick ITU-R modelled value for vTEC analysis and GPS measurements for sTEC analysis.

TEC_{mod} denotes the corresponding modelled TEC value.

	Absolute	Relative
Bias	$\langle TEC_{ref} - TEC_{mod} \rangle$	$\left\langle \frac{TEC_{ref} - TEC_{mod}}{TEC_{ref}} \right\rangle$
Maximum	$\max\left(TEC_{ref} - TEC_{mod}\right)$	$\max\left(\frac{TEC_{ref} - TEC_{mod}}{TEC_{ref}}\right)$
RMS	$\left\langle \left(TEC_{ref} - TEC_{mod}\right)^2 \right\rangle$	$\left\langle \left(\frac{TEC_{ref} - TEC_{mod}}{TEC_{ref}}\right)^2 \right\rangle$

Table 7.1: Statistical characterization of differences in vTEC and sTEC analysis

Furthermore these tests should be realized for **both uses** of the model, physical and effective.

A thorough study implies to take **various conditions** into account following the general ionospheric variations (figure 3.6 and table 3.3).

For example, the *profiles* treatment should use

1. several positions or rather latitudes – low (Dakar (DAKA): $14.68^{\circ}N$, $-17.46^{\circ}E$), mid (ESTEC: $52.217^{\circ}N$, $4.42^{\circ}E$) and high (Ny-Alesund (NYAL): $78.9^{\circ}N$, $11.9^{\circ}E$) ;
2. several seasons – winter (December), equinox (March) and summer (June) ;
3. several solar activity levels – low ($\Phi_{12} = 63$), mid ($\Phi_{12} = 123$) and high ($\Phi_{12} = 183$) ;
4. and several times-of-day paying attention to the different longitudes – approximately 0 and 12LT (UT: 0 and 12 for Dakar, 1 and 13 for ESTEC, 2 and 14 for Ny-Alesund).

Similarly, the $vTEC$ should involve

1. several positions by means of a grid of different latitudes and longitudes – steps of 5° in latitude and 10° in longitude – with the higher endpoints at specific height – $23222km$ corresponding to the GALILEO constellation ;
2. several seasons – winter (December), equinox (March) and summer (June) ;
3. several solar activity levels – low ($\Phi_{12} = 63$), mid ($\Phi_{12} = 123$) and high ($\Phi_{12} = 183$) ;
4. and several times-of-day – two hours (0 and 12 UT) for maps and a set of hours (0 to 23 with step 1) for differences.

Finally the $sTEC$ error examination could treat

1. different positions – all available stations and satellites at $20200km$ for the GPS constellation ;
2. different seasons – winter (January) and summer (July) ;
3. different solar activity levels – high in 2000 and mid in 2004 ;
4. and different times-of-day – all available hours from 0 to 23.9 as the last measurement should be 10 minutes before midnight ;
5. particular days as the measurements vary from day to day – using their position during the year called Day-Of-Year (DOY), 1 DOY (21) and 5 DOYs (17 to 21) without geomagnetic storms ($Kp < 5$; cf. subsection 3.2.2).

In this last case, it is first necessary to list the usable files (on the basis of primary table of contents toc.txt) because

1. the available stations are not the same every day – a file called char.txt in the directory corresponding to the year allows to select the relevant stations available for the chosen DOYs ;
2. and the available UTs vary from station to station – another file named char.txt in the directory corresponding to chosen DOY is scanned in order to discard stations if they do not include all wanted UTs.

By way of example, **first results** are presented in the following sections for a physical behaviour study.

7.2 Profiles

The chosen situations allow to **understand** the **consequences of the modifications** described in subsection 5.2.2.

They correspond to **average conditions**.

1. Position: mid latitude (ESTEC: $52.217^{\circ}N,\ 4.42^{\circ}E$)
2. Season: equinox (March)
3. Solar activity level: mid ($\Phi_{12} = 123$)
4. Time-of-day: 13UT

The **resulting profiles** are presented below. Figure 7.1 shows the ITU-R baseline. In figure 7.2, unrealistic peculiarities in the height profiles are avoided thanks to simplifications from NeQuick 2002. In this case, the modification of the k parameter from NeQuick 2005a implies a denser topside (cf. figure 7.3) which can reveal itself problematic for equatorial regions as the modelled ionosphere is already too dense for these regions. NeQuick 2005b brings a "big" modification in the sense that the most important feature (anchor point F_2 layer peak) changes (cf. figure 7.4). With its less dense topside in figure 7.5, an interesting compromise with figure 7.3 seems possible from NeQuick 2006b. Finally figure 7.6 includes all modifications and shows the compromise reached for the topside.

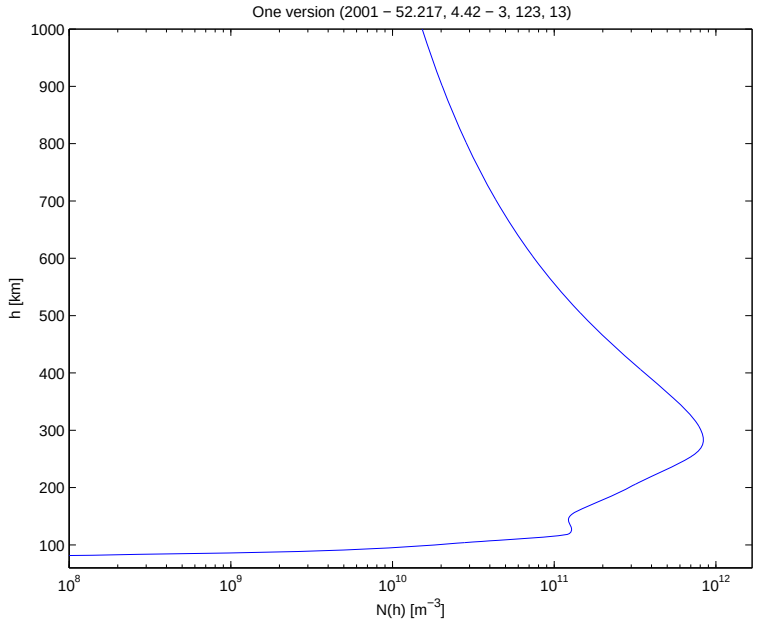

Figure 7.1: Electron density profile from NeQuick 2001 (version 1, ITU-R)

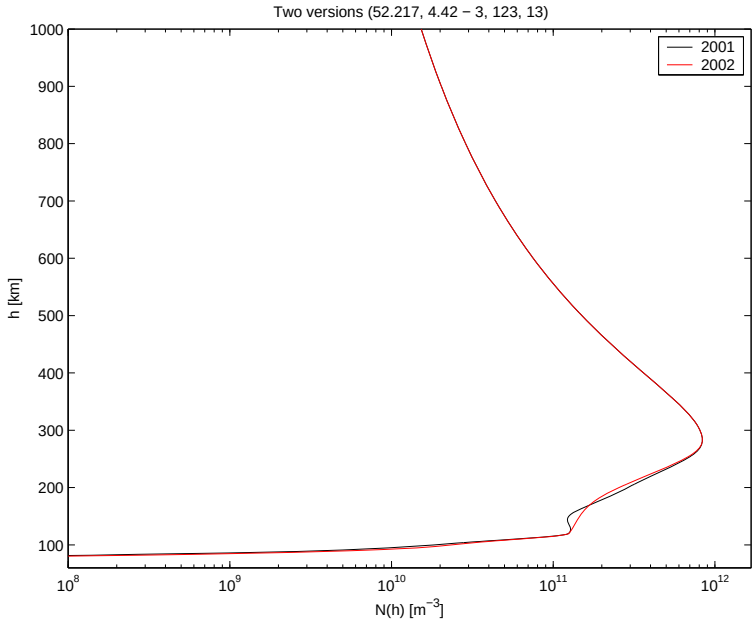

Figure 7.2: Electron density profiles comparison between NeQuick 2002 and NeQuick 2001 (version 1, ITU-R)

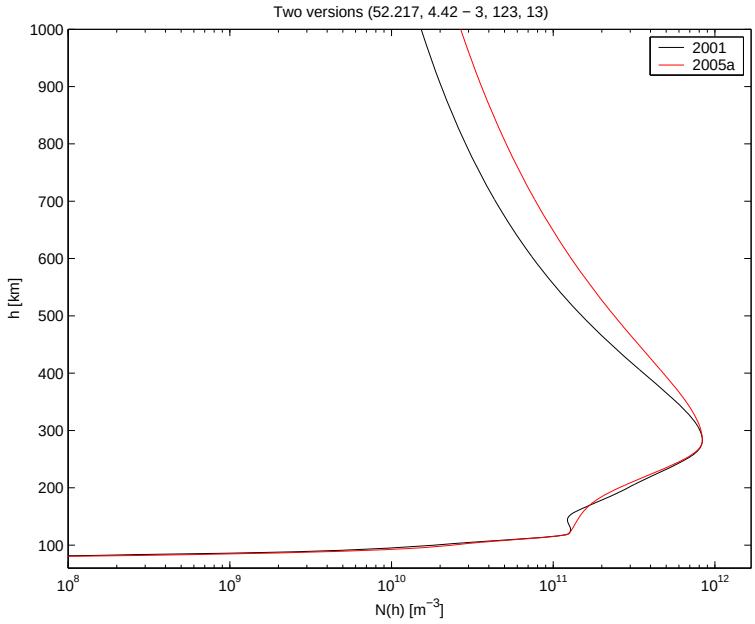

Figure 7.3: Electron density profiles comparison between NeQuick 2005a and NeQuick 2001 (version 1, ITU-R)

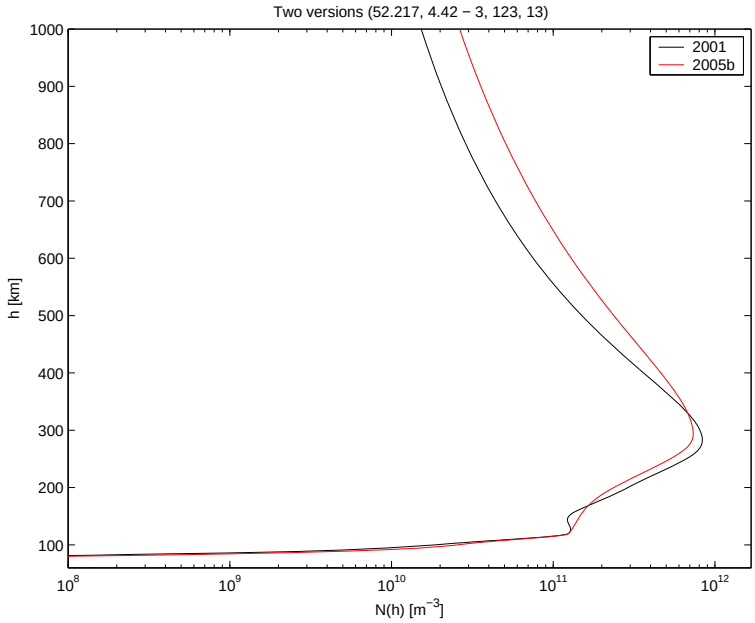

Figure 7.4: Electron density profiles comparison between NeQuick 2005b (version 2) and NeQuick 2001 (version 1, ITU-R)

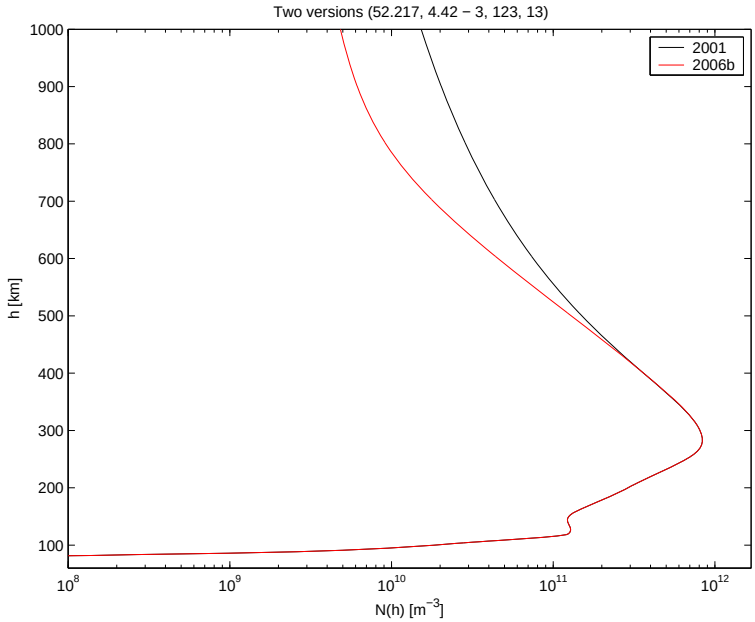

Figure 7.5: Electron density profiles comparison between NeQuick 2006b and NeQuick 2001 (version 1, ITU-R)

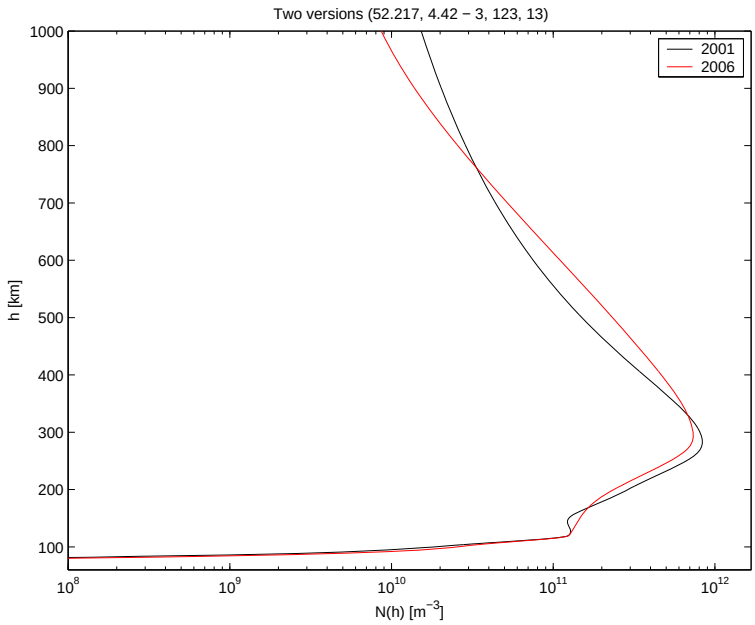

Figure 7.6: Electron density profiles comparison between NeQuick 2006 and NeQuick 2001 (version 1, ITU-R)

7.3 vTEC

The highlighted indices of improvements from previous subsection have now to be studied on a **global scale**. As a consequence,

- the global evolution will be characterized to establish whether the modifications have beneficial consequences such as a weaker latitudinal dependence of NeQuick error (cf. subsection 4.3.4) ;
- and only the main versions will be considered: versions 1 (2001, ITU-R), 2 (2005b) and 2006.

Similar **average conditions** are used.

1. Position: grid of latitude and longitude (5° in latitude and 10° in longitude)
2. Season: equinox (March)
3. Solar activity level: mid ($\Phi_{12} = 123$)
4. Time-of-day: 12UT

The first result to be presented still consists of the ITU-R reference (cf. figure 7.7). It shows the well-known feature of vTEC maps, the equatorial anomaly at the geomagnetic equator described in subsection 3.2.2) with a maximum value of 82 $TECu$. Figure 7.8 reinforces the **feeling of an improvement from NeQuick version 2** with its maximum value of 65 $TECu$ and, if the overestimation was still present, NeQuick 2006 could maybe solve the problem as it gives further lower values (58 $TECu$ in figure 7.9). However the overall shape of the map did not change so that it could only represent an offset due to its simplicity (cf. subsection 5.2.3).

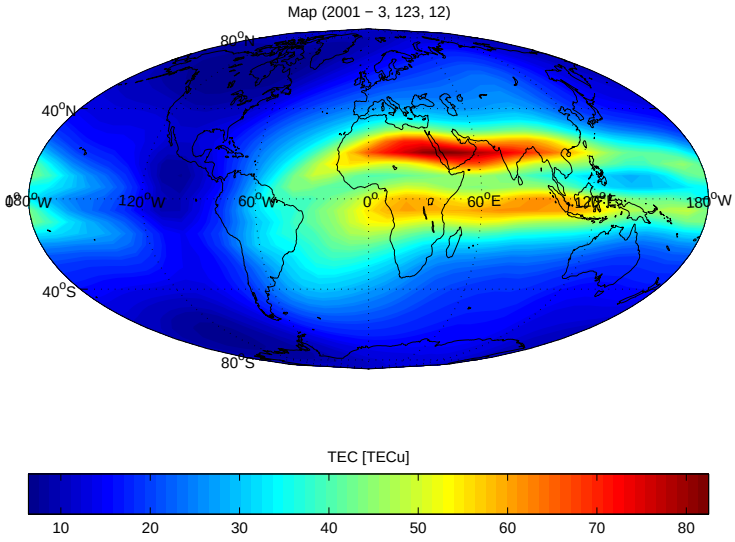

Figure 7.7: vTEC map from NeQuick 2001 (version 1, ITU-R)

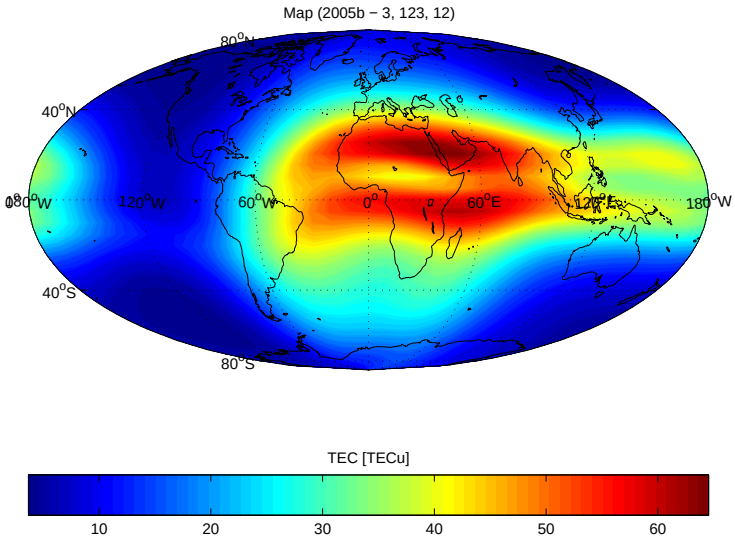

Figure 7.8: vTEC map from NeQuick 2005b (version 2)

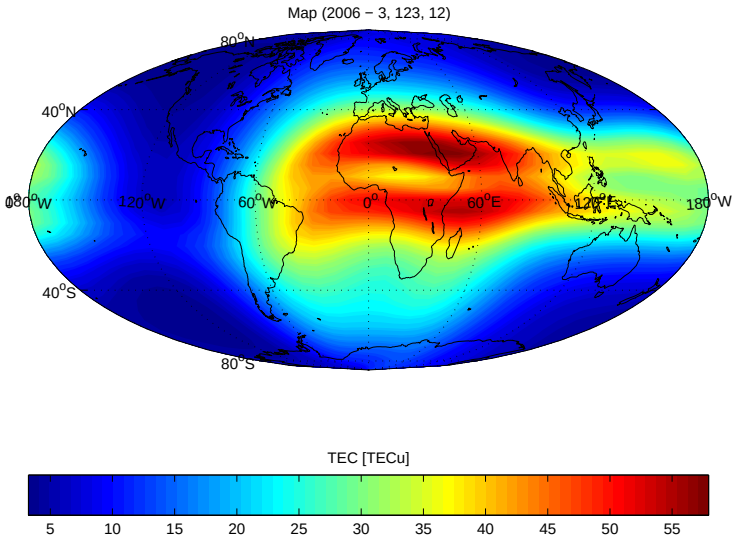

Figure 7.9: vTEC map from NeQuick 2006

7.4 sTEC

The sTEC analysis should bring the **final answer** to the question of the relevance of modifications. However only the evolution from the reference is significant as the monthly "physical" behaviour herein considered implies varying error from day to day.

According to available data, following **conditions** have been chosen.

1. Position: all available stations and satellites
2. Season: winter (January)
3. Solar activity level: high in 2000
4. Times-of-day: all available hours between 0h30 and 23h30 UT[1]
5. Days: 5 DOYs (17 to 21)

[1]The number of available stations was considerably increased without taking hours around midnight into account.

The 45 selected stations[2] are located in figures 7.10 to 7.12.

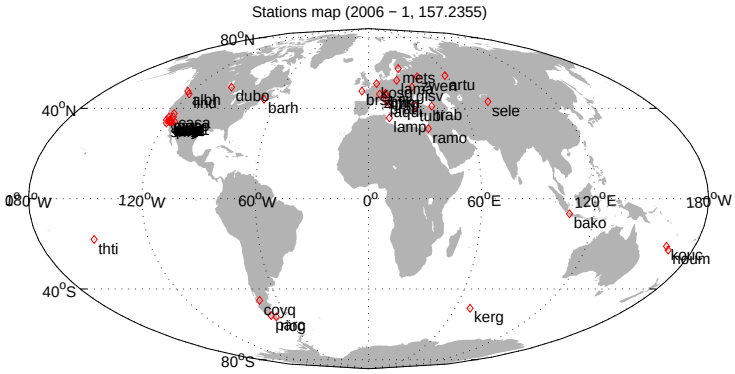

Figure 7.10: Selected stations for sTEC analysis

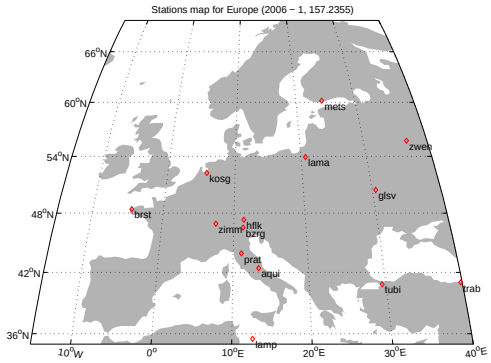

Figure 7.11: Selected European stations for sTEC analysis

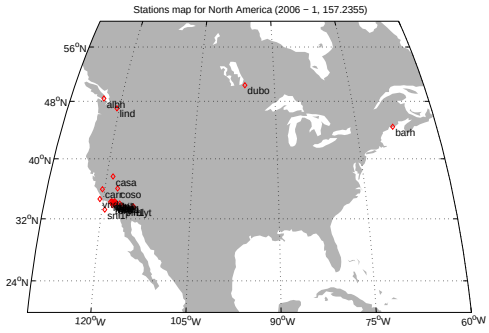

Figure 7.12: Selected North-American stations for sTEC analysis

The negative bias of NeQuick version 1 (cf. figure 7.13) highlights its average overestimation which seems quite high for chosen days regarding the RMS error of 80%. The huge maximum value comes from unrealistic 0 values in sTEC measurements supposed to include ionospheric electron densities from ground to 20200km. Figure 7.13 indicates the **correct average behaviour of NeQuick version 2** according to the almost 0 bias and the **better RMS error** of 49%. The last version (2006) seems even better because of its lower RMS error of 46% (cf. figure 7.13) but the offset effect suggested by the vTEC analysis is confirmed by the positive bias leading to an average underestimation, underlining the need for further investigation of the topside formulation.

[2]Their complete name can be found on IGS website (http://igscb.jpl.nasa.gov).

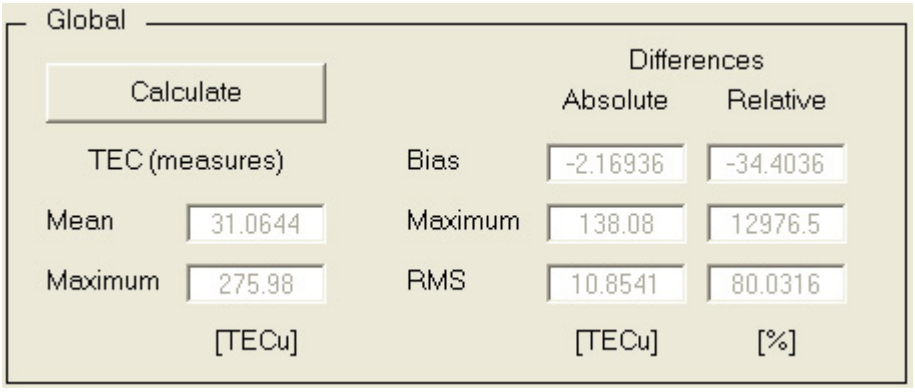

Figure 7.13: Results of sTEC analysis for NeQuick 2001 (version 1, ITU-R)

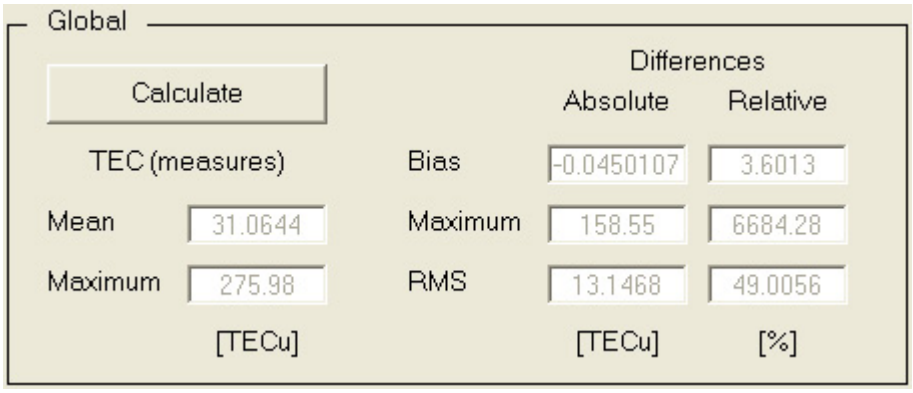

Figure 7.14: Results of sTEC analysis for NeQuick 2005b (version 2)

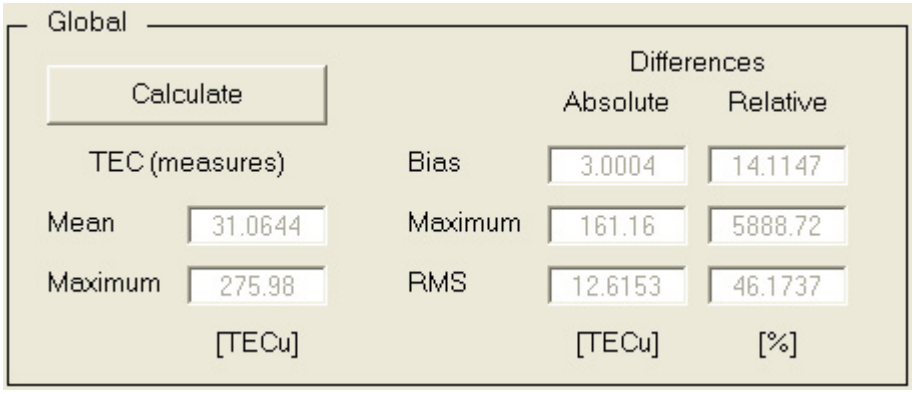

Figure 7.15: Results of sTEC analysis for NeQuick 2006

Part III

A path to the future

Chapter 8

Conclusion

8.1 Benefits for GALILEO

As intended, the present study has provided a **structured basis** for future improvements of NeQuick, including

- a deep understanding,
- a check list of noticeable issues,
- analysis tools allowing to visualize the evolution of the model constitutive parameters and results
- and first tests demonstrating the procedure to characterize possible improvements.

It has already highlighted the interest of using *NeQuick version 2 as a new baseline* as its error behaviour towards latitude shows a better agreement with reality. It should be coupled to a less simplistic topside formulation involving several layers with appropriate transitions like in the simple proposal of this study. Getting to the use of the model in GALILEO single frequency algorithm, the need of a different treatment as also been stated, such as the dismissal of negative f_0F_2 critical frequency values.

However the work is due to be *continued* through

- a broader "physical" behaviour analysis,
- topside formulations research,
- an optimization of the Az calculation method,
- intrinsic modification considerations for daily use
- and finally an "effective" use analysis.

Anyway, it was for me the occasion to be involved in team working in an **international, high-technology environment** as I got into contact with various actors from the field. Beside engineers from the GALILEO Project, I shared information with receivers specialists from some companies and scientists working on the model who are currently undergoing research about precise topics such as the transition height in the topside.

8.2 Towards further related research

To a broader extent, some **ionospheric issues absent from NeQuick** are also investigated for their impact on satellite navigation. The *ionospheric storms*, corresponding to geomagnetic storms, have already been suggested and constitute the most widespread features. *Travelling ionospheric disturbances* (TIDs) may also cause TEC variations depending on their scale, from tens of kilometres and several minutes to thousands and several hours [68]. Finally the smallest-scale structures give birth to a phenomenon called ionospheric *scintillation* resulting in loss of receiver lock on satellites signals [67].

Surprisingly navigation systems on other planets have also been imagined: **Mars Communications and Navigation satellite network** (MC&N) is also concerned by ionospheric related questions [65]. It consists of a constellation of microsatellites (Microsats) and one or more relatively large Mars Areostationary Relay Satellites (MARSats) (cf. figure 8.1). The Microsats would serve both as *communication relays* between Mars exploration devices and the Earth and as *navigational aids* allowing for example to improve drastically the precision of approach and surface descent of probes which is currently targeted from the Earth by means of Deep Space Network (DSN) tracking. The current uncertainty of position, about $15km$ when $125km$ above the surface and about $75km$ when on the surface, could decrease, at 125 km above the surface, to less than 1 km and, on the surface, to within 10 to 100 meters!

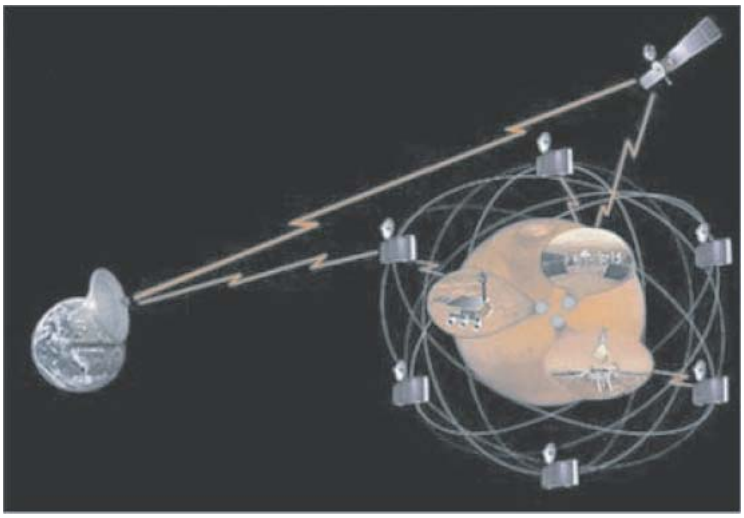

Figure 8.1: Mars Communications and Navigation satellite network (MC&N) [66]

In order to *assess the impact of Mars ionosphere* – dominated by 0_2^+ ions – on the potential satellite navigation systems, sets of electron density versus altitude profiles from the Mars Global Surveyor radio occultation experiment have been examined. These local measurements were extended to more global morphologies showing quite low values of TEC by comparison to Earth characteristic measurements, of an order of magnitude of 1 $TECu$.

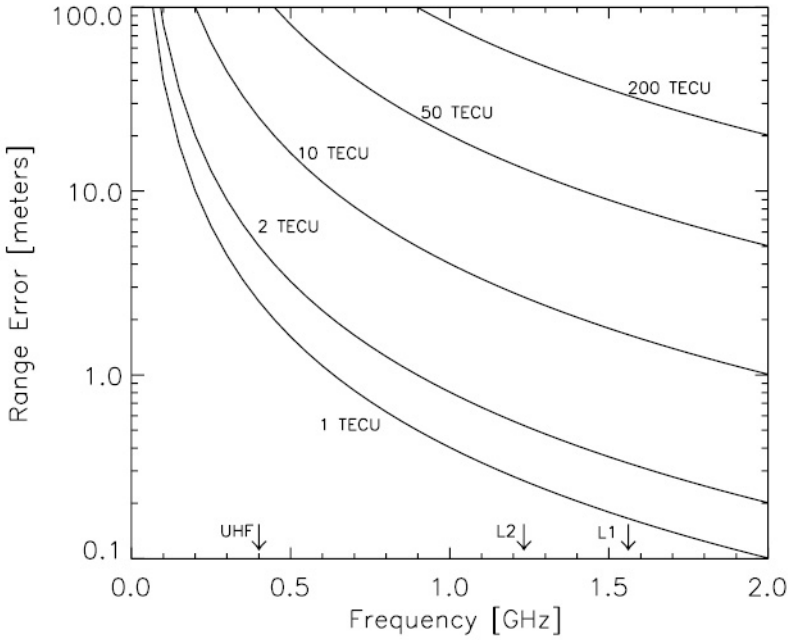

Figure 8.2: Ionospheric range errors for different vTEC values versus the frequency used in a satellite navigation system [65]

These ridiculously low values for a terrestrial navigation system could however lead to significant errors for the MC&N system considering its possible lower operating frequencies, in the low end of the UHF band (cf. figure 8.2).

All these examples show clearly that navigation and ionospheric effects in particular are promised to a fruitful future. Research in those growing and interesting fields will continue to allow people to say, despite of the different sources of errors affecting satellite navigation:

And yet it does work!

Part IV

Appendixes

Appendix A

NeQuick details

A.1 Variables and parameters

Variables and units The main variables used in NeQuick and their units are given in table A.1.

Position and geomagnetism	
Height	h $[km]$
Latitude	ϕ [°]
Longitude	θ [°]
Magnetic latitude	λ [°]
Magnetic dip	I [°]
Modified dip latitude	μ [°] (cf. equation 3.5)
Solar activity	
Monthly mean of $F10.7$	Φ $[10^{-22}\ W\ m^{-2}\ Hz^{-1}]$
Monthly smoothed value of $F10.7$	Φ_{12} $[10^{-22}\ W\ m^{-2}\ Hz^{-1}]$
Monthly smoothed sunspot number	R_{12} (cf. equation 3.3)
Time and season	
Universal time	UT [hours]
Local time	LT [hours]
Month	month
Zenith angle of the sun	χ [°]

Table A.1: Main variables and units for NeQuick

Parameters and units The main parameters used in NeQuick and their units are given in table A.2.

Electron density of layer L	N^L $[10^{11}\ el.\ m^3]$
Peak electron density of layer L	N^L_{max} $[10^{11}\ el.\ m^3]$
Global electron density at the peak height of layer L	NmL $[10^{11}\ el.\ m^3]$
Peak height of layer L	h^L_{max} $[km]$
Thickness parameter of layer L	B^L $[km]$
Critical frequency of of layer L	f_0L $[MHz]$
Transmission factor	$M(3000)F_2$

Table A.2: Main parameters and units for NeQuick

A.2 Version 1 (ITU-R)

Electron density For the *lowest part* of the ionosphere, a Chapman formulation (equation A.3) is used as described in [42]. The equation for b is translated from the code[1].

$$N_{low}(h) = N_{bot}(100)\ e^{1-\ b\frac{h-100}{10}\ -\ e^{-\frac{h-100}{10}}}$$

$$b = 1 - \frac{1}{10\ N_{bot}(100)} \left[\frac{4\ N^{F_2}_{max} \left(1 - e^{\frac{100-h^{F_2}_{max}}{B^{F_2}_{bot}}}\right) e^{\frac{100-h^{F_2}_{max}}{B^{F_2}_{bot}}}}{B^{F_2}_{bot} \left(1 + e^{\frac{100-h^{F_2}_{max}}{B^{F_2}_{bot}}}\right)^3} \right.$$
$$+ \frac{4\ N^{F_1}_{max} \left(1 - e^{\zeta(100)\frac{100-h^{F_1}_{max}}{B^{F_1}_{bot}}}\right) e^{\zeta(100)\frac{100-h^{F_1}_{max}}{B^{F_1}_{bot}}}}{B^{F_1}_{bot} \left(1 + e^{\zeta(100)\frac{100-h^{F_1}_{max}}{B^{F_1}_{bot}}}\right)^3}$$
$$\left. + \frac{4\ N^{E}_{max} \left(1 - e^{\zeta(100)\frac{100-h^{E}_{max}}{B^{E}_{bot}}}\right) e^{\zeta(100)\frac{100-h^{E}_{max}}{B^{E}_{bot}}}}{B^{E}_{bot} \left(1 + e^{\zeta(100)\frac{100-h^{E}_{max}}{B^{E}_{bot}}}\right)^3} \right] \quad \text{(A.1)}$$

[1]The second and third terms in the parenthesis corresponding to the F_1 and E layers are equalled to 0 if $|\zeta(100)\frac{100-h^L_{max}}{B^L}| > 25$.

$$\zeta(100) = e^{\frac{10}{1+2|100-h_{max}^{F_2}|}}$$

The shape of the following equations can be found into [62].

For the *bottomside* (equation A.2 when $100km \leq h \leq h_{max}^{F_2}$), the shape of the sum was first defined into [35]. The height h determines whether to use the top thickness parameter B_{top}^{L} or the bottom one B_{bot}^{L} [2].

$$\begin{aligned} N_{bot}(h) &= N^{F_2}(h) + N^{F_1}(h) + N^{E}(h) \\ &= 4\ N_{max}^{F_2}\ \frac{e^{\frac{h-h_{max}^{F_2}}{B^{F_2}}}}{\left(1+e^{\frac{h-h_{max}^{F_2}}{B^{F_2}}}\right)^2} + 4\ N_{max}^{F_1}\ \frac{e^{\zeta(h)\frac{h-h_{max}^{F_1}}{B^{F_1}}}}{\left(1+e^{\zeta(h)\frac{h-h_{max}^{F_1}}{B^{F_1}}}\right)^2} \\ &\quad + 4\ N_{max}^{E}\ \frac{e^{\zeta(h)\frac{h-h_{max}^{E}}{B^{E}}}}{\left(1+e^{\zeta(h)\frac{h-h_{max}^{E}}{B^{E}}}\right)^2} \end{aligned} \tag{A.2}$$

$$\zeta(h) = e^{\frac{10}{1+2|h-h_{max}^{F_2}|}}$$

The *topside* ($h > h_{max}^{F_2}$) corresponds to a semi-Epstein layer (cf. equation 4.1) with H as thickness parameter.

$$N_{top}(h) = 4\ N_{max}^{F_2}\ \frac{e^{\frac{h-h_{max}^{F_2}}{H}}}{\left(1+e^{\frac{h-h_{max}^{F_2}}{H}}\right)^2} \tag{A.3}$$

Peak electron densities The following equation can be found into [48] taking into account the fading out effect described in [42][3].

$$N_{max}^{F_2} = NmF_2 \tag{A.4}$$

$$N_{max}^{F_1} = NmF_1 - N^{F_2}(h_{max}^{F_1}) \tag{A.5}$$

$$N_{max}^{E} = NmE - N^{F_1}(h_{max}^{E}) - N^{F_2}(h_{max}^{E}) \tag{A.6}$$

The *global electron densities* at the peak height of layer L NmL are calculated from the critical frequencies f_0L by means of equation 3.2 repeated here under.

[2] The second and third terms corresponding to the F_1 and E layers are equalled to 0 if $|\zeta(h)\frac{h-h_{max}^{L}}{B^{L}}| > 25$.

[3] $N_{max}^{F_1}$ and N_{max}^{E} are limited at a minimum value of 0.005. The transition is computed by means of equation A.27 with $\alpha = 60$.

$$NmL = 0.124\ f_0 L^2 \tag{A.7}$$

Peak heights The following equations can be found into [48] and is based on a formula from [34][4].

$$\begin{aligned} h_{max}^{F_2} &= \frac{1490\ MF}{M + DM} - 176 \\ DM &= \frac{0.253}{f_0F_2/f_0E - 1.215} - 0.012 \\ MF &= M\sqrt{\frac{0.0196M^2 + 1}{1.2967M^2 - 1}} \\ M &= M(3000)F_2 \end{aligned} \tag{A.8}$$

The following equation can be found into [48] and was originally defined in [45][5].

$$h_{max}^{F_1} = 108.8 + 14\ NmF_1 + 0.71\ |I| \tag{A.9}$$

$$h_{max}^{E} = 120km \tag{A.10}$$

Thickness parameters The following equations can be found into [48].

$$\begin{aligned} B_{bot}^{F_2} &= \frac{0.385\ NmF_2}{0.01\ (dN/dh)_{max}} \\ \ln\left((dN/dh)_{max}\right) &= -3.467 + 0.857 \ln\left(f_0F_2\right)^2 \\ &\quad + 2.02 \ln\left(M(3000)F_2\right) \end{aligned} \tag{A.11}$$

$(dN/dh)_{max}$ $[10^9\ el.\ m^{-3}\ km^{-1}]$ is the gradient of $N(h)$ at the characteristic point at the base of the F_2 layer i.e. the first derivative of equation 4.1 for F_2 layer at the inflection point.

The following equations can be found into [48] and [49] ([62] for a correct version of H)[6].

[4]The ratio f_0F_2/f_0E is limited at a minimum value of 1.75. The transition is computed by means of equation A.27 with $\alpha = 20$.

[5]The transition at $I = 0$ is computed by means of equation A.27 with $\alpha = 12$.

[6]The transitions at $k = 2$ and $k = 8$ are computed by means of equation A.27 with $\alpha = 1$.

$$H = B_{top}^{F_2}\left(1 + \frac{12.5(h - h_{max}^{F_2})}{100B_{top}^{F_2} + 0.125(h - h_{max}^{F_2})}\right) \tag{A.12}$$

$$B_{top}^{F_2} = \frac{k\ B_{bot}^{F_2}}{\nu}$$

$$k = \begin{cases} -7.77 + 0.097\left(\frac{h_{max}^{F_2}}{B_{bot}^{F_2}}\right)^2 + 0.153\ NmF_2 & \text{from October to March} \\ 6.705 - 0.014\ R_{12} - 0.008\ h_{max}^{F_2} & \text{from April to September} \end{cases} \tag{A.13}$$

$$2 \leq k \leq 8$$

$$\nu = (0.041163\ x - 0.183981)\ x + 1.424472$$

$$x = \frac{k\ B_{bot}^{F_2} - 150}{100}$$

The formula for $B_{top}^{F_1}$ (from [48]) is obtained from a simplification of the top F_1 semi-Epstein layer (equation 4.1 adapted to F_1), the shape of F_1 peak amplitude from equation 4.5 and the same assumption as in equation 4.6[7].

$$\begin{aligned} NF_1(h_{max}^{F_2}) &\approx 4\ N_{max}^{F_1}\ e^{-\frac{h_{max}^{F_2} - h_{max}^{F_1}}{B_{top}^{F_1}}} \\ &\approx 4\ \left(NmF_1 - N^{F_2}(h_{max}^{F_1})\right)\ e^{-\frac{h_{max}^{F_2} - h_{max}^{F_1}}{B_{top}^{F_1}}} \\ &\approx 0.1\ NmF_1 \end{aligned} \tag{A.14}$$

$$B_{top}^{F_1} = \frac{h_{max}^{F_2} - h_{max}^{F_1}}{\ln\left(4\ \frac{NmF_1 - N^{F_2}(h_{max}^{F_1})}{0.1\ NmF_1}\right)} \tag{A.15}$$

[7]The ratio $4\frac{NmF_1 - N^{F_2}(h_{max}^{F_1})}{0.1\ NmF_1}$ is limited at a minimum value of 1.5. The transition is computed by means of equation A.27 with $\alpha = 20$.
$B_{top}^{F_1}$ is limited at a maximum value of $B_{bot}^{F_2} + 50$. The transition is computed by means of equation A.27 with $\alpha = 20$.

The following equations can be found into [48].

$$B_{bot}^{F_1} = 0.7 B_{top}^{F_1} \tag{A.16}$$

$$B_{top}^{E} = \begin{cases} 0.5\ B_{top}^{F_1} & \text{if } F_1 \text{ is present} \\ 7km & \text{if not} \end{cases} \tag{A.17}$$

$$B_{bot}^{E} = 5km \tag{A.18}$$

Critical frequencies and transmission factor The shape of the following equations, which were originally defined into [41], can be found into [42][8].

$$\begin{gathered} (f_0 E)^2 = a_E^2\ \sqrt{\Phi}\ \cos^{0.6}\chi_{eff} + 0.49 \\ a_E = 1.112 - 0.019\ s_E\ \frac{e^{0.3\phi} - 1}{e^{0.3\phi} + 1} \\ s_E = \begin{cases} -1 & \text{for "Winter" (November to February} \\ 0 & \text{for "Equinox" (March, April, September and October)} \\ 1 & \text{for "Summer" (May to August)} \end{cases} \\ \chi_{eff} = \begin{cases} \chi & \text{for daytime } (\chi < \chi_0) \\ 90 - 0.24\ e^{20-0.2\chi} & \text{for nighttime } (\chi > \chi_0) \end{cases} \end{gathered} \tag{A.19}$$

$\chi_0 = 86.23^\circ$ denotes the limit between day and night.

$$f_0 F_1 = \begin{cases} 1.4\ f_0 E & \text{for daytime } (\chi < \chi_0) \\ 0 & \text{for nighttime } (\chi > \chi_0) \end{cases} \tag{A.20}$$

The following equation can be found into [25]. This general form of the *numerical map* function Ω providing the evaluation of the monthly median of f_0F_2 or $M(3000)F_2$ has the shape of a Fourier time series.

$$\Omega(\phi, \theta, T) = \sum_{k=0}^{K} U_{0,k} G_k(\phi, \theta) + \sum_{j=1}^{H} \sum_{k=0}^{K} \left[U_{2j,k} \cos(jT) + U_{2j-1,k} \sin(jT) \right] G_k(\phi, \theta) \tag{A.21}$$

[8] The transitions between day and night for χ_{eff} and f_0F_1 at $\chi = \chi_0$ are computed by means of equation A.27 with $\alpha = 12$.

T denotes the universal time UT expressed as an angle ($-180^\circ \leq T \leq 180^\circ$).

H denotes the maximum number of harmonics used to represent the diurnal variation (6 for f_0F_2 and 4 for $M(3000)F_2$).

The coefficients $U_{i,k}$ are calculated from the CCIR files by linear combination with R_{12} as weighting coefficient (low solar activity: $R_{12} = 0$, $U^-_{i,k}$; high solar activity: $R_{12} = 100$, $U^+_{i,k}$).

$$U_{i,k} = U^-_{i,k}\left(1 - \frac{R_{12}}{100}\right) + U^+_{i,k}\,\frac{R_{12}}{100} \tag{A.22}$$

The geographic coordinate functions G_k are composed of three trigonometric functions in the following way.

$$G_k(\phi,\theta) = \sin^{q(k)}\mu\ \cos^{m(k)}\phi \left\{ \begin{array}{c} \cos \\ \sin \end{array} \right\} (m(k)\theta) \tag{A.23}$$

$q(k)$, the order in modified dip latitude, and $m(k)$, the order in longitude, are linked to the order of current harmonic.

The following formulation allows to *understand the code easier*.

$$\begin{aligned}\Omega(\mu,\phi,\theta,UT) = &\sum_{L=1}^{q(1)+1} C_{i(1,L)}(UT)\ \sin^{L-1}\mu \\ &+ \sum_{j=2}^{k_1}\sum_{L=1}^{q(j)+1}\left[C_{i(j,L)}(UT)\ \cos\left((j-1)\theta\right) + C_{i(j,L)+1}(UT)\ \sin\left((j-1)\theta\right)\right] \\ &\cos^{j-1}\phi\ \sin^{L-1}\mu\end{aligned} \tag{A.24}$$

The first term could be included in the sum noticing that, for $j = 1$, $\cos^{j-1}\phi = 1$, $\cos\left((j-1)\theta\right) = 1$ and $\sin\left((j-1)\theta\right) = 0$.

$q(j)$ denotes the maximum order in modified dip latitude for current order in longitude.

k_1 denotes the maximum order in longitude.

$$i(j,L) = \left\{ \begin{array}{ll} L & \text{if } j = 1 \\ q(1) + 2\left(\sum_{l=2}^{j-1} q(l) + j + L\right) - 4 & \text{else} \end{array} \right.$$

$$C_i(UT) = U_{1,i} + \sum_{j=1}^{H} U_{2j,i}\sin\left(j\left(\frac{\pi}{12}UT - \pi\right)\right) + U_{2j+1,i}\cos\left(j\left(\frac{\pi}{12}UT - \pi\right)\right) \tag{A.25}$$

Implementation tools To represent the *piecewise function* $f(x)$ (cf. equation A.26), NeQuick uses an exponential transition (cf. equation A.27) depending on the (steepness) parameter α related to steepness of the transition between the two pieces $f_+(x)$ and $f_-(x)$. An interesting interpretation of this formulation is obtained considering the limits for $x \to \pm\infty$.

$$f(x) = \begin{cases} f_+(x) & \text{if } x > 0 \\ f_-(x) & \text{if } x < 0 \end{cases} \tag{A.26}$$

The following equation is translated from the code.

$$f(x) = \frac{f_+(x)\ e^{\alpha x} + f_-(x)}{e^{\alpha x} + 1} \tag{A.27}$$

Finally it is important to mention that NeQuick *restricts the argument of exponential functions* within the interval $[-80, 80]$ to avoid extreme values which could result (cf. equation A.28).

$$e^x_* = \begin{cases} e^{80} \approx 5.5406\ 10^{34} & \text{if } x > 80 \\ e^x & \text{if } -80 \leq x \leq 80 \\ e^{-80} \approx 1.8049\ 10^{-35} & \text{if } x < -80 \end{cases} \tag{A.28}$$

A.3 Version 2

Epstein parameters The first modifications related to the *peak electron densities* and $h^{F_2}_{max}$ are translated from the code as they are not published yet.

As a consequence of the modified formulation of f_0F_1 (cf. equation A.35), $N^{F_1}_{max}$ is equalled to 0 if $f_0F_1 \leq 0.5$ and N^E_{max} is obtained from equation A.6 taking into account the disappearing of the F_1 layer. In the other case, $N^{F_1}_{max}$ and N^E_{max} are calculated by means five successive iterations of equations A.29 and A.6[9].

$$N^{F_1}_{max} = NmF_1 - N^{F_2}(h^{F_1}_{max}) - N^E(h^{F_1}_{max}) \tag{A.29}$$

The roles of $h^{F_2}_{max}$ and $M(3000)F_2$ have been inverted as $h^{F_2}_{max}$ is now computed by means of a numerical map (cf. equation A.37).

The following modifications to the equations in section A.2 are described into [62].

[9] N^E_{max} is still limited at a minimum value of 0.005 and the transition is still computed by means of equation A.27 with $\alpha = 60$.
At each iteration, $N^{F_1}_{max}$ is limited at a minimum value of 0.8 NmF_1. The transition is computed by means of equation A.27 with $\alpha = 1$.

$$h_{max}^{F_1} = \frac{h_{max}^{F_2} + h_{max}^{E}}{2} \tag{A.30}$$

$$\begin{gathered} B_{top}^{F_2} = k\ B_{bot}^{F_2} \\ k = 3.22 - 0.0538\ f_0F_2 - 0.00664\ h_{max}^{F_2} + 0.113\frac{h_{max}^{F_2}}{B_{bot}^{F_2}} + 0.00257\ R_{12} \\ k \geq 1 \end{gathered} \tag{A.31}$$

$$B_{top}^{F_1} = 0.3\ (h_{max}^{F_2} - h_{max}^{F_1}) \tag{A.32}$$

$$B_{bot}^{F_1} = 0.5\ (h_{max}^{F_1} - h_{max}^{E}) \tag{A.33}$$

$$B_{top}^{E} = \max \left\{ \begin{array}{c} 0.5\ (h_{max}^{F_1} - h_{max}^{E}) \\ 7km \end{array} \right\} \tag{A.34}$$

Ionosonde parameters and $h_{max}^{F_2}$ The following modifications to equation A.20 are described into [62].

$$f_0F_1 = \left\{ \begin{array}{ll} 1.4\ f_0E & f_0E \geq 2 \\ 0 & f_0E < 2 \\ 0.85\ 1.4\ f_0E & 1.4\ f_0E > 0.85\ f_0F_2 \end{array} \right. \tag{A.35}$$

The last condition represents a 15% reduction when f_0E is too close to f_0F_2.

As above-mentioned, the roles of $h_{max}^{F_2}$ and $M(3000)F_2$ have been inverted so that

- Ω is now equal to f_0F_2 or $h_{max}^{F_2}$ in equation A.37
- and $M(3000)F_2$ is now calculated from $h_{max}^{F_2}$ by means of the following equation.

$$M(3000)F_2 = \frac{1490}{hmF2 + 176} - 0.3 \tag{A.36}$$

The following modification to equation A.21 associated to the simplified CCIR files (CCsim) is translated from the code. It consists of a *spherical harmonics approximation* which does not use latitude anymore and replaces universal time by local time. The shape of the associated Legendre polynomials P_n^m can be found in [64] taking into account the fact that the Condon-Shortley phase $(-1)^m$ is not included. For the chosen approximation, the maximum orders are $n = 6$ and $m = 3$ (the polynomials with $m > n$ are assumed 0).

$$\begin{aligned}\Omega(\mu, \theta, LT) = C_0(LT) + \sum_{n=1}^{6} C_{j(n,0)}(LT)\ P_n^0(-\sin\mu) \\ + \sum_{n=1}^{6}\sum_{m=1}^{3}\left[C_{j(n,m)}(LT)\ \cos(m\theta) + C_{k(n,m)}(LT)\ \sin(m\theta)\right]\ P_n^m(-\sin\mu)\end{aligned} \tag{A.37}$$

The first terms could still be included in the sum for $n = 0$ and $m = 0$.

$$j(n,m) = \begin{cases} \frac{n(n+1)}{2} + m & \text{if } n \leq 2 \\ 4n - 6 + m & \text{else} \end{cases}$$

$$k(n,m) = \begin{cases} \frac{n(n-1)}{2} + 21 + m & \text{if } n \leq 2 \\ 3n + 15 + m & \text{else} \end{cases}$$

$$C_k(LT) = U_{0,k} + \sum_{i=0}^{3} U_{i,k}\cos\left(i\frac{\pi}{12}LT\right) - U_{i+3,k}\sin\left(i\frac{\pi}{12}LT\right) \tag{A.38}$$

List of Figures

1.1 Galileo Galilei (1564 - 1642) - Original portrait by Justus Sustermans painted in 1636 [1] 1

2.1 Satellite navigation principle [6] 6
2.2 GPS satellite (Block IIA) (Credit: NASA) 8
2.3 GPS constellation [6] 8
2.4 GALILEO satellite (Credit: ESA) 11
2.5 GALILEO constellation (Credit: ESA) 11
2.6 Different components of the positioning error 12

3.1 Possible subdivisions of the Earth's atmosphere [28] 14
3.2 Global profile of electron density, gas density and intensity of solar radiation with altitude [28] 15
3.3 Typical bottomside vertical electron density profile 15
3.4 General behaviour of the sunspot number (Credit: SIDC, RWC Belgium, World Data Center for the Sunspot Index, Royal Observatory of Belgium) 17
3.5 vTEC map example from NeQuick version 1 (ITU-R) (May, average solar flux – $\Phi = 100$ –, 15h universal time) 18
3.6 General ionospheric variations 19
3.7 Ray geometry (sender on Earth) for different frequencies [29] . . 20
3.8 Elevation angle $\frac{\pi}{2} - a_T$ as a function of f/f_0 - Distance as parameter [29] 20
3.9 Comparison between sunspot numbers (Credit: SIDC, RWC Belgium, World Data Center for the Sunspot Index, Royal Observatory of Belgium) 22
3.10 Relationship between R_{12} and Φ_{12} [23] 23
3.11 Shape of μ 24

4.1 IRI vTEC map example [51] . . . 28
4.2 KLOBUCHAR vTEC map example [51] . . . 29
4.3 KLOBUCHAR algorithm scheme [51] . . . 29
4.4 NeQuick vTEC map example [51] . . . 30
4.5 NeQuick algorithm scheme [51] . . . 31
4.6 Peak amplitude N_{max} sensibility . . . 32
4.7 Peak height h_{max} sensibility . . . 33
4.8 Thickness parameter B sensibility . . . 33
4.9 Bottomside profile example (ESTEC location – $52.217^{\circ}N$, $4.42^{\circ}E$ –, May, average solar flux – $\Phi_{12} = 100$ –, midday universal time) 34
4.10 Bottomside profile example from NeQuick version 1 (ITU-R) (ESTEC location – $52.217^{\circ}N$, $4.42^{\circ}E$ –, May, average solar flux – $\Phi_{12} = 100$ –, midday universal time) . . . 37
4.11 Profile example from NeQuick version 1 (ITU-R) (ESTEC location – $52.217^{\circ}N$, $4.42^{\circ}E$ –, May, average solar flux – $\Phi_{12} = 100$ –, midday universal time) . . . 38
4.12 NeQuick structure . . . 40
4.13 slQu structure . . . 43
4.14 Principle of the effective ionization level Az . . . 44
4.15 GALILEO single-frequency algorithm . . . 45

5.1 Analysis structure . . . 48
5.2 $B_{top}^{F_1}$ map from NeQuick 2001 (November, $\Phi_{12=122}$, 11h universal time) . . . 50
5.3 $B_{top}^{F_1}$ map from NeQuick 2002 (November, $\Phi_{12=122}$, 11h universal time) . . . 50
5.4 Transition between 0^+ and H^+ dominated ionosphere [60] . . . 53
5.5 Proposed topside formulations and NeQuick version 1 (ITU-R) (ESTEC location – $52.217^{\circ}N$, $4.42^{\circ}E$ –, May, average solar flux – $\Phi_{12} = 100$ –, midday universal time) . . . 53
5.6 f_0F_2 map for $Az = 10$ (ESTEC location – $52.217^{\circ}N$, $4.42^{\circ}E$ –, May, midnight universal time) . . . 54
5.7 New "effective" limits . . . 55

6.1 Main GUI . . . 58
6.2 Electron densities module . . . 58

6.3 Profiles module 61
6.4 vTEC analysis module 63
6.5 sTEC analysis module 65
6.6 Flux module 66

7.1 Electron density profile from NeQuick 2001 (version 1, ITU-R) . 71
7.2 Electron density profiles comparison between NeQuick 2002 and NeQuick 2001 (version 1, ITU-R) 72
7.3 Electron density profiles comparison between NeQuick 2005a and NeQuick 2001 (version 1, ITU-R) 72
7.4 Electron density profiles comparison between NeQuick 2005b (version 2) and NeQuick 2001 (version 1, ITU-R) 73
7.5 Electron density profiles comparison between NeQuick 2006b and NeQuick 2001 (version 1, ITU-R) 73
7.6 Electron density profiles comparison between NeQuick 2006 and NeQuick 2001 (version 1, ITU-R) 74
7.7 vTEC map from NeQuick 2001 (version 1, ITU-R) 75
7.8 vTEC map from NeQuick 2005b (version 2) 75
7.9 vTEC map from NeQuick 2006 76
7.10 Selected stations for sTEC analysis 77
7.11 Selected European stations for sTEC analysis 77
7.12 Selected North-American stations for sTEC analysis 77
7.13 Results of sTEC analysis for NeQuick 2001 (version 1, ITU-R) . 78
7.14 Results of sTEC analysis for NeQuick 2005b (version 2) 78
7.15 Results of sTEC analysis for NeQuick 2006 78

8.1 Mars Communications and Navigation satellite network (MC&N) [66] 82
8.2 Ionospheric range errors for different vTEC values versus the frequency used in a satellite navigation system [65] 82

List of Tables

2.1 Comparison between GPS and GALILEO 11
2.2 Different components of the residual positioning error [14] . . . 13

3.1 Horizontal layers in the ionosphere [28] 16
3.2 Typical values of solar indices 23
3.3 Main variables for general ionospheric variations 24

4.1 Epstein parameters corresponding to figure 4.9 34
4.2 Ionosonde parameters and peak height electron densities corresponding to figure 4.9 36

7.1 Statistical characterization of differences in vTEC and sTEC analysis 69

A.1 Main variables and units for NeQuick 85
A.2 Main parameters and units for NeQuick 86

Bibliography

References for chapter 1

[1] O'Connor, J. J., Robertson, E. F. *The MacTutor History of Mathematics archive: Galileo Galilei* [on line]. St Andrews: University of St Andrews, 2002. Available on http://www-history.mcs.st-andrews.ac.uk/Mathematicians/Galileo.html. (cited May 29th, 2006)

References for chapter 2

[2] Arbesser-Rastburg, B. "Propagation issues for the GALILEO project". Presented at the *European Conference Propagation and Systems (ECPS) 2005*, Brest, 2005.

[3] Benedicto, J., Dinwiddy, S. E., Gatti, G., et al. *GALILEO: Satellite System Design and Technology Developments* [on line]. Noordwijk: ESA, 2000, 21 p. Available on http://esamultimedia.esa.int/docs/galileo_world_paper_Dec_2000.pdf. (cited February 17th, 2006)

[4] ESA. Navigation. *The future - GALILEO* [on line]. Available on http://www.esa.int/esaNA/galileo.html. (cited February 17th, 2006)

[5] EU. EC. Directorate-General Energy and Transport. *GALILEO* [on line]. Available on http://ec.europa.eu/dgs/energy_transport/galileo. (cited February 17th, 2006)

[6] FAA. Satellite Navigation Product Teams. *Global Positioning System* [on line]. Available on http://gps.faa.gov/GPSbasics/index.htm. (cited May 28th, 2006)

[7] Falcone, M., Erhard, P., Hein, G. W. "GALILEO". In Kaplan, E., Hegarty, C. J. Eds. *Understanding GPS: Principles and Applications*. 2nd ed. Boston: Artech House, 2005, Chap. 10, p. 1-20. ISBN 1-58053-894-0

[8] JPO. *NAVSTAR Global Positioning System* [on line]. Available on http://gps.losangeles.af.mil. (cited May 28th, 2006)

[9] GJU. *GALILEO Joint Undertaking* [on line]. Available on http://www.galileoju.com. (cited February 17th, 2006)

[10] Kaplan, E. "Introduction". In Kaplan, E., Hegarty, C. J. Eds. *Understanding GPS: Principles and Applications*. 2nd ed. Boston: Artech House, 2005, Chap. 1, p. 1-20. ISBN 1-58053-894-0

[11] Kaplan, E., Leva, L., Milbert, D. et al. "Fundamentals of Satellite Navigation". In Kaplan, E., Hegarty, C. J. Eds. *Understanding GPS: Principles and Applications*. 2nd ed. Boston: Artech House, 2005, Chap. 2, p. 21-66. ISBN 1-58053-894-0

[12] Parkinson, B. W. "GPS Error Analysis". In Parkinson, B. W., Spilker, J. J. Jr. Eds. *Global Positioning System: Theory and Applications*. Washington, DC: AIAA, 1996, Vol. I, Part II, Chap. 11, p. 469-484. ISBN 1-56347-106-X

[13] USNO. *GPS Timing Operations* [on line]. Available on http://tycho.usno.navy.mil/gps.html. (cited May 28th, 2006)

[14] Warnant, R. *Théorie des erreurs et GNSS* [*Error theory and GNSS*]. Master course GEOG0615. Liège: ULg (Geography), 2005.

[15] Wilson, A. Ed. *Galileo: The European Programme for Global Navigation Services* [on line]. 2nd ed. Noordwijk: ESA Publications Division, 2005, BR-186(E). ISBN 92-9092-738-0 Available on http://www.esa.int/esapub/br/br186/br186e.pdf. (cited February 17th, 2006)

References for chapter 3

[16] BIRA-IASB. *Background information in SPENVIS: Indices* [on line]. Available on http://www.spenvis.oma.be/spenvis/help/background/indices.html. (cited April 7th, 2006)

[17] Conley, R., Cosentino, R., Hegarty, C. et al. "Performance of Stand-Alone GPS" In Kaplan, E., Hegarty, C. J. Eds. *Understanding GPS: Principles and Applications*. 2nd ed. Boston: Artech House, 2005, Chap. 7, p. 301-378. ISBN 1-58053-894-0

[18] Davies, K. "Radio soundings of the ionosphere". In *Ionospheric Radio*. London: Peter Peregrinus, 1990, Chap. 4, p. 89-110. (IEE, Electromagnetic Wave Series 31). ISBN 0-86341-186X

[19] DAVIES, K. "Morphology of the ionosphere". In *Ionospheric Radio*. London: Peter Peregrinus, 1990, Chap. 5, p. 125-142. (IEE, Electromagnetic Wave Series 31). ISBN 0-86341-186X

[20] GEOFORSCHUNGSZENTRUM POTSDAM. *Indices of Global Geomagnetic Activity* [on line]. Available on http://www.gfz-potsdam.de/pb2/pb23/niemegk/kp_index. (cited April 7th, 2006)

[21] GÉRARD, J. C. "Interaction rayonnement solaire-atmosphère" ["Interaction solar radiation-atmosphere"]. In *Physique de l'atmosphère et de l'environnement terrestres* [*Physics of terrestrial atmosphere and environment*]. Master course ASTR0208. Liège: ULg (AGO), 2004, Chap. II, p. 21-77.

[22] GÉRARD, J. C. "L'ionosphère" ["The ionosphere"]. In *Physique de l'atmosphère et de l'environnement terrestres* [*Physics of terrestrial atmosphere and environment*]. Master course ASTR0208. Liège: ULg (AGO), 2004, Chap. V, p. 152-167.

[23] ITU-R. *Choice of indices for long-term ionospheric predictions*. Rec. ITU-R P.371-8, 1999.

[24] ITU-R. *Ionospheric propagation data and prediction methods required for the design of satellite services and systems*. Rec. ITU-R P.531-8, 2005.

[25] ITU-R. *Reference ionospheric characteristics*. Rec. ITU-R P.1239, 1997.

[26] KLOBUCHAR, J. A. "Ionospheric Effects on GPS". In PARKINSON, B. W., SPILKER, J. J. Jr. Eds. *Global Positioning System: Theory and Applications*. Washington, DC: AIAA, 1996, Vol. I, Part II, Chap. 12, p. 469-484. ISBN 1-56347-106-X

[27] NOAA. NESDIS. NGDC. SOLAR TERRESTRIAL PHYSICS. *Solar and Interplanetary Phenomena: Penticton/Ottawa 2800 MHz Solar Flux* [on line]. Available on http://www.ngdc.noaa.gov/stp/SOLAR/FLUX/flux.html. (cited April 7th, 2006)

[28] ODIJK, D. "The ionospheric error in GPS observations". In *Fast precise GPS positioning in the presence of ionospheric delays* [on line]. Ph.D thesis. Delft: TU Delft, 2002, PoG 52, Chap. 4, p. 69-102. ISBN 90-6132-278-2 Available on http://www.ncg.knaw.nl/Publicaties/Geodesy/pdf/52Odijk.pdf. (cited March 27th, 2006)

[29] RAWER, K. "Propagation of Decameter Waves (HF-Band)". In LANDMARK, B. Ed. *Meteorological and Astronomical Influences on Radio Wave Propagation*. New York: Academic Press, 1963, Chap. 11, p. 221-250.

[30] Van der Linden, R.A.M., and the SIDC team. *Online catalogue of the sunspot index* [on line]. Available on http://www.sidc.be/sunspot-data. (cited April 7th, 2006)

References for chapter 4

[31] Aragon-Angel, M. A., Orus, R., Hernandez-Pajares, M. et al. "Preliminary NeQuick assessment for future single frequency users of GALILEO". Presented at the *6th Geomatic Week Conference*, Barcelona, 2005.

[32] Aragon-Angel, A., Amarillo Fernandez, F. "Advanced Ionospheric modelling for GNSS single frequency users". Presented at the *IEEE/ION Position Location And Navigation Symposium 2006*, San Diego, 2006.

[33] Arbesser-Rastburg, B., Prieto Cerdeira, R. *GALILEO Ionospheric Model for Single Frequency Receivers.* ESA-APPNG-SPEC/00344-BAR. Issue 5. Noordwijk: ESA, 2005.

[34] Bradley, P. A., Dudeney, J. R. "A simple model of the vertical distribution of electron concentration in the ionosphere". *J. Atmos. Terr. Phys.*, 1973, Vol. 35, p. 2131-2146.

[35] Di Giovanni, G., Radicella, S. M. "An analytical model of the electron density profile in the ionosphere". *Adv. Space Res.*, 1990, Vol. 10, No. 11, p. 27-30.

[36] Gérard, J. C. "Le magnétisme terrestre" ["The terrestrial magnetism"]. In *Physique de l'atmosphère et de l'environnement terrestres* [*Physics of terrestrial atmosphere and environment*]. Master course ASTR0208. Liège: ULg (AGO), 2004.

[37] Hochegger, G., Nava, B., Radicella, S. M. et al. "A Family of Ionospheric Models for Different Uses". *Phys. Chem. Earth (C)*, 2000, Vol. 25, No. 4, p. 307-310.

[38] ICTP. ARPL. *Nequick TEC On-line Calculation* [on line]. Trieste, 2003. Available on http://arpl.ictp.trieste.it/nq-online/index.html. (cited March 7th, 2006)

[39] ITU-R. *NeQuick software* [on line]. Rec. P.531, 2002. Available on http://www.itu.int/ITU-R/study-groups/software/rsg3-p531-electron-density.zip. (cited May 5th, 2006)

[40] Klobuchar, J. A. "Ionospheric Time-Delay Algorithm for Single-Frequency GPS Users". *IEEE Transactions on Aerospace and Electronic Systems*, 1987, Vol. AES-23, No. 3, p. 324-331.

[41] Leitinger, R., Titheridge, J. E., Kirchengast, G. et al. "Ein "einfaches" globales empirisches Modell für die F-Schicht der Ionosphäre" ["A "simple" global empirical model for the F layer of the ionosphere"]. *Kleinheubacher Ber.*, 1996, Vol. 39, p. 697-704.

[42] Leitinger, R., Radicella, S.M., Nava, B. et al. "NeQuick - COSTprof - NeUoG-plas, a family of 3D electron density models". In *Proceedings of the COST 251 Madeira Workshop*, Madeira, 1999. p. 75-89.

[43] Litt, F. X. "Approximation par interpolation" ["Approximation by interpolation"]. In *Analyse numérique II* [*Numerical analysis II*]. Master course MATH0012. Liège: ULg (Montefiore Institute), 1999, Chap. 1, p. 5-56.

[44] Litt, F. X. "Intégration et dérivation numérique" ["Numerical integration and derivation"]. In *Analyse numérique II* [*Numerical analysis II*]. Master course MATH0012. Liège: ULg (Montefiore Institute), 1999, Chap. 3, p. 93-117.

[45] Mosert de Gonzalez, M., Radicella, S. M. "An empirical model of the F_1 intermediate layer true-height characteristics". *Adv. Space Res.*, 1987, Vol. 7, No. 6, p. 65-68.

[46] NASA. GSFC. Space Physics Data Facility. *Geophysical Models* [on line]. Available on http://modelweb.gsfc.nasa.gov. (cited May 22nd, 2006)

[47] Pita, J. *GALILEO Reference Ionosphere*. ESA-APPNG-SPEC/00171-JP. Issue 2. Noordwijk: ESA, 2004.

[48] Radicella, S. M., Zhang, M.-L. "The improved DGR analytical model of electron density height profile and total electron content in the ionosphere". *Ann. Geofis*, 1995, Vol. XXXVIII, No. 1, p. 35-41.

[49] Radicella, S. M., Leitinger, R. "The evolution of the DGR approach to model electron density profiles". *Adv. Space Res.*, 2001, Vol. 27, No. 1, p. 35-40.

[50] Radicella, S. M., Leitinger, R., Hochegger, G. et al. "Ionospheric model developments for satellite navigation and communication applications". In *Proceedings of the XXVIIth URSI General Assembly* [on line], Maastricht, 2002. p. 1480-1483. Available on http://www.ursi.org/Proceedings/ProcGA02/papers/p1480.pdf. (cited March 30th, 2006)

[51] Radicella, S. M., Arbesser-Rastburg, B., Leitinger, R. "An improved Ionospheric Correction Model for Single Frequency Satellite Navigation". Presented at the *7th SBAS meeting*, Graz, 2003.

[52] Radicella, S. M., Leitinger, R. "Are models predicting a realistic picture of vertical total electron content?". *Radio Science*, 2004, Vol. 39, RS1S14, doi:10.1029/2002RS002823.

[53] Rawer, K. "Replacement of the present sub-peak plasma density profile by a unique expression". *Adv. Space Res.*, 1983, Vol. 2, No. 10, p. 183-190.

[54] Rogers, N. C., Cannon, P. S., Angling, M. J. et al. "Validation of an ionospheric pseudo-range error correction model for GALILEO". Presented at the *11th International Ionospheric Effects Symposium*, Alexandria (USA), 2005.

[55] VEGA Group PLC. GSSF Team. *GALILEO System Simulation Facility - Algorithms and Models*. GSSFP2.OM.002 [on line]. Issue 5. Darmstadt: VEGA Informations-Technologien GmbH, 2005. Available on http://www.gssf.info/Documents_CGSSFP2.OM. 002 - Algorithms and Models - Issue 5.zip. (cited February 17th, 2006)

[56] Weisstein, E. W. "Lagrange Interpolating Polynomial". In *MathWorld - A Wolfram Web Resource* [on line]. Available on http://mathworld.wolfram.com/LagrangeInterpolatingPolynomial.html. (cited March 22nd, 2006)

[57] Weisstein, E. W. "Legendre-Gauss Quadrature". In *MathWorld - A Wolfram Web Resource* [on line]. Available on http://mathworld.wolfram.com/Legendre-GaussQuadrature.html. (cited March 22nd, 2006)

References for chapter 5

[58] Coïsson, P., Radicella, S. M., Nava, B. "Tests of NeQuick with modified topside formulation". Presented at the *11th SBAS meeting*, Noordwijk, 2005.

[59] Fonda, C., Coïsson, P., Nava, B. et al. "Comparison of analytical functions used to describe topside electron density profiles with satellite data" [on line]. *Ann. Geophys.*, 2005, Vol. 48, No. 3, p. 491-495. Available on http://www.earth-prints.org/bitstream/2122/916/1/08Fonda.pdf. (cited March 28th, 2006)

[60] Jakowski, N., Kutiev, I. S., Heise, S. et al. "A topside ionosphere/plasmasphere model for operational applications". In *Proceedings of the XXVIIth URSI General Assembly* [on line], Maastricht, 2002. p. 2174-2177. Available on http://www.ursi.org/Proceedings/ProcGA02/paper/p2174.pdf. (cited March 30th, 2006)

[61] Knezevich, M., Radicella, S. M. "Development of an ionospheric NeQuick model algorithm for GNSS receivers". In *Proceedings of the 2nd ESA Workshop on Satellite Navigation User Equipment Technologies NAVITEC 2004*, Noordwijk, 2004.

[62] Leitinger, R., Zhang, M.-L., Radicella, S. M. "An improved bottomside for the ionospheric electron density model NeQuick" [on line]. *Ann. Geophys.*, 2005, Vol. 48, No. 3, p. 525-534. Available on http://www.earth-prints.org/bitstream/2122/920/1/12Leitinger1.pdf. (cited March 28th, 2006)

[63] Weisstein, E. W. "Gauss-Kronrod Quadrature". In *MathWorld - A Wolfram Web Ressource* [on line]. Available on http://mathworld.wolfram.com/Gauss-KronrodQuadrature.html. (cited April 22nd, 2006)

[64] Weisstein, E. W. "Legendre Polynomial". In *MathWorld - A Wolfram Web Resource* [on line]. Available on http://mathworld.wolfram.com/LegendrePolynomial.html. (cited May 22nd, 2006)

References for chapter 8

[65] Mendillo, M., Pi, X., Smith, S. et al. "Ionospheric effects upon a satellite navigation system at Mars" [on line]. *Radio Science*, 2004, Vol. 39, RS2028, doi:10.1029/2003RS002933. Available on http://sirius.bu.edu/aeronomy/2003RS002933.pdf. (cited May 5th, 2006)

[66] NASA. JPL. *Mars Network* [on line]. Available on http://marsnet.jpl.nasa.gov. (cited May 5th, 2006)

[67] Pita, J. *Characterization of Ionosphere Scintillations for GALILEO*. ESA-APPNG-TN/00255-JP. Issue 2. Noordwijk: ESA, 2004.

[68] Schaer, S. "Extracting Ionospheric Information from GPS Data". In *Mapping and Predicting the Earth's Ionosphere Using the Global Positioning System* [on line]. Ph.D thesis. Bern: University of Bern (Astronomical Institute), 1999, Chap. 3, p. 41-72. Available on http://www.aiub.unibe. ch/download/papers/ionodiss.pdf. (cited March 22nd, 2006)

Acronyms

Satellite navigation

AS	GPS Anti Spoofing
CS	GALILEO Commercial Service
DOP	Dilution Of Precision
EGNOS	European Geostationary Navigation Overlay System, European SBAS
GAGAN	GPS and GEO Augmented Navigation system, Indian SBAS
GCC	GALILEO Control Centre
GCS	GALILEO Ground Control Segment
GLONASS	GLObal NAvigation Satellite System, Russian contribution to GNSS
GMS	GALILEO Ground Mission Segment
GNSS	Global Navigation Satellite System
GOC	GALILEO Operating Company
GPS	Global Positioning System, US contribution to GNSS
GSS	GALILEO Sensor Station
GSSF	GALILEO System Simulation Facility
MARSat	MC&N Mars Areostationary Relay Satellite
MC&N	Mars Communications and Navigation satellite network
MCS	GPS Master Control Station
MS	GPS Monitor Stations
MSAS	Multifunctional transport Satellite space-based Augmentation System, Japanese SBAS
NAVSTAR	NAVigation Satellite Timing And Ranging, official name for GPS
OS	GALILEO Open Service
PPS	GPS Precise Positioning Service
PRS	GALILEO Public Regulated Service
QZSS	Japanese Quasi-Zenith Satellite System

SA	GPS Selective Availability
SAR	GALILEO Search And Rescue service
SBAS	Satellite-Based Augmentation System
SIS	Signal In Space
SoL	GALILEO Safety of Life service
SPS	GPS Standard Positioning Service
TOA	Time Of Arrival
TT&C	GALILEO Telemetry, Tracking and Command stations
UERE	User Equivalent Range Error
ULS	GALILEO UpLink Stations
WAAS	Wide Area Augmentation System, US SBAS

Ionosphere

DGR	Di Giovanni-Radicella
IRI	International Reference Ionosphere
RINEX	Receiver INdependent EXchange format, used to exchange GPS data
TEC	Total Electron Content
sTEC	slant TEC
vTEC	vertical TEC
TID	Travelling Ionosphere Disturbance

Other

DOY	Day Of Year
DRMS	Distance Root Mean Square
FAQ	Frequently Asked Questions
GUI	Graphical User Interface
LT	Local Time
MEO	Medium Earth Orbit
MODIP	MOdified DIP latitude
NaN	Not a Number
RMS	Root Mean Square
SPENVIS	SPace ENVironment Information System, developed for ESA by BIRA-IASB, http://www.spenvis.oma.be
UHF	Ultra High Frequency
UT	Universal Time
UTC	Coordinated Universal Time
UV	UltraViolet radiation

Organisms

A&M	Aerospace and Mechanical Engineering department of the FAS of the ULg, http://www.ltas.ulg.ac.be
AGO	Astrophysics, Geophysics and Oceanography department of the FS of the ULg, http://www.astro.ulg.ac.be
ASE	Agence Spatiale Européenne, cf. ESA
AIAA	American Institute of Aeronautics and Astronautics, USA, http://www.aiaa.org
ARPL	ICTP Aeronomy and RadioPropagation Laboratory, http://arpl.ictp.it
BIRA	Belgisch Instituut voor Ruimte-Aëronomie, Belgian Institute for Space Aeronomy, Brussels, Belgium, http://www.aeronomie.be
CCIR	Consultative Committee for International Radio, former ITU-R
COSPAR	Committee on Space Research, http://www.cosparhq.org
COSPAS-SARSAT	Cosmicheskaya Sistyema Poiska Avariynich Sudow (Space System for the Search of Vessels in Distress), Search and Rescue Satellite-Aided Tracking, http://www.cospas-sarsat.org
COST	European Cooperation in the field of Scientific and Technical Research, http://www.cost.esf.org
DSN	NASA JPL Deep Space Network, http://deepspace.jpl.nasa.gov/dsn
EC	European Commission, one of EU institutions, http://ec.europa.eu/index_en.htm
ESA	European Space Agency, http://www.esa.int
ESTEC	ESA European Space Research and Technology Centre, Noordwijk, The Netherlands, http://www.esa.int/esaCP/SEMOMQ374OD_index_0.html
EU	European Union, http://europa.eu
FAA	Federal Aviation Administration, USA, http://www.faa.gov
FAS	Faculty of Applied Sciences of the ULg, http://www.facsa.ulg.ac.be
FS	Faculty of Sciences of the ULg, http://www.facsc.ulg.ac.be
FSA	Faculté des Sciences Appliquées, cf. FAS
GJU	GALILEO Joint Undertaking, Brussels, Belgium, http://www.galileoju.com

GSFC	NASA Goddard Flight Space Center, http://www.nasa.gov/centers/goddard/home/index.html
IASB	Institut d'Aéronomie Spatiale de Belgique, Belgian Institute for Space Aeronomy, Brussels, Belgium, http://www.aeronomie.be
ICTP	Abdus Salam International Centre for Theoritical Physics, Trieste, Italy, http://www.ictp.it
IEE	Institution of Electrical Engineers, former part of IET not to be confused with IEEE
IET	Institution of Engineering and Technology, result of the merging of IEE and IIE in September 2005, http://www.theiet.org
IEEE	Institute of Electrical and Electronics Engineers, http://www.ieee.org
IIE	Institution of Incorporated Engineers, former part of IET
ION	Institute of Navigation, http://www.ion.org
IGAM	Institute for Astrophysics, Geophysics and Meteorologie, Graz, Austria, http://www.uni-graz.at/en/igamwww.htm
IGS	International GNSS Service, JPL, http://igscb.jpl.nasa.gov
ITU	International Telecommunication Union, http://www.itu.int
ITU-R	ITU Radiocommunication Sector, http://www.itu.int/ITU-R/index.asp
JPL	NASA Jet Propulsion Laboratory, Pasadena, USA, http://www.jpl.nasa.gov
JPO	GPS Joint Program Office, USA, http://gps.losangeles.af.mil
NASA	National Aeronautics and Space Administration, USA, http://www.nasa.gov
NESDIS	NOAA National Environmental Satellite, Data, and Information Service, http://www.nesdis.noaa.gov
NGDC	NESDIS National Geophysical Data Center, Boulder, USA http://www.ngdc.noaa.gov
NOAA	National Oceanic & Atmospheric Administration, Silver Spring, USA, http://www.noaa.gov
ROB	Royal Observatory of Belgium, Brussels, Belgium, http://www.observatoire.be
SIDC	ROB Solar Influences Data analysis Centre, http://sidc.oma.be

TEC	ESTEC Technical and Quality Management Directorate, http://www.esa.int/techresources/index.html
TEC-E	TEC Electrical Engineering Department, http://www.esa.int/techresources/ESTEC-Page-Electrical_1082551445348.html
TEC-EE	TEC-E Electromagnetics and Space Environments Division, http://www.esa.int/techresources/ESTEC-Article-fullArticle_item_selected-7_5_00_par-29_1069167509934.html
TEC-EEP	TEC-EE Wave Interaction & Propagation Section, http://www.esa.int/techresources/ESTEC-Article-fullArticle_item_selected-7_5_00_par-29_1069167508470.html
TU Delft	(Technische Universiteit Delft) Delft University of Technology, Delft, The Netherlands, http://www.tudelft.nl
ULg	University of Liège, Liège, Belgium, http://www.ulg.ac.be
URSI	Union Radio-Scientifique Internationale, International Union of Radio Science, http://www.ursi.org